PERIPHERAL EXPRESSION OF PLASMA GELSOLIN AS A TREATMENT FOR ALZHEIMER'S DISEASE

By

AARON HIRKO

A DISSERTATION PRESENTED TO THE GRADUATE SCHOOL
OF THE UNIVERSITY OF FLORIDA IN PARTIAL FULFILLMENT
OF THE REQUIREMENTS FOR THE DEGREE OF
DOCTOR OF PHILOSOPHY

UNIVERSITY OF FLORIDA

2006

To my daughter, Ava Wrenn Hirko; and to her brother, Elliott Todd Hirko

ACKNOWLEDGMENTS

I would like to thank my parents, Robert and Theresa Hirko, for all of their love and support. I also need to thank my wife, Laura; daughter, Ava; and my son Elliott for their inspiration, love, and support.

I owe a deep debt of gratitude to my mentor, Dr. Jeffrey Hughes, for giving me the opportunity to study in the pharmaceutics program. I also need to thank Dr. Edwin Meyer for taking me in as an undergrad, introducing me to Dr. Hughes, and giving me space in his laboratory. I thank my supervisory committee members (Dr. Michael King, Dr. Guenther Hochhaus, and Dr. Sihong Song) for all the excellent advice and insight. I acknowledge Dr. Raj Rao, Dr. Ke Wu, Dr. Ron Klein, Dr. Yan Gong, Dr. Ke Ren, and Dr. Preeti Yadava for their friendship, help, and advice. Finally, I thank all of the students and staff from the Department of Pharmaceutics.

TABLE OF CONTENTS

LIST OF FIGURES

Abstract of Dissertation Presented to the Graduate School
of the University of Florida in Partial Fulfillment of the
Requirements for the Degree of Doctor of Philosophy

PERIPHERAL EXPRESSION OF PLASMA GELSOLIN AS A TREATMENT FOR ALZHEIMER'S DISEASE

By

Aaron Hirko

August 2006

Chair: Jeffrey Hughes
Major Department: Pharmacy

Alzheimer's disease (AD) is a progressive neurodegenerative disorder affecting memory, thinking, behavior, and emotion. It is characterized by a progressive accumulation of extracellular amyloid plaques and intracellular neurofibrillary tangles. Evidence suggests that the deposition of amyloid triggers a cascade that ultimately leads to Alzheimer's pathology, making amyloid a promising target for the treatment of AD. Amyloid plaques are composed mainly of the 4.5 kD peptide fragment amyloid β (Aβ). One strategy targeting Aβ is to deliver an Aβ binding agent outside the brain, creating a peripheral sink that causes efflux of Aβ across the blood-brain barrier.

One such agent is the 89 kD protein plasma gelsolin. However, administering such a large compound poses formidable formulations challenges, and proteins generally have poor pharmacokinetic properties. Taking a gene-therapy approach by delivering a DNA vector coding for plasma gelsolin offers an alternative to repeated injections of protein.

We developed a plasmid vector for human plasma gelsolin. We determined that plasma gelsolin may have enzymatic-like functions toward Aβ, shifting the equilibrium from fibrillization and deposition to solubilization and elimination. We obtained expression of our plasmid vector for plasma gelsolin in the periphery of 2 different mouse models of Alzheimer's, and showed that it results in a significant reduction in the amount of Aβ in the brain. We also showed that this reduction of Aβ in the brain may occur along with an increase in microglia activity. These results show the validity of using plasma gelsolin as a peripheral gene therapy of Alzheimer's disease.

CHAPTER 1
INTRODUCTION

Alzheimer's disease (AD) is the most common form of dementia. In the next 45 years, the number of Americans afflicted with AD is expected to quadruple: from about 2.5 million cases today, to nearly 10 million in 2050 (Sloane et al., 2002). This increased prevalence of AD can be attributed to aging of the population: in the year 2000, 5.9% of the population was over age 75; in 2050, this is expected to be 11.4% (Kawas and Brookmeyer, 2001). Age is the single strongest risk factor for AD. It afflicts 10% of people over 65, and almost 50% of people older than 85 (Evans et al., 1989). Alzheimer's disease has a huge impact on a person's quality of life (e.g., memory loss, impaired activities of daily living, depression, and behavioral disturbances) (Sloane et al., 2002). As the disease progresses, independence decreases, placing an increased financial and psychological burden on family caregivers. Koppel estimated that in 2001, the total economic impact of AD in the US was between $183 and 207 billion (2002). With the expected increased prevalence of AD, finding efficacious treatments will be critical to ease the social burden of this disease.

Dementia

In Latin "dementia" is defined as irrationality. Medically speaking, dementia describes a collection of symptoms that robs an individual of his/her cognitive functions, resulting in the loss of the ability to carry out normal daily activities eventually requiring the full-time care of family or professionals. These symptoms can be caused by a number of different diseases that affect the brain. Typically the diagnosis of dementia requires

significant deficits in at least two or more brain functions, such as reasoning, judgment, perception, language, and memory.

Discovery of Alzheimer's disease

In March 1901 the husband of a 50-year-old woman (Auguste D) noticed a paranoid symptomalogy in his wife, which rapidly progressed to include sleep disorders, aggressiveness, crying, confusion, and disturbances of memory. By November, the deteriorating mental state of Auguste D forced her husband to admit her for inpatient treatment at the Community Psychiatric Hospital at Frankfurt. A senior assistant at the hospital, Dr. Alois Alzheimer, thoroughly documented the progression of August D's symptoms. On her death on April 8, 1906, Alzheimer was able to examine her brain both histologically and morphologically. His examination showed that Auguste D's brain was atrophied, and included histological abnormalities later considered the hallmarks of AD, known as neurofibrillary tangles (NFT) and senile plaques. He described these findings (along with their relationship to more than 4 years of clinical observations) at the 37th meeting of South-West German Psychiatrists in Tübingen on November 3, 1906.

Although Alzheimer's lecture was not well received, his observation would be later recognized as the first demonstrated relationship between clinical history of specific cognitive changes and neurological lesions at autopsy. After reports of the case of Auguste D, a number of other patients with similar ailments were described (Moller and Graeber, 1998). The term Alzheimer's disease was first coined to describe the condition by a colleague of Alzheimer in Munich, Dr. Emil Kraepelin (1910). Since then Alzheimer's disease has been recognized as the most common form of dementia worldwide.

Current Therapies

To date, the only FDA-approved treatments for AD are acetylcholinesterase inhibitors (tacrine, donepezil, rivastigmine, and galantamine) and an NMDA antagonist (memantine). The aim of using acetylcholinesterase inhibitors is to enhance selective cholinergic transmission in the brain by decreasing the catabolism of acetylcholine. Basal forebrain cholinergic neurons, critical for memory and learning, are diminished in AD, resulting in a reduction of choline acetyltransferase and acetylcholine (Coyle et al., 1983; Terry and Katzman, 1983). Increasing the levels of acetylcholine can help ameliorate deficits in memory and learning (Weinstock, 1995). The aim of using NMDA antagonist is to block the effects of elevated levels of glutamate which may lead to neuronal dysfunction (Mattson et al., 1992). Both treatment strategies have shown modest improvements in maintaining independence, function, and decreasing cost to society (Trinh et al., 2003; Wimo et al., 2003). However, these modest improvements are far from ideal and only delay the onset of the inevitable dependency of care by a short period of time. These treatments only address biochemical symptoms of AD rather than preventing progression of the underlying cause.

Inherited Alzheimer's

It was not until 75 years after Alzheimer described the case of August D that the main constituent of the senile plaques was biochemically identified. Allsop and coworkers (1983) identified that these plaques consisted mainly of a 40-42 amino acid peptide named amyloid β (Aβ). This peptide was later discovered to originate from a larger precursor given the name amyloid precursor protein (APP) (Kang et al., 1987). The subsequent discovery that a single missense mutation on the APP gene corresponded with an inheritable form of Alzheimer's disease (Goate et al., 1991) led to the

formulation of the amyloid cascade hypothesis, which states the underlying cause of AD is the result of an increased concentration and deposition of Aβ (Hardy and Allsop, 1991). This hypothesis was bolstered by the later discovery that every inheritable form of AD results from mutations involved in the processing of Aβ from APP: either on APP itself, Presenilin-1, or Presenilin-2 (Clark and Goate, 1993; Levy-Lahad et al., 1995; Sherrington et al., 1996). Although inherited forms of AD comprise fewer than 10% of all Alzheimer's cases, every inheritable form involves the facilitation of the oligomerization and later precipitation of Aβ.

Amyloid Precursor Protein

In humans, amyloid precursor protein is a large transmembrane glycoprotein that exists as three major isoforms (APP695, APP751, and APP770) that are all the result of alternative processing of pre-mRNA generated from the APP gene on Chromosome 21.

The function of APP is poorly understood. However, evidence suggests it may have cell adhesive, intracellular communication, membrane to nucleus communication, neurotrophic, or neuroproliferative activity (Turner et al., 2003). Even though APP may play a role in many biological functions, compensatory mechanisms allow for the viability of APP knockout mice (Zheng et al., 1996). These mice show reductions in body weight and synaptic transmission, impaired locomotor activity and grip strength, and a hypersensitivity to epileptic seizures and forebrain commissural defects (Zheng et al., 1995).

Three proteolytic cleavage sites have been identified on APP: two near the plasma membrane on the extracellular side, and one within the plasma membrane. The protease complexes responsible for the cleavage are known as α, β, and γ secretase. Cleavage by

α secretase and β secretase releases large amino-terminal fragments known as APP_s-α and APP_s-β respectively. These fragments differ in size by 17 amino acids at the carboxy-terminus of the fragments (APP_s-α is larger than APP_s-β). The remaining fragments of APP stay anchored to the plasma membrane, and are referred to as C99 for the β secretase product and C83 for the α secretase product. Both C83 and C99 are substrates for γ secretase which cleaves within the plasma membrane. Amyloid β (Aβ) is formed after C99 is cleaved by γ secretase. This cleavage usually results with a 40 amino acid length peptide Aβ 1-40. However, γ secretase cleavage of C99 can also result in the more hydrophobic 42 amino acid peptide product Aβ 1-42. The Aβ 1-42 is more prone to oligomerzation and fibril formation than Aβ 1-40 (Hasegawa et al., 1999). The inheritable forms of AD invariably increase the relative amounts of Aβ 1-42 as compared to Aβ 1-40 (Scheuner et al., 1996; Sinha and Lieberburg, 1999; Suzuki et al., 1994; Tamaoka et al., 1994).

Amyloid β is first released from neurons as a soluble monomer which has an α-helical secondary structure. During the process of oligomerization this undergoes a series of conformational changes to form cross β-sheet structures as oligomers. These soluble oligomeric forms of Aβ may have a protofibular-like structure (Lashuel et al., 2002) or an amorphous micellular-like structure (Hoshi et al., 2003). In the fibrillar model for amyloid deposition the soluble oligomers begin to aggregate forming first protofibrils, and then fibrils that finally come together to make up the plaques (Figure 1-1).

Amyloid Cascade Hypothesis

One of the central controversies in the AD research community is whether Aβ is the cause or result of the pathogenic process. The hypothesis that Aβ is central to the

pathogenesis of AD is known as the amyloid cascade hypothesis (Selkoe, 1989, 1990). This hypothesis states that something causes either an over- production or a decreased clearance of Aβ. The increased levels of Aβ result in the formation of oligomeric forms of Aβ. These then aggregate and deposit as plaques. This deposition of plaques causes the activation of microglia and astrocytes, resulting in the release of pro-inflammatory cytokines and reactive oxygen species (Akama et al., 1998; Hoozemans et al., 2005; Johnstone et al., 1999). Together microglia activation, astrocytic activation, and oligomeric Aβ can all cause synaptic and neuritic injury, including neurofibrillary tangles, which then lead to dementia.

Evidence Supporting the Amyloid Cascade Hypothesis

The main evidence supporting the amyloid cascade hypothesis is that every form of familial Alzheimer's disease (FAD) involves mutations on either APP itself or the enzymes that cleave APP, resulting in an overproduction of Aβ 1–42. The presence of an extra copy of chromosome 21, in which the gene for APP is located, is found in Down's syndrome; this inevitably leads to an early onset of Alzheimer's-like pathology. In the more common sporadic form of AD, the presence of the apolipoprotein E4 (apoE4) allele is considered a risk factor for the disease (Corder et al., 1993); evidence suggests that apoE is involved with the clearance of Aβ (Brendza et al., 2002). Further evidence supporting the amyloid cascade hypothesis is the fact that, *in vitro,* Aβ itself has been found to be neurotoxic (Dahlgren et al., 2002; Pike et al., 1991).

Critics of the Amyloid Cascade Hypothesis

Critics of the amyloid cascade hypothesis argue that Aβ accumulation may occur secondary to other pathological events and actually play a role in neuroprotection. They

point out that although specific forms of Aβ can be toxic *in vitro*; this toxicity is less reliable in animal models, providing the argument that the *in vitro* toxicity may be an artifact. They make the point that amyloid deposition is poorly correlated with cognitive deficits, and that neurofibrillary tangles (NFT) and neuron number are much better indicators of cognitive decline (Giannakopoulos et al., 2003).

It is true that when Aβ deposits in humans are measured histochemically, they do not correlate well with cognitive decline. However, soluble forms of Aβ measured biochemically from brain extracts correlates very well with synaptic density and can be used to discriminate between AD patients and non-AD controls that do have a high degree of amyloid deposit pathology (Lue et al., 1999; Naslund et al., 2000). Total Aβ 40 and 42 levels of nursing home resident brain extracts measured biochemically has also been correlated to cognitive decline as measured by the Clinical Dementia Rating (CDR) scale (Naslund et al., 2000).

There is evidence that Aβ may play a role as an antioxidant (Curtain et al., 2001) or a neurotrophin (Yankner et al., 1990). In fact, Lopez-Tolendano and Shelanski (2004) recently found that Aβ was neurogenic in a dose-dependent manner when treating neural stem cells. However, Liu et al. (2004) demonstrated that Aβ's toxicity in primary neuronal cultures was dependent on the expression of the microtubule-associated protein tau, cyclin-dependent kinase 5 (Cdk5), and the cell's state of differentiation.

This is an interesting observation, providing evidence for a mechanism of how Aβ can cause NFTs. Hyperphosphorylated tau is the main component of NFTs and Cdk5 is one of the enzymes thought responsible for tau's phosphorylation (Cruz and Tsai, 2004; Noble et al., 2003). Although both sides can make strong arguments supporting their

point of view, it is unlikely that there will be any consensus over what role Aβ plays in the progression of AD until human trials are completed that target Aβ.

Elan and Wyeth Trial

The observations that active immunization in transgenic mice dramatically reduced the accumulation of Aβ (Schenk et al., 1999), and showed protection against memory deficits (Janus et al., 2000; Morgan et al., 2000) led to the phase II trial undertaken by the pharmaceutical companies Elan and Wyeth in late 2001. They actively immunized patients against Aβ, hoping to trigger an immune response that would increase clearance of Aβ from the CNS. These trials were halted early because about 6% of the patients developed meningoencephalitis (Orgogozo et al., 2003). Follow-up studies on the participants indicated that antibody responders had significantly improved memory function as measured by the neuropsychological test battery and decreased cerebral spinal fluid levels of tau protein (Gilman et al., 2005).

Sink-Hypothesis

One proposed mechanism for how immunization works is that anti-Aβ antibodies enter the CNS and stimulate microglial phagocytosis of Aβ-antibody complexes. This has been demonstrated by Bacskai et. al. (2001). Another possible mechanism for how anti-Aβ antibodies can clear plaques is by shifting the equilibrium of Aβ from the CNS to the periphery. The so called "sink hypothesis" is supported by the finding that less than 0.1% of antibodies in the serum gain access across the blood brain barrier (BBB) (Bard et al., 2000) and studies performed by separate groups using different Aβ binding agents administered peripherally(Deane et al., 2003; Matsuoka et al., 2003).

For the sink-hypothesis to be valid, carrier or receptor mediated transport of Aβ must occur, because the BBB normally prevents free exchange of polar solutes between blood and brain or brain and blood. The main transporter identified being responsible for transport out of the CNS is low-density lipoprotein receptor-related protein-1 (LRP-1) (Shibata et al., 2000). LRP-1 is a large endocytic receptor responsible for the transport of apoE and cholesterol-containing lipoproteins.

Likewise the receptor for advanced glycation end products (RAGE) has been identified as a membrane-bound receptor that transports Aβ from the circulation into the CNS (Deane et al., 2003). RAGE is a multiligand receptor in the immunoglobin superfamily. Generally there is little expression of RAGE in most tissues. However the accumulation of RAGE ligands, such as Aβ, triggers RAGE expression, in contrast to a decrease of LRP-1 expression seen in an Aβ rich environment (Shibata et al., 2000). Exacerbating this effect, RAGE transport of Aβ results in the increased expression of proinflammatory cytokines and endothelin-1 at the BBB causing decreased cerebral blood flow (Deane et al., 2003).

Deane et al. (2003) demonstrated that when PD-hAPP mice were treated with intraperitoneal injections of a truncated soluble form of RAGE (sRAGE), Aβ transport into the CNS was interfered with and significant increases in plasma Aβ levels along with a decrease in brain Aβ levels and plaque loads was observed. Likewise Matsuoka et al. saw similar results when they treated PS/APP mice with the Aβ binding agents GM1 and plasma gelsolin (Matsuoka et al., 2003; Morgan et al., 2000).

Gelsolin

Plasma gelsolin is a highly conserved 93 kD actin-binding protein, also known as brevin or actin-depolymerizing factor, normally found in the plasma at concentrations of about 179 mg/L (Chauhan et al., 1999). Its main function is thought to be part of the actin-scavenging system, to protect the microcirculation from the effects of long F-actin polymers released during cell death (Lee and Galbraith, 1992). However recent evidence points to the possibility that plasma gelsolin may play a variety of roles in the body, including mediating inflammatory responses by binding to pro-inflammatory compounds (Bucki et al., 2005; Bucki et al., 2004; Chauhan et al., 1999; Lind and Janmey, 1984; Smith et al., 1987), or by altering cell motility and endocytosis(Witke et al., 2001).

There are three known forms of gelsolin [cytoplasmic (Yin and Stossel, 1979), plasma (Nodes et al., 1987), and gelsolin-3 (Vouyiouklis and Brophy, 1997)] all coded for by the same gene, resulting from alternative post-transcriptional processing. The cytoplasmic form of gelsolin was first described as a factor able to solubilize gels formed by macrophage extracts, hence the name **gel**-**sol**-in (Yin and Stossel, 1979). Plasma gelsolin differs from the other two by the presence of an N-terminal 23 amino acid signal peptide, which causes plasma gelsolin to be secreted outside the cell producing it.

Gelsolin is regulated by polyphosphoinositide and Ca^{+2}. Gelsolin severs and caps F-actin in response to Ca^{+2}, and phosphoinositides block the capping function (Bucki et al., 2004; Kwiatkowski, 1999). It alters cell shape by remodeling actin filaments and is involved with cell motility (Cooper et al., 1987; Janmey et al., 1987; McLaughlin et al., 1993). Data from gelsolin knockout mice indicates gelsolin is necessary for rapid motile responses in cell types involved in responding to stress such as hemostasis, wound healing, and inflammation (Witke et al., 1995). A mutated form of gelsolin (either

D187N or D187Y) results in aberrant proteolytic cleavage by furin causing a 68kD gelsolin fragment to be secreted and then deposited as amyloid in the Finish type of amyloidosis (Chen et al., 2001; Kazmirski et al., 2000).

Gelsolin has been shown to be an effector of apoptosis through its interaction with the cysteinyl-protease caspase-3. A gelsolin cleavage fragment of caspace-3 has been shown to cause numerous cell types to "round up, detach from the plate, and undergo nuclear fragmentation"(Kothakota et al., 1997), most likely the result of the N-terminal gelsolin fragment's ability to activate DNase-1 (Chhabra et al., 2005).

Gelsolin has also been shown to be protective against excitotoxic induced apoptosis by altering the actin cytoskeleton in response to Ca^{+2} influx, preventing the reduction of the mitochondrial permeability transition pore opening and membrane potential loss, and preventing caspase-3 activation (Harms et al., 2004).

Plasma gelsolin has been shown to protect against inflammatory reactions associated with injury (Christofidou-Solomidou et al., 2002a; Rothenbach et al., 2004). Vasconcellos et al. showed that plasma gelsolin reduced the viscosity of cystic fibrosis sputum (1994). In fact Biogen Inc. evaluated recombinant plasma gelsolin in phase 2 clinical trials as a treatment for cystic fibrosis.

Chauhan et al. showed that human plasma gelsolin binds to Aβ, prevents fibrillization, and disassembles preformed Aβ fibrils, suggesting a possible role for gelsolin in the clearance of amyloid β (Chauhan et al., 1999; Ray et al., 2000). Plasma gelsolin is found in the cerebral spinal fluid (CSF), and produced in the choroid plexus (Matsumoto et al., 2003). At the 2004 International Conference on Alzheimer's and Related Disorders Chauhan et al. reported that gelsolin levels in AD patients' CSF was

significantly reduced as compared to nondemented age matched controls, suggesting that decreased gelsolin may play a role in the increased amyloid β content seen in AD (2004). Matsuoka et al. showed injections with bovine plasma gelsolin can prevent deposition of gelsolin in younger $_{hu}$APP $_{K670N,M671L}$/ PS-1 $_{M146L}$ (2003). The focus of our study will be on the effects plasma gelsolin gene expression has on amyloid deposition in transgenic mouse models of Alzheimer's disease.

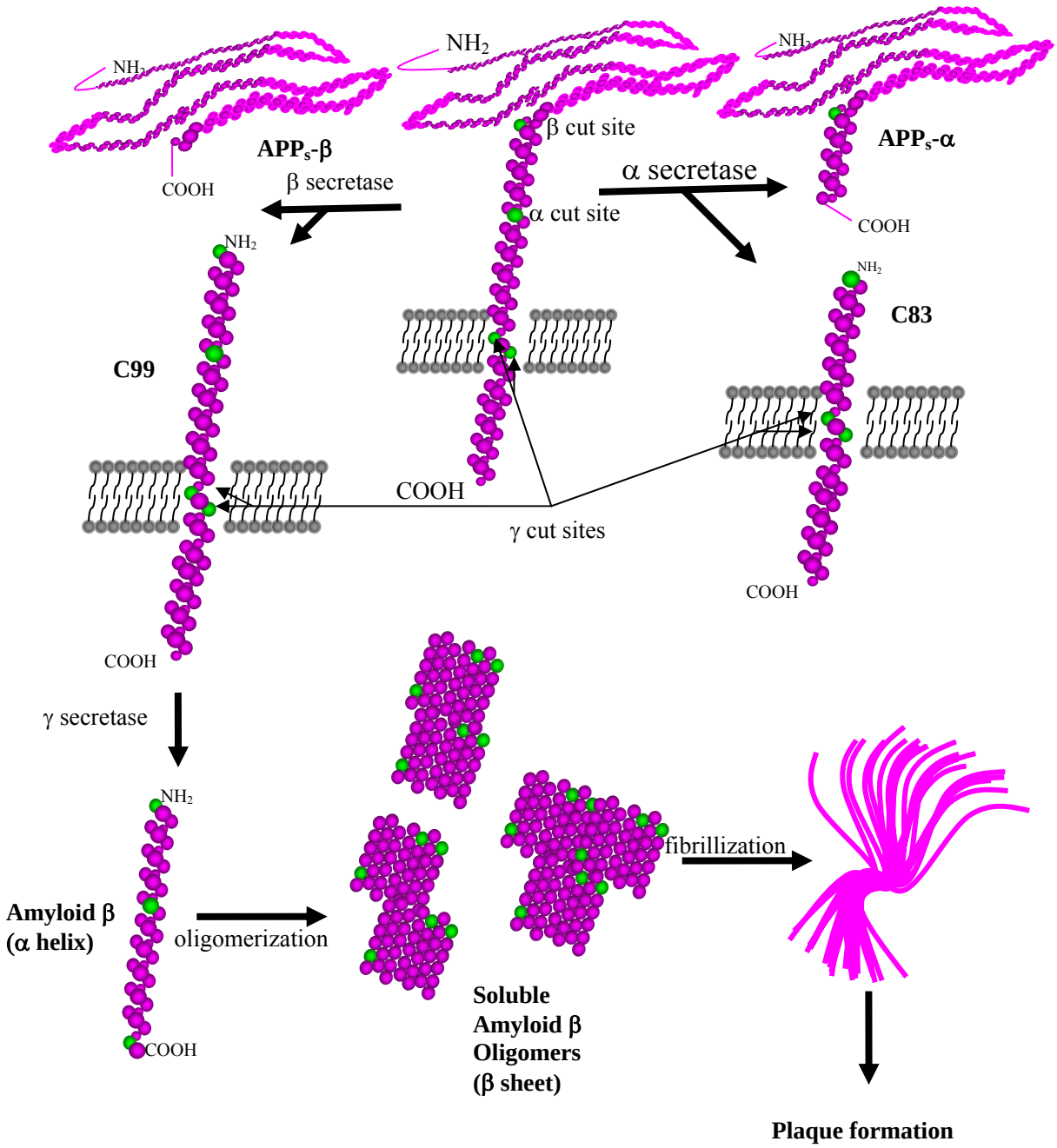

Figure 1-1. Amyloid precursor protein processing.

CHAPTER 2
MATERIALS AND METHODS

Reagents

Except where noted, all chemicals used were purchased from Fisher Scientific (Hampton, NH). Molecular biology reagents and enzymes were purchased from New England Biolabs (Ipswich, MA). Amyloid peptides were purchased from Anaspec (San Jose, CA). ThePCR primers were ordered from Sigma Genosys (The Woodlands, TX). The ELISA kits were purchased from Biosource (Camarillo, CA). Precast polyacrilamide gels and PVDF membranes were purchased from Bio-Rad Laboratories (Hercules, CA)

Subcloning Vectors

An expression plasmid for plasma gelsolin, pPGLE (Figure 2-1A), that is based on the commercially available plasmid (pCDM8) was kindly provided by Dr. Hisakazu Fujita (Kwiatkowski et al., 1989). The coding sequence for plasma gelsolin was removed from the pCDM8 backbone by a HindIII and XbaI digest, followed by separation on a 1% agarose gel, and purification using a Qiagen gel purification kit. Blunt ends were made by treating with T4 DNA polymerase in the presence of dNTPs. HindIII linkers were ligated to the blunted ends using T4 DNA ligase. Samples were then run on a 1% agarose gel. The blurred band containing the gelsolin insert, along with different amounts of linkers, was purified from the gel using a Qiagen gel purification kit. This purified band was then subject to a HindIII digest.

A plasmid backbone containing the cytomegalovirus/chicken beta-actin hybrid (CBA) promoter and the woodchuck hepatitis virus post-transcriptional regulatory element (WPRE) was prepared from our pGFP vector (Figure 2-1B)((Klein et al., 2002) by excising the Green Fluorescent Protein (GFP) coding sequence with a HindIII digest followed by separation on a 1% agarose gel; and was then purified using a Qiagen gel purification kit. The 5'phosphate groups were removed with calf intestine alkaline phosphatase in order to prevent self-ligation.

The purified backbone along with the plasma gelsolin insert were ligated together overnight with T4 DNA ligase. Electrocompetent SURE cells (Stratagene, Garden Grove, CA) were transformed with the resultant ligated product, using a Bio-Rad electroporator, with the resistance set at 400 Ω, the capacitance at 25 μF, and the voltage at 2.2kv. Transformed bacteria were grown for an hour in 1mL of NZY broth at 37°C, followed by plating on NZY agar plates containing ampicillin (50mg/L), and then grown overnight at 37°C. Several colonies were selected for screening, and each was grown overnight in 5 mL of ampicillin-containing NZY broth. Plasmids were purified from the cultures, using Qiagen mini plasmid prep kits. Plasmids were then subjected to a BglII digest to confirm orientation of the insert (Figure 2-2). A clone (W16) with the forward insert was given the name pUFGL (Figure 2-1C).

Large Scale Plasmid Preparation

For large-scale preps, plasmids were propagated overnight in 5 mL of ampicillin containing NZY broth. This was used to inoculate 2 L of ampicillin containing NZY broth, and then grown overnight again. The cultures were pelleted by centrifugation. They were then resuspended in a lysozyme buffer (80 mL/L of culture) and treated with lysozyme (2 mg/mL, Sigma, St. Louis, MO). Next the cultures were subject to alkaline

lysis by adding a 1% SDS 0.2N NaOH solution at 196 mL/L of culture. The mixture was neutralized with a 3M NaAc (pH4.8) 0.6% chloroform solution (144 mL/L of culture). The resultant chromosomal and protein precipitates were separated by centrifugation.

Plasmid DNA in the supernatant was then precipitated by bringing the solution to 10% polyetheleneglycol (PEG). The precipitates were separated by centrifugation, and then resuspended in distilled water (40 mL/L of culture). The RNA was precipitated and separated by adding 5.5 M LiCl (40 mL/L of culture), followed by centrifugation. Plasmid DNA was precipitated from the supernatant by bringing the solution to 36% isopropanol. Precipitated plasmid DNA was resuspended in a 5.3M CsCl solution containing 1 mM ethidium bromide. The resultant solution was centrifuged in a Beckman 70.1 Ti rotor at 55,000 rpm for 19 hours. The lower band containing the plasmid DNA was removed using an 18 g syringe. Ethidium bromide was removed by performing four extractions with isoamyl alcohol.

The plasmid DNA was precipitated from the aqueous layer by bringing the solution to a 40% Ethanol concentration. The plasmid precipitate was pelleted by centrifugation, and resuspended in TE (10 mM Tris-HCl 1 mM EDTA pH 8.0). Any residual protein contamination was removed from this solution by performing four extractions with phenol-chloroform, followed by one extraction with chloroform alone. Plasmid DNA was precipitated once again by adding one tenth volume of 3 M NaAC pH 4.8 and 2.5 volumes of 100% ethanol. Precipitates were pelleted by centrifugation, followed by washing excess salt with a 75% ethanol solution. The plasmids were resuspended in sterile TE buffer. Concentration and purity of the samples were determined by UV absorbance at 260/280 nm.

Cell Culture

Human embryonic kidney (HEK) 293 cells were cultured in DMEM with 10% fetal bovine serum (FBS), 100 units/mL penicillin and 100 μg/mL streptomycin (Gibco, Invitrogen, CA) in a 5% CO_2 incubator at 37°C. Cells were grown on 10cm dishes to 50% and 80% confluency. One half hour before transfection using the $CaPO_4$ precipitation method, culture media was replaced with fresh media. To prepare transfection complexes 20 μg of either pUFGL or pGFP in 700 μl of 250 mM $CaCl_2$ solution was added in a dropwise fashion to 700 μl 2X HEPES Buffered Saline while vortexing slowly (for 2X HBS, 300 mM NaCl, 1.8 mM Na_2HPO_4, 11 mM dextrose, and 40 mM HEPES, pH 7.12).

The transfection solutions were then incubated at room temperature for 20 minutes. Following incubation, the transfection solutions were mixed gently then added to cell culture dishes in a drop wise fashion. Culture dishes were incubated with transfection media for 12 hours then replaced with fresh media. Forty-eight hours later, media was collected, a proteinase inhibitor cocktail was added (Sigma P8340), and it was either used for immunoprecipitation, or concentrated ten fold with Centricon 50,000 nmw cutoff centrifugal filters for western blot analysis.

Animals and Procedures

All procedures were done with prior approval and oversight of the University of Florida's institutional animal use and care committee. Double transgenic mice expressing both Swedish mutant $_{\text{mouse /human}}$APP695 $_{\text{K594N,M595L}}$ and exon 9 deleted mutant presenilin-1 ($_{\text{mo/hu}}$APP /PS1$_{\delta E9}$) were supplied by Jackson Laboratories (Bar Harbor, ME) (Jankowsky et al., 2004). Double transgenic mice expressing both Swedish mutant

human $APP_{K670N,M671L}$ ($_{hu}APP_{K670N,M671L}$, Tg2576)(Hsiao et al., 1996) and mutant presenilin-1 $_{M146L}$ (PS-1 $_{M146L}$)(Duff et al., 1996), and transgenic mice expressing only mutant PS-1 $_{M146L}$ were supplied by The Nathan Kline Institute (NY,NY).

One litter of $_{mo/hu}APP$ /$PS1_{\delta E9}$ mice was aged until 36 weeks, at which time the mice were either injected with our test plasmid pUFGL (n=3) or left untreated (n=3). Mice expressing $_{hu}APP_{K670N,M671L}$/ PS-1 $_{M146L}$ were aged until 32 weeks, at which time they were either injected with plasmid DNA, pUFGL (n=5), pGFP (n=3), or left untreated (n=7). PS-1 mice used for western blot detection of plasma gelsolin were injected at the age of 36 weeks with either pUFGL (n=2), pGFP (n=2), or left untreated (n=2).

For injections, plasmid DNA was diluted in lactated Ringer's solution to a concentration such that there was 25 μg of plasmid DNA/10% of body weight volume of ringers (e.g. a 30 g mouse received a 3 mL injection). DNA solutions were warmed to a temperature of 37°C. Animals were warmed briefly under a heat lamp, mildly anesthetized with isoflourane, and restrained in a custom-made harness. A three milliliter syringe was used with a 27 g half inch needle. The injection solution was injected in a time period of 5-10 seconds. Animals were then recovered on a heating pad, and returned to their cages.

Blood samples were taken from PS-1 mice from the retro-orbital sinus using heparinized capillary tubes. Animals were mildly anesthesized with isoflourane, and then the capillary tube was used to puncture the retro-orbital sinus. The tube was allowed to fill with blood, and then plugged on one end with clay. Plasma was separated

immediately by centrifugation, snap frozen in liquid nitrogen, and stored at -80º C for analysis by western blot.

Two and one half weeks following injections, double transgenic mice were sacrificed along with age-matched untreated controls. Animals were deeply anesthetized with isoflourane and perfused with PBS. Livers and brains were excised, hemi-brains and a sample of liver were snap frozen in liquid nitrogen and stored at -80° C for analysis by ELISA and RT-PCR. The remaining hemi-brain and liver tissue was fixed for 48 hours in a 4% paraformaldehyde in PBS solution, and then equilibrated in 30% sucrose in PBS solution for cryoprotection.

Immunoprecipitation and Western Blot

An immunoprecipitation kit from Sigma (IP-50, St. Louis, MO) was used for the immunoprecipitation reactions. 600 μL of media from cell cultures with or without being spiked with Aβ 1-42 to 5 μM along with 2 μl anti-Gelsolin monoclonal antibody clone GS-2C4 (Sigma G-4896, St. Louis, MO) was added to the spin columns provided with the kit and incubated overnight at 4° C. 30 μL/column of protein-G agarose was washed in 1X IP buffer, then resuspended in 50 μL of 1X IP buffer and added to the samples in the columns. These samples were then incubated overnight at 4°C. The tips were broken from the columns, then the columns were centrifuged and the effluent was discarded. The beads in the columns were washed five times with 1X IP buffer, followed by a sixth wash in 0.1X IP buffer. 50 μL of Laemmli sample buffer containing 5% β-mercaptoethanol was then added to the beads and incubated at 95° C for ten minutes. Samples were spun through the columns and then 50 μl loaded onto a precast SDS 4-20% PAGE Tris-HCl gel.

For Western blots of concentrated media 25μL of sample was mixed with 25 μL of 2X Laemmli sample buffer with 5% β-mercaptoethanol, boiled for 5 minutes, and then loaded onto a precast SDS 10% PAGE Tris-HCl gel. For western blot analysis of plasma samples 4μL of plasma was diluted in 21 μL of distilled water and then mixed with 25 μL of 2X Laemmli sample buffer with 5% β-mercaptoethanol, boiled for 5 minutes, and then loaded onto a precast SDS 10% PAGE Tris-HCl gel. Gels were run using a Biorad power supply set at 100 V for one hour.

Separated proteins were then transferred to a PVDF membrane at 75V for 2 hours on ice. Membranes were incubated overnight in a blocking solution (5% nonfat dry milk and 0.05% Tween 20 in PBS) at 4°C. Primary antibodies were then added [for anti-Aβ, 6E10 from Chemicon(Temecula, CA) was used at 1:1000 dilution, for anti-gelsolin GS-2C4 from Sigma was used at 1:1000 dilution] and incubated at room temperature for 2 hours. Membranes were washed three times in PBS with 0.05% Tween 20, and incubated with horseradish peroxidase (HRP)-conjugated anti-mouse antibody [Amersham (Piscataway, NJ) at 1:5000] in blocking solution for 1 hr at room temperature. Following three more washes, they were incubated with substrate [electrochemiluminescence (ECL), Amersham(Piscataway, NJ)] for 1 min and exposed (Kodak, Rochester, NY).

Detection of Message

A Qiagen (Valencia, CA) RNeasy mini-kit was used for RNA extractions. 30 mg of frozen liver or brain tissue was homogenized on ice using a Polytron homogenizer (Brinkmann Instruments, Westbury, NY) in 600 mL of buffer RLT containing β-mercaptoethanol. RNA was purified and washed using the columns and reagents

provided by the Qiagen kit as recommended by the manufacturer. RNA was eluted from the column to a final volume of 60μL in RNase-free water provided with the kit.

Primers were designed to yield ~900 b.p. product from mRNA transcribed from our vector pUFGL or ~1800b.p. product from unprocessed RNA or DNA contamination, by having the forward primer (GGC TCT GAC TGA CCG CGT TTA C, Tm = 68.7°C) anneal to sequence from Exon 1 in the vector, and reverse primer (CTG TTG GAA CCA CAC CAC TGG, Tm = 67.7°C) anneal to sequence from the coding region of gelsolin. Primers for β-Actin (ATG AGG TAG TCT GTC AGG T, Tm = 52.9°C, & ATG GAT GAC GAT ATC GCT G, Tm = 52.7°C) were used as a positive control.

A Qiagen one-step RT-PCR kit was used for the RT-PCR reaction. One microliter of RNA was used in each 25 μL reaction with final primer concentrations of 0.6 μM, and Q solution was included in the mixture. A MJ Research PTC-200 Peltier Thermal Cycler was used for the RT-PCR reaction. Reverse transcription was done for 30 minutes at 50°C, followed by PCR activation at 95°C for 15 minutes. Next came thirty cycles that consisted of: denaturation for one minute at 94°C, annealing for 30 seconds at 50°C, and extension for two minutes at 72°C. There was one final extension for 10 minutes at 72°C, and then samples were held at 4°C. Samples were then loaded onto a 2% agarose gel and run at 85 volts. Bands were then imaged by ethidium bromide staining.

Enzyme Linked Immunosorbent Assay

For enzyme linked immunosorbent assay (ELISA) Biosource colorimetric immunoassay kits were used for both β amyloid 1-40 and 1-42. Frozen hemi-brains were weighed. Eight times the mass of 5 M guanidine HCl, 50 mM Tris HCl, pH 8.0 was added to the brains then homogenized using a Polytron homogenizer (Brinkmann

Instruments). The homogenate was mixed at room temperature for four hours, and then aliquotted and stored at -80°C. The guanidine extracted homogenates were diluted 3000 times in BSAT-DPBS [Dulbecco's phosphate buffered saline with 5% bovine serum albumin, 0.03% Tween-20 and 1 mM 4-(2-Aminoethyl)benzenesulfonylfluoride (AEBSF)]. Mixtures were centrifuged at 16,000 G and 4°C for twenty minutes. The supernatants were diluted four fold in the standard diluent buffer provided with the Biosource kit, with AEBSF at 1mM. Samples were then incubated on a shaking platform at room temperature for two hours in the wells provided with the Biosource kit with an equal volume of primary antibody solution. Samples were then washed four times, and incubated in HRP solution four one half hour. Samples were washed four times again and then incubated for a half hour with HRP substrate, in a box to protect the samples from light. Stop solution was then added and absorbance at 450 nm was measured using a Dynex Technologies MRX microplate reader. Concentrations of Amyloid β (1-42) were determined from standards provided with the kit.

Histochemistry

Coronal sections (50 μm thick) were cut from the hemi-brains on a sliding microtome with a freezing stage. Four sections, six sections apart each, were mounted on slides for thioflavine S staining. Sections were allowed to dry on the slides for 15 minutes. The slides were then placed in deionized water for five minutes. They were then placed in filtered Mayer's Hematoxylin for five minutes. Next, the slides were rinsed under running tap water for five minutes, followed by a five minute rinse in deionized water. The slides were then placed in a 1% thioflavine S solution (in dH_2O, filtered, Sigma) for five minutes. The slides were differentiated in 70% ethanol for five

minutes, given short rinses in deionized water followed by PBS, and cover slipped with glycerol gelatin (Sigma).

Immunohistochemistry

Antigen detection on 50 μm thick coronal hemibrain sections was conducted on free-floating sections by incubating the sections overnight at 4°C in blocking solution (3% goat serum, 0.3% Triton X-100, 0.05% azide in PBS). Endogenous peroxidase activity was quenched by incubating the sections for 10 minutes in 0.5% H_2O_2 in PBS at room temperature prior to blocking.

Primary antibodies used were: 6E10 (1:1000, Signet, Dedham, MA), OX-42 (1:200, Serotec, Raleigh, NC), and anti-amyloid oligomer (1:250 Chemicon). Sections were incubated with primary antibodies diluted in blocking solution at 4°C for three days. Sections were then washed with PBS three times for 5 minutes each wash. Then the sections were incubated overnight at 4°C with secondary antibody (biotinylated anti-mouse IgG or biotinylated anti-rabbit IgG, 1:1000, Dako, CA) diluted in blocking solution. Sections were again washed three times in PBS. Next the sections were incubated for two hours at room temperature in PBS with ExtrAvidin peroxidase (HRP) conjugate (1:1000, Sigma). Washing was performed again, and then development of tissue labeled with HRP was performed with a solution of 0.67 mg/mL diaminobenzidine (DAB, Sigma) and 0.13 μL of 30% H_2O_2 per mL of 80 mM sodium acetate buffer containing 8 mM imidazole and 2% $NiSO_4$.

The sections were mounted on Superfrost plus microscopic slides (Fisher, NH), air dried and dehydrated by passing through water, followed by 70%, then 95%, and 2

changes of 100% ethanol. Then they were passed through two changes of xylene and coverslipped with Eukitt (Calibrated Instruments, NY).

For immunofluorescence Alexa Flour® 555 goat anti-rabbit IgG (H+L) (1:2000, Molecular Probes, OR), Alexa Flour® 488 goat anti-mouse IgG (H+L) (1:1000, Molecular Probes), AMCA conjugated F(ab')2 fragment goat anti-mouse IgG, F(ab')2 fragment specific (1:100, Jackson ImmunoResearch Laboratories, PA) secondary antibodies were used diluted in blocking solution following the primary antibody incubation. Nuclear counter staining was performed by incubating the sections in 4',6-diamidino-2-phenylindole (DAPI, 1 μg/mL, Sigma) for 15 minutes at room temperature. Fluorescent slides were cover slipped with glycerol gelatin mounting medium (Sigma).

Image Analysis

For percent amyloid burden measurements (both dense cored and diffuse) sections were analyzed in a blinded manner using the NIH Image J software. Regions of interest (ROI) were created encompassing both the hippocampus and neocortex of digital micrographs of each stained section. The ROI's area was measured in pixels^2. The number of plaques stained, plaque sizes (in pixels^2), and total stained areas in the hippocampus and cortex (in pixels^2) were determined by thresholding segmentation. Total stained areas were divided by total area, and then multiplied by 100% to give the percent amyloid burden.

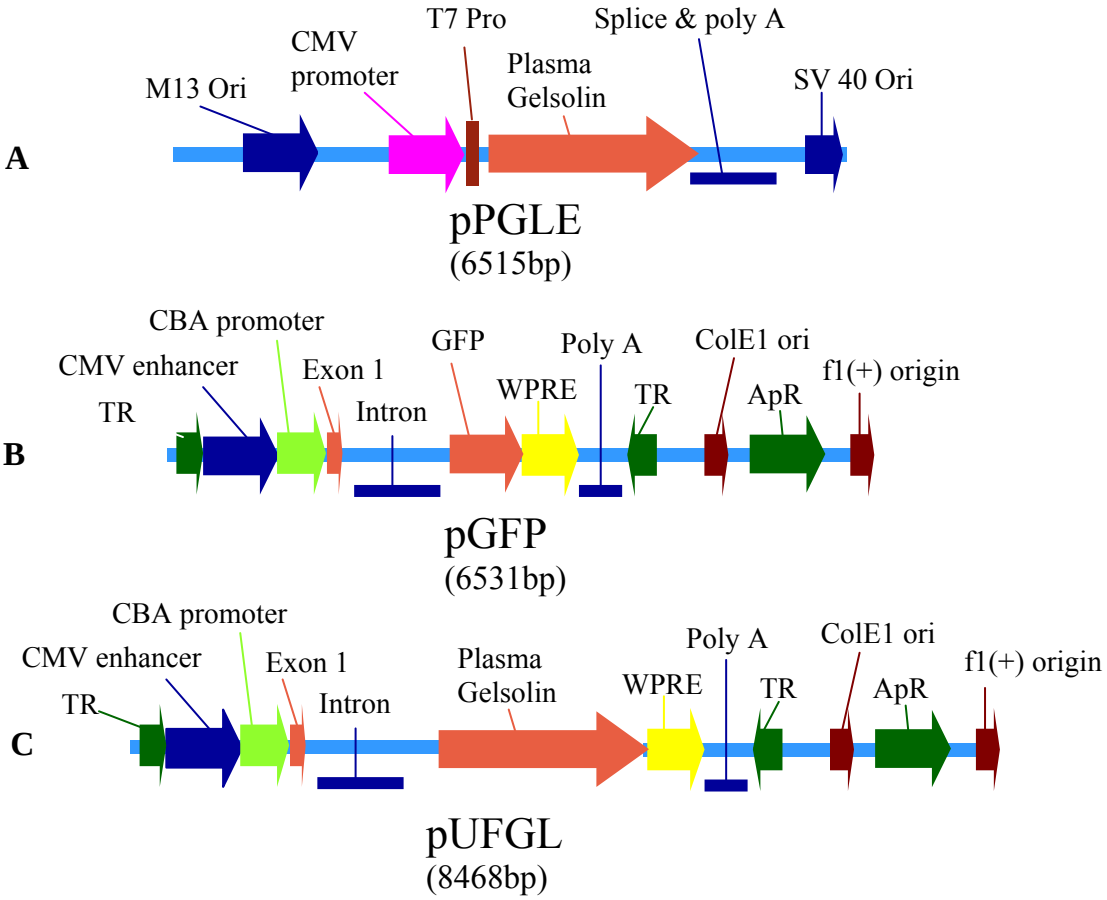

Figure 2-1 Vectors, **pPGLE** kindly provided by Dr. Hisakazu Fujita (A), The coding sequence for plasma gelsolin was excised and then inserted into the CBA promoter and WPRE containing backbone from the control plasmid **pGFP** (B) to make our test plasmid **pUFGL** (C).

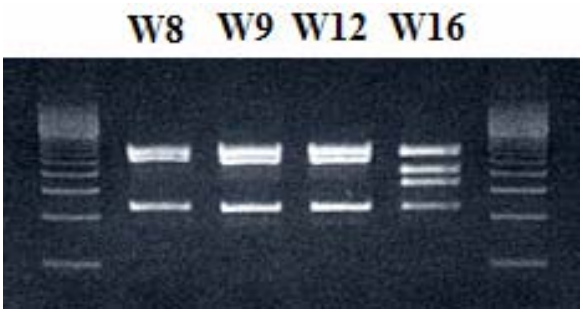

Figure 2-2 Restriction digest to confirm orientation of clones. **W8, W9,** and **W12** are all clones representing antisense orientation, having bands of 3173, 3013, 1137, & 1088 base pairs long. **W16** is a sense clone given the name **pUFGL** having bands of 3173, 2103, 1998, & 1137 base pairs long.

CHAPTER 3
THE INTERACTION OF PLAMA GELSOLIN AND AMYLOID β

Introduction

Studies by Chauhan et al. showed that human plasma gelsolin binds to amyloid β, prevents fibrillization, and disassembles preformed amyloid β fibrils, suggesting a possible role for gelsolin in the clearance of amyloid β (Chauhan et al., 1999; Ray et al., 2000). Chauhan used a solid phase binding assay to measure the dissociation rate constants (K_d) for two binding sites on human gelsolin, and found them to be 1.38 and 2.55 μM. Matsuoka et al. showed injections with bovine plasma gelsolin can prevent deposition of amyloid β in young $_{hu}$APP $_{K670N,M671L}$/ PS-1 $_{M146L}$ (2003). Our hypothesis for how gelsolin prevents amyloid β deposition was based on its ability to bind amyloid β in the periphery shifting its equilibrium from deposition in the CNS to clearance in the periphery. Chauhan's measurement of human plasma gelsolin's K_d indicates human plasma gelsolin does not have a very high affinity for amyloid β. On the other hand Matsouka's use of bovine plasma gelsolin in mice showed encouraging results. The different species forms of gelsolin used in Chauhan's studies and Matsuoka's study triggered us to ask the question of whether bovine gelsolin has a higher affinity for amyloid β than the human form of gelsolin. In this chapter we further characterize the interaction between amyloid β, and human and bovine plasma gelsolin.

Experimental Methods and Results

Measurement of ^{125}I Labeled Aβ (1-42) Binding to Recombinant Human Plasma Gelsolin

An attempt to measure the binding affinity of ^{125}I labeled Aβ 1-42 to human plasma gelsolin was carried out using standard binding protocol. Labeled Aβ at concentrations of 2.0, 5.0, and 10.0 μM were incubated with or without 2 μM recombinant human plasma gelsolin in PBS for one day. The following day the samples were run through Whatman GF/C filters that had been preincubated for 30 min with 0.5% polyethylenimine, followed by three washes with cold Krebs Ringer buffer (KRB; 118 mM NaCl, 5 mM KCl, 10 mM glucose, 1 mM $MgCl_2$, 2.5 mM $CaCl_2$, 20 mM HEPES; pH 7.5). The filters were counted for radioactivity, and it was found that the samples with plasma gelsolin had lower counts (Figure 3-1).

Because the molecular weight of plasma gelsolin is ~ twenty times that of amyloid β we were expecting that plasma gelsolin would bind the glass filters and in the presence of amyloid β more radioactivity would be detected and be representative of how much amyloid β is binding to plasma gelsolin. However it is apparent from our results that a significant amount of amyloid β itself binds to the glass filters and in the presence of plasma gelsolin less amyloid β binds to the filters. This experimental approach was subsequently abandoned; however theses results are discussed further later.

Measuring Binding of HiLyte Fluor 488 Labeled Amyloid β (1-42) to Bovine Plasma Gelsolin Using Fluorescence Anisotropy

Another approach at measuring the binding of amyloid β (1-42) to plasma gelsolin is to use the property of fluorescence anisotropy. The change of orientation of a population of fluorophores, from that of a specific orientation, isotropy, to a random

orientation, anisotropy can be measured by monitoring the rate at which fluorescence decays in a population of fluorophores when observed through polarized filters and is termed the fluorescence anisotropic decay. This change occurs via Brownian rotational diffusion. This property can be expressed using Equation 3-1 as the molecular diffusion coefficient (D_r) and is dependent on absolute temperature (T), the viscosity of the solution (η), and the molecular volume (V); R is the gas constant (Weber, 1953).

$$D_r = \frac{RT}{6\eta V} \qquad (3\text{-}1)$$

Protein-protein interactions can be measured by fluorescence anisotropy by observing changes in the rotational molecular motion due to the increase in molecular volume when two or more species associate with each other. The fluorescence anisotropy can be expressed as a function of molecular volume using Equation 3-2 (Perrin's equation) (Lakowicz, 2002). The value of anisotropy in the absence of rotational diffusion is defined as A_0; and τ is the fluorescence lifetime of the fluorophores. As the molecular volume increases (V), as when two or more proteins bind to one another, the numerator of Equation 3-2 will decrease, increasing the value of the anisotropy.

$$A = \frac{A_0}{1 + RT\tau/\eta V} \qquad (3\text{-}2)$$

Understanding the principles of fluorescent anisotropy, we decided use the change in anisotropy to measure the binding of fluorescently labeled amyloid β (1-42) (HiLyte Fluor 488 labeled amyloid β (1-42) from Anaspec). We first used the monoclonal antibody 6E10 (Chemicon) as a positive control for our binding study. The fluorescent amyloid β concentration was kept between 547-516 nM the fluorescence measurements through out the assay maintained values of 90-100 relative units (RU). The 6E10 was

added stepwise with a starting concentration of 0 nM and a final concentration of 369 nM. Results show a clear sigmoidal relationship (Figure 3-2) indicating a saturatable binding of amyloid β (1–42) to 6E10, validating our approach of using anisotropy to measure the binding of amyloid β (1-42).

The same experiment was then repeated with bovine plasma gelsolin (Sigma) substituted for the 6E10. The fluorescent amyloid β concentration was kept between 547-526 nM and the plasma gelsolin was added stepwise with a starting concentration of 0 nM and a final concentration of 423 nM. As the gelsolin was added, instead of rising, the anisotropy fell from about 0.060 to about 0.048, at the same time the fluorescence rose dramatically from 51 RU and then leveled off at about 210 RU(Figure 3-3). A hypothesis was formulated as a result of the data: the anisotropy decreased with an increasing concentration of gelsolin was representative of gelsolin disassembling oligomeric forms of amyloid β and the fluorescence increase is representative of more fluorophores interacting with the aqueous phase of the solution, rather than being tied up into hydrophobic areas of the oligomers.

Using a sample from the experiment an attempt was made to separate the free amyloid β from the amyloid β bound to gelsolin, to determine if a Scatchard analysis was possible, using ultra-filtration using Centricon filters with a 30 kD nmw cutoff. Prior to the spin the volume was brought up to 1 mL by adding distilled water, making the concentration of gelsolin 418 nM. To control for Aβ adsorbing to the filter material, the same amount of amyloid β was added to 1 mL of water (0.4 μg making the final amyloid β concentration 82 nM) with no gelsolin. The fluorescence of the samples was

measured prior to centrifugation and afterwards the retentate and the flow through were measured (Table 3-1).

After filtration the retentate was taken from the sample containing only amyloid β and gelsolin was added in a stepwise fashion, bringing the concentration of gelsolin from 0-1758 nM. As the gelsolin was added the fluorescence increased from about 1 to 9, while the anisotropy declined from 0.363 to 0.118 (Figure 3-4).

HiLyte Fluor 488 Labeled Aβ (1-42) Fibril Formation

The fibrillation of amyloid β is thought to be a major event in the pathology of AD. As Aβ is formed it is soluble and has an α-helical confirmation. Fibril formation involves a conformational change to a cross β-pleated sheet structure, oligomerization, followed by aggregation. *In vitro,* both synthetic β 1-40 and synthetic amyloid β (1-42) at 100 μM form fibrils spontaneously within 48 hours(Wegiel et al., 1996). In this experiment we monitor the fibril formation of HiLyte Fluor 488 labeled amyloid β (1-42) as a decrease in fluorescence. A 3.2 μM solution of HiLyte Fluor 488 labeled amyloid β (1-42) (chosen due to availability of labeled peptide) in distilled water was incubated at room temperature. A rapid decrease in fluorescence of the solution was seen along with the appearance of visible precipitates (Figure 3-5).

HiLyte Fluor 488 Labeled Aβ (1-42) Fibril Disassembly with Gelsolin

It has been well demonstrated that human plasma gelsolin has the ability to disassemble preformed Aβ fibrils (Ray et al., 2000). The administration of bovine plasma gelsolin has prevented amyloid deposition in transgenic mice (Matsuoka et al., 2003). Due to theses observations we decided to determine if there are species'

differences between bovine plasma gelsolin and human plasma gelsolin in the ability to disassemble preformed Aβ fibrils.

Under sterile conditions, dialysis tubes with a 10 kD molecular weight cutoff were used as a membrane in order to separate the monomer or dimer forms of labeled amyloid β 1-42 from more aggregated oligomeric forms. Inside the dialysis tubes100 µl of 1.6 µM fibrillized HiLyte Fluor 488-Labeled amyloid β (1-42), from the previous experiment, was added. On the outside of the dialysis tubes 200µl of distilled water was added.

The experimental groups included adding 0.5, 1.0, 2.0, 3.0, 5.0, and 8.0 µg of human plasma gelsolin or 1.0, 2.0, 3.0, 5.0, and 8.0 µg of bovine plasma gelsolin on the inside of the dialysis tubes, with the amyloid β. As a control, only amyloid β inside the dialysis tube and no plasma gelsolin, was used. To determine the maximum amount of diffused labeled amyloid β possible, a group with only labeled amyloid β (1–42) on the inside of the dialysis tube was used with 5M urea in distilled water on the outside of the tube for complete disassembly of amyloid β fibers to amyloid β monomers,

The dialysis reactions were set up in triplicate under sterile conditions and allowed to incubate at room temperature for 1 week. At this point the fluorescence was measured outside the dialysis tubes, revealing the amount of amyloid that was diffusible across the filters. This experiment was repeated twice using triplicate samples each time. The results are displayed in Figure 3-6.

Measuring Binding Amyloid β to Plasma Gelsolin Using Surface Plasmon Resonance

Surface plasmon resonance (SPR) is method that can be employed to observe interactions between macromolecules by measuring local changes in the refractive index of a solution containing a substrate flowing across a metal surface to which a ligand has been attached.

Amyloid β 1-40 and 1-42 were coupled to a gold chip modified with carboxymethylated dextran layer, Biacore CM5 chip, using amino-coupling chemistry. Reactive sucinimide esters were produced on the surface of the CM5 chip by using a 1:1 mixture of 1-ethyl-3-[3-(dimethylamino)propyl]carbodiimide hydrochloride (EDC) and N-hydroxysuccinimide (NHS). Then an acetate solution, pH 4, containing 50μg/ml amyloid β 1-40 (Figure 3-7) or 1-42 (Figure 3-8) was passed across the activated surface of the CM5 chip. Free amino groups in the amyloid are able to react with the activated surface of the CM5 chip becoming covalently bound. Following attachment of the amyloid β a high concentration of ethanolamine was passed over the surface to block any unreacted carboxymethyl groups on the surface of the chip. For amyloid β 1-40 an increase of 650 resonance units (RU) was observed, and for amyloid β 1-42 an increase of 3880 RU was observed.

Following coupling of amyloid β to the CM5 chip a solution containing 50 μg/ml of the antibody 6E10 was injected across both surfaces bound with amyloid β 1-40 and 1-42 for 240 seconds, and also a blank surface of the chip, as a positive control for binding. The resultant sensorgram is displayed in Figure 3-9. This shows that the 6E10 binds to both surfaces coupled with amyloid β 1-40 or 1-42 showing a response of 4000 RU and

5000 RU respectively, and no binding to the blank surface. The off-rate for 6E10 appears quite slow with no loss of response occurring after cessation of injection. The surface of the chip was then regenerated with a solution of 4M guanidine HCL removing any unconjugated protein or peptide. Following regeneration a solution containing 50 μg/ml of human plasma gelsolin was injected across the surfaces for 240 seconds. The resultant sensorgram (Figure 3-10) shows response increases of about 750 RU for the amyloid β 1-40, 1-42, and the blank channel. This indicates that the observed response results from bulk flow changes resulting from differences in buffer composition that cause changes in the refractive index. Specific binding of gelsolin to the coupled amyloid β is difficult to detect in this case.

Another CM5 chip was then coupled with human plasma gelsolin using the same amino coupling chemistry (EDC/NHS) as described for the amyloid β coupling. The coupling procedure resulted in a final increase of 1650 RU for the surface of the chip (Figure 3-11). Following the coupling procedure with human plasma gelsolin a solution containing 30 second injection of 50 mg/ml of GS-2C4 antibody (recognizes human plasma gelsolin) was injected across the surface of the human plasma gelsolin coupled CM5 chip (Figure 3-12). There was a bulk increase in response of 225 RU, with only a small amount of response increase due to GS-2C4 binding (~40 RU). After binding with GS-2C4 antibody the surface of the chip was regenerated with 4M guanidine HCL.

A solution of 50 mg/ml of amyloid β 1-40 was then injected across the surface of the chip. After a bulk increase in response of 8000 RU, the increase in response attributable to amyloid b binding was ~ 20 RU (Figure 3-13). In order to confirm the presence of bound amyloid β 1-40, 50 μg/ml of 6E10 was then injected across the

surface. 6E10 resulted in an increase in response of ~ 1200 RU. The surface was then regenerated with 4M guanidine HCL. A solution containing 50 μg/ml of amyloid β 1-42 was then injected across the surface of the chip again resulting in a bulk response of ~8000 RU, and a response increase attributable to binding of amyloid β 1-42 of ~ 30 RU (Figure 3-14). 6E10 was again used to confirm the presence of bound amyloid β 1-42, resulting in a response increase of ~1020 RU.

Conclusions

The preceding experiments were undertaken in an effort to determine if there were species differences in the binding affinities of bovine and human plasma gelsolin. Human gelsolin had been shown to bind to and disassemble amyloid fibrils (Chauhan et al., 1999) and bovine gelsolin had been shown to have an effect *In Vivo* in mice that deposit a human form of amyloid β (Matsuoka et al., 2003). We hypothesized that plasma gelsolin may be an effective peripherally expressed gene therapy for Alzheimer's disease based on a sink-hypothesis, that binding amyloid β peripherally will shift the equilibrium of amyloid β from depositing in the CNS to the periphery where it can be cleared. So we set out to measure binding affinities in order to determine if one species form would be advantageous over the other.

Although we were unable to measure specific on and off rates of the binding interaction between plasma gelsolin and amyloid β, our results demonstrate that the presence of plasma gelsolin alters the binding activity of amyloid β. The data from the ^{125}I labeled amyloid β (1-42) binding experiment (Figure 3-1) and centrifugal filtration experiment (Table 3-1) both demonstrate that in the presence of gelsolin amyloid β has an improved ability to pass through either 30 kD filter or glass filter paper. This is most

likely due to gelsolin's ability to disassemble amyloid β fibrils. Our data shows that HiLyte Fluor 488 Labeled amyloid β (1-42) forms insoluble fibril precipitates (Figure 3-5B). While this occurs the fluorescence activity decreases (Figure 3-5A), most likely due to fluorophores being sequestered in the non-aqueous phase of the precipitates.

As gelsolin is added to the amyloid β fibril suspension there is a fluorescence increase that is accompanied by a decrease in the anisotropy (Figures 3-3 and 3-4**)**. This decrease in anisotropy can be attributed to an increase in rotational diffusion caused by a decrease in size as amyloid β fibrils are disassembled. The fact that gelsolin can do this across a membrane (Figure 3-6) suggest that gelsolin may have enzyme-like activity shifting the equilibrium from amyloid β fibril formation to soluble α-helical amyloid β monomers.

Gelsolin does have similar enzyme-like activity with its interaction with actin. It disassembles actin filaments and can cap actin monomers in preparation for actin filament elongation. If gelsolin's interaction with amyloid β is enzyme-like, it may have a high affinity for oligomeric amyloid β that has a β-sheet secondary structure, and a low affinity for than soluble monomeric amyloid with α-helical secondary structure. This may lead to quick off rates, which can be difficult to measure. Supporting the idea that gelsolin may have fast off rates are measurements for the interaction (Kd) between amyloid β (1-40) and human plasma gelsolin reported by Chauhan et al. to be in the μM range (1999). To conclude our data suggest that gelsolin may in fact have an enzymatic-like property that makes it an even more attractive agent for the treatment of amyloid related disorders than just an amyloid β binding agent, because one molecule of gelsolin potentially have an effect on a large population of amyloid β molecules.

Table 3-1 Measurements of Fluorescence and Anisotropy before and after centrifugal filtration through 30,000 NMW cutoff filters. Anisotropy is reported as ± SEM, values > 0.400 were excluded.

	Fluorescence	Anisotropy
Aβ (82nM) prefilter	7.30	0.060 ± 0.002
Aβ flow through	0.94	0.400 ± na
Aβ retentate	1.00	0.363 ± 0.025
Aβ (82nM) + Gelsolin (418nM) prefilter	26.50	0.050 ± 0.001
Aβ + Gelsolin flow through	4.80	0.047 ± 0.002
Aβ + Gelsolin retentate	16.46	0.076 ± 0.001

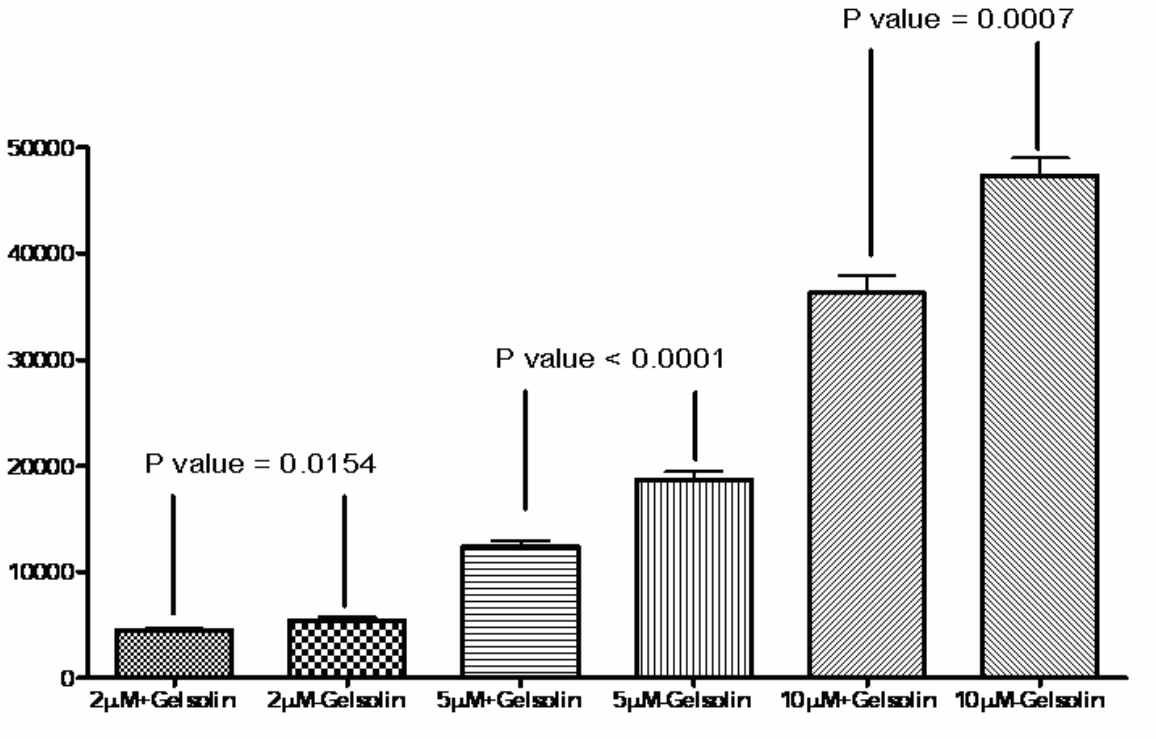

Figure 3-1 Binding of ^{125}I labeled Aβ 1-42 to Whatman GF/C filters. P values from t-tests performed show there is consistently lower binding of Aβ 1-42 (at 2, 5, and 10 μM) in the presence of 2μM recombinant gelsolin.

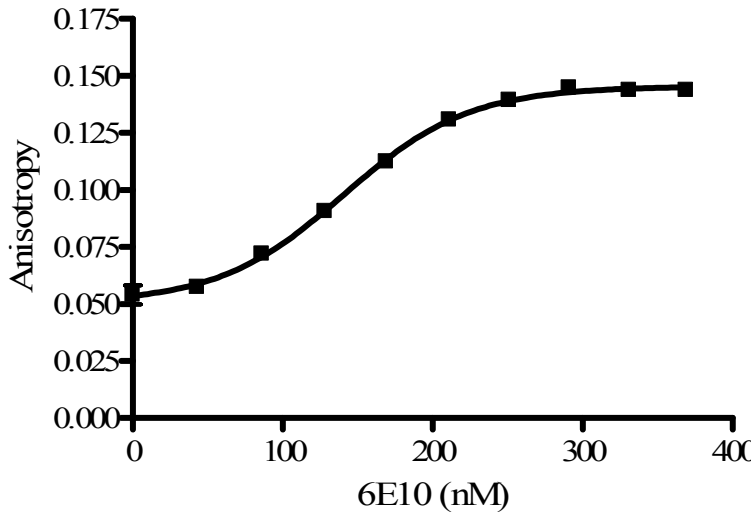

Figure 3-2 Binding of amyloid β (1-42) to the antibody 6E10. Blocks represent means ± SEM of triplicate measurements. Line represents best fit with GraphPad Prism software with a minimum anisotropy of 0.05035, a maximum of 0.1453, a log EC50 of 140.7 nM, and a hillslope of 0.01037. The fit had an r^2 of 0.9938, and an absolute sum of squares of 2.342×10^{-4}.

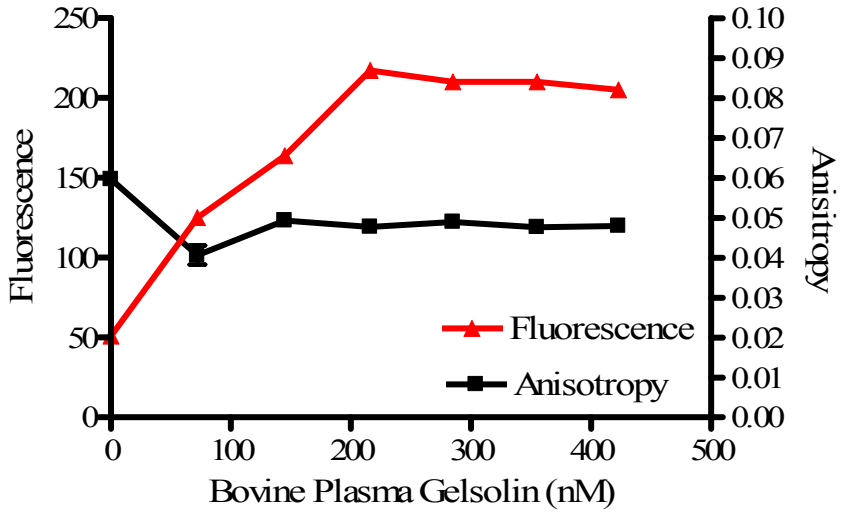

Figure 3-3 Binding of plasma gelsolin to fluorescently labeled amyloid β (1-42)

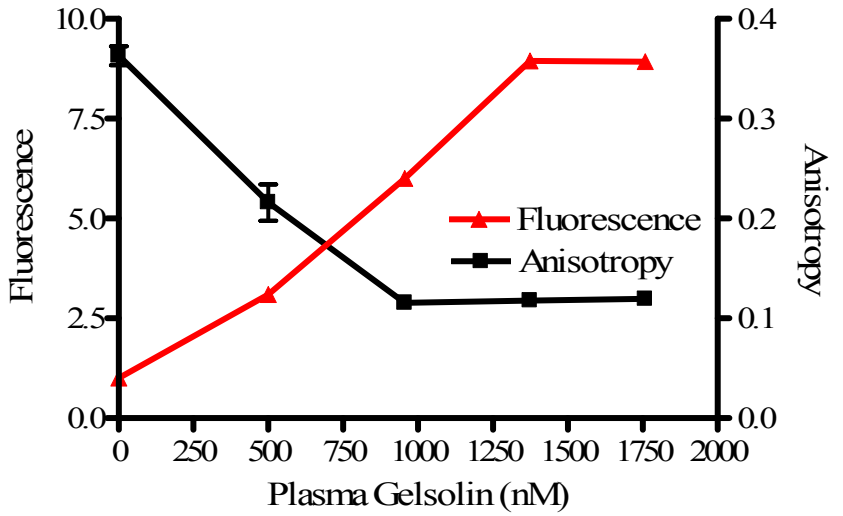

Figure 3-4 Amyloid β (1-42) binding to plasma gelsolin after concentration by centrifugal filtration

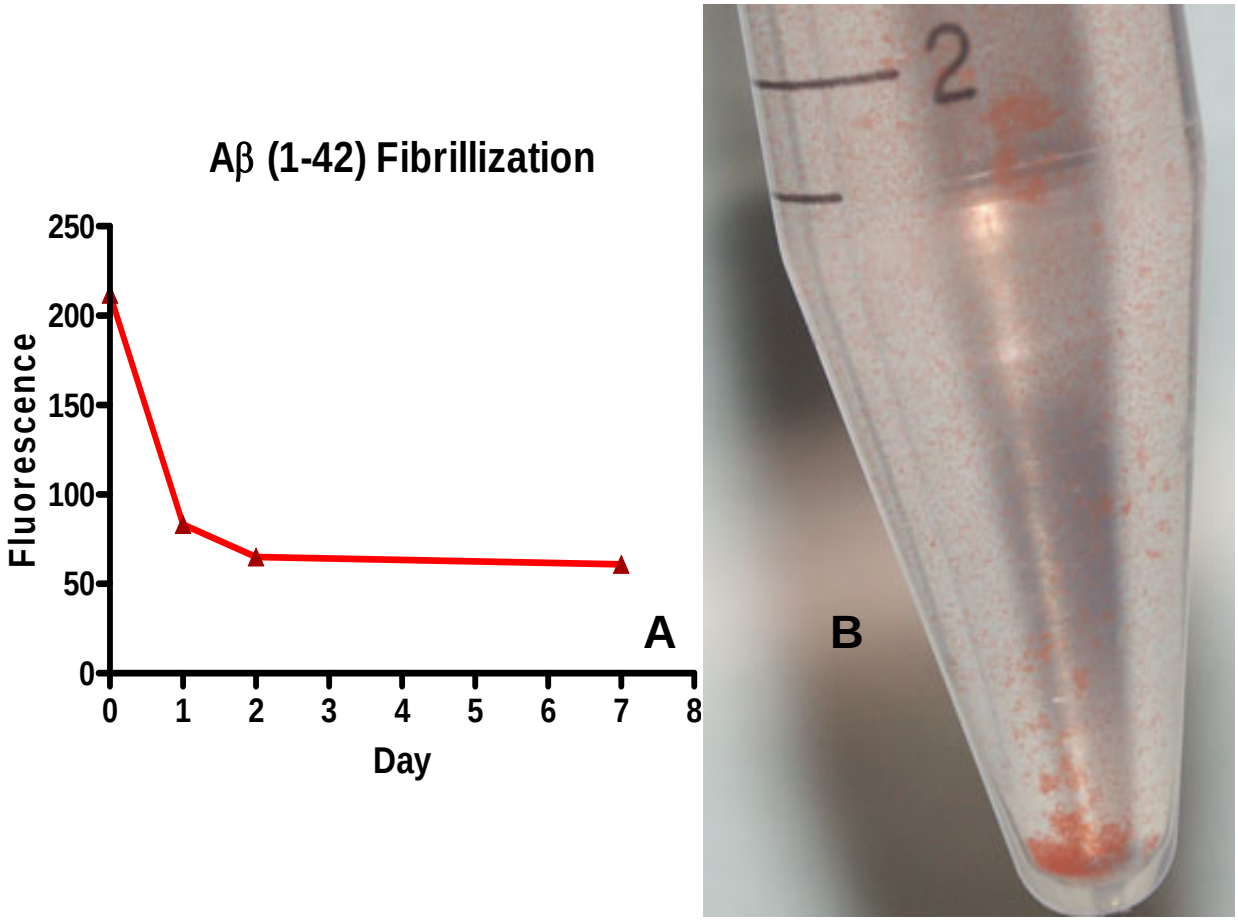

Figure 3-5 Fibril formation of HiLyte Fluor 488 Labeled Aβ (1-42) fluorescence rapidly decreases (A), while visible precipitates are formed (B). Photo taken at day 7.

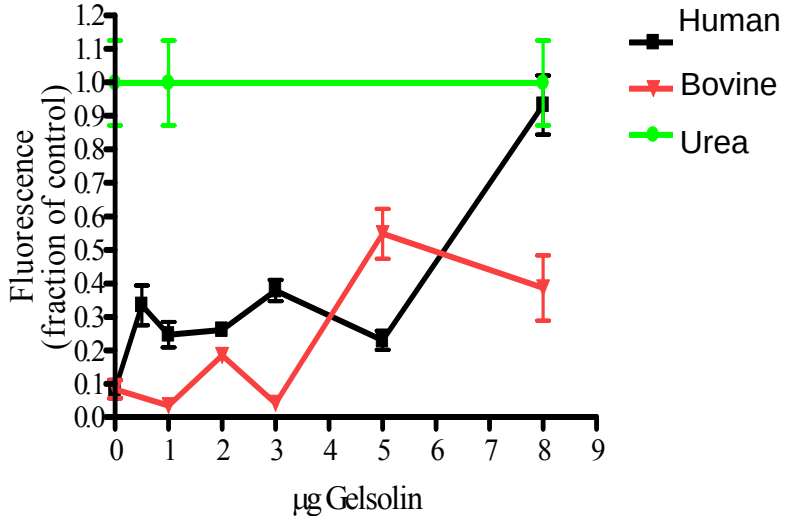

Figure 3-6 Dialysis experiment. Amyloid β fibril disassembly by gelsolin across a membrane**.** Human and bovine refer to the species of gelsolin added. Outside and inside refers to whether the gelsolin was added outside the dialysis tubing or inside the dialysis tubing. Fibrillized Aβ was added to the inside of dialysis tubes in all samples. Fluorescence was measured outside the dialysis tubes for all samples. The urea samples contain no gelsolin, just added as a line to represent the maximum fluorescence obtainable.

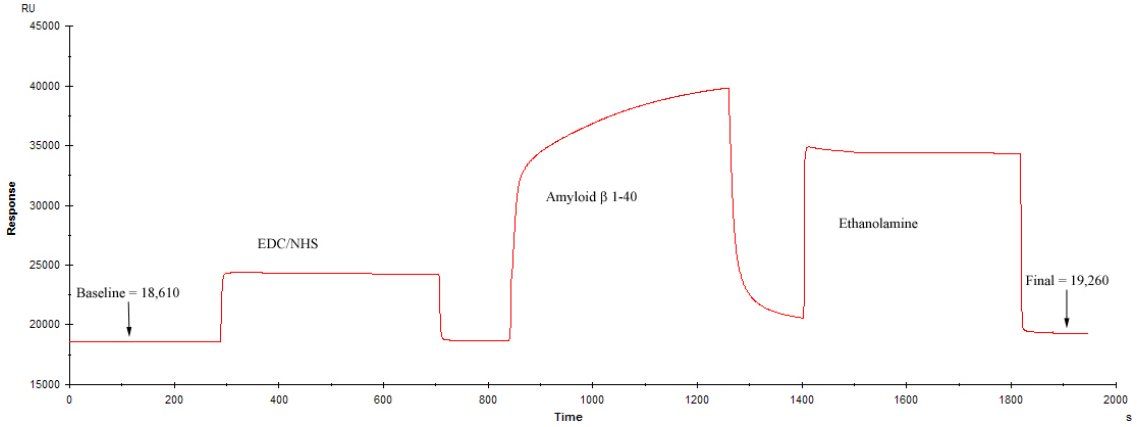

Figure 3-7 Amino-coupling of amyloid β 1-40 to CM5 chip. A rise in the response is observed at around 300 seconds when the injection of EDC/NHS reagents occurs, likewise a drop back to baseline is observed when the injections ends at 700 seconds this change in response is due to bulk differences in buffer composition. At 850 seconds the injection of amyloid β 1-40 begins corresponding with another increase in response. Upon completion of the amyloid injection the response does not fall completely back to base line indicative of covalently attached amyloid. Ethanolamine is then injected between 1400 to 1800 seconds to block any unreacted carboxymethyl groups. Another rise in response is observed attributed to bulk changes buffer composition again. At the completion of attachment there is a rise in baseline of about 650 RU.

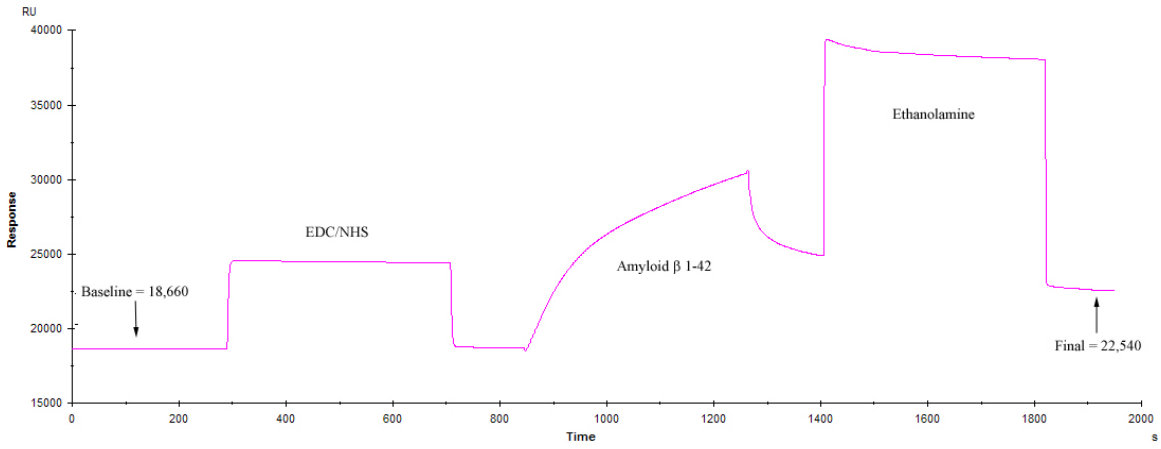

Figure 3-8 Amino-coupling of amyloid β 1-42 to CM5 chip. A rise in the response is observed at around 300 seconds when the injection of EDC/NHS reagents occurs, likewise a drop back to baseline is observed when the injections ends at 700 seconds this change in response is due to bulk differences in buffer composition. At 850 seconds the injection of amyloid β 1-42 begins corresponding with another increase in response. Upon completion of the amyloid injection the response does not fall completely back to base line indicative of covalently attached amyloid. Ethanolamine is then injected between 1400 to 1800 seconds to block any unreacted carboxymethyl groups. Another rise in response is observed attributed to bulk changes buffer composition again. At the completion of attachment there is a rise in baseline of about 3880 RU.

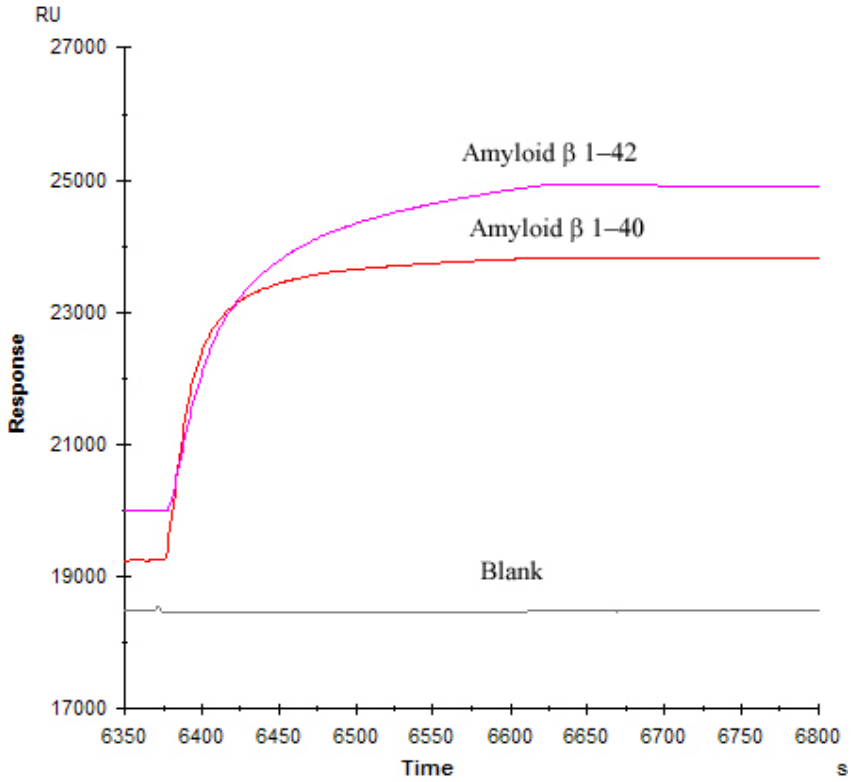

Figure 3-9 Antibody binding to amyloid coupled CM5 chip. Response increases of 4000 RU and 5000 RU, for amyloid β 1-40 and 1-42 respectively, are observed after a 240 second injection of a solution containing 50 μg/ml of the antibody 6E10. No response is observed when the solution is injected across the blank channel of the chip.

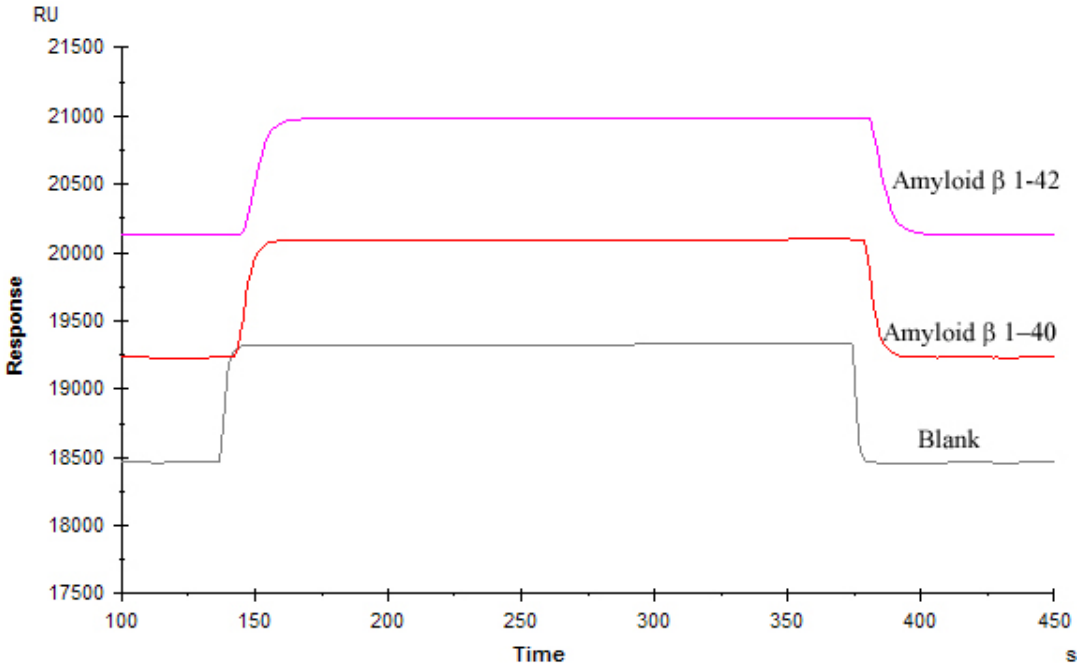

Figure 3-10 Human plasma gelsolin binding to amyloid coupled CM5 chip. Response increases of about 750 RU for the amyloid β 1-40, 1-42, and the blank channel are observed during a 240 second injection of 50 µg/mL solution of human plasma gelsolin. This indicates that the observed response results from bulk flow changes caused from differences in buffer composition resulting in changes in the refractive index.

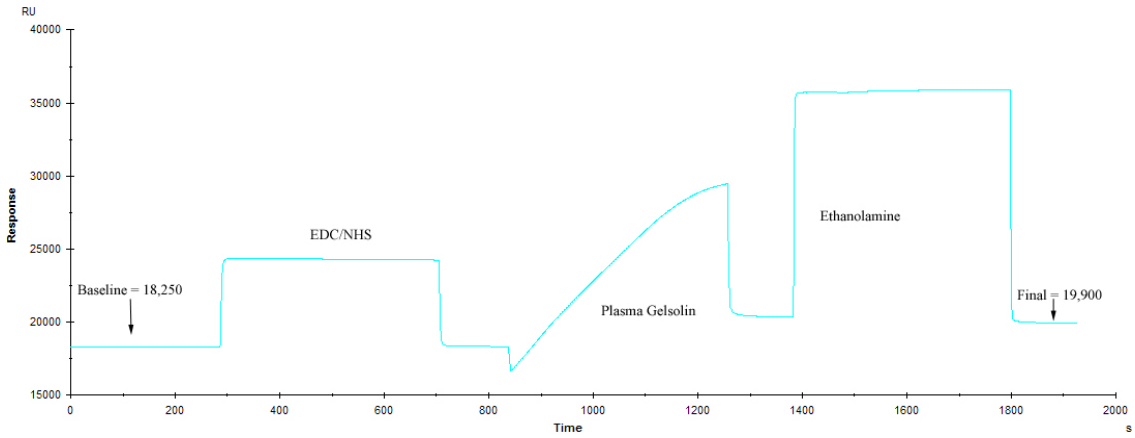

Figure 3-11 Amino-coupling of human plasma gelsolin to CM5 chip. A rise in the response is observed at around 300 seconds when the injection of EDC/NHS reagents occurs, likewise a drop back to baseline is observed when the injections ends at 700 seconds this change in response is due to bulk differences in buffer composition. At 850 seconds the injection of plasma gelsolin begins corresponding with another increase in response. Upon completion of the amyloid injection the response does not fall completely back to base line indicative of covalently attached amyloid. Ethanolamine is then injected between 1400 to 1800 seconds to block any unreacted carboxymethyl groups. Another rise in response is observed attributed to bulk changes buffer composition again. At the completion of attachment there is a rise in baseline of about 1650 RU

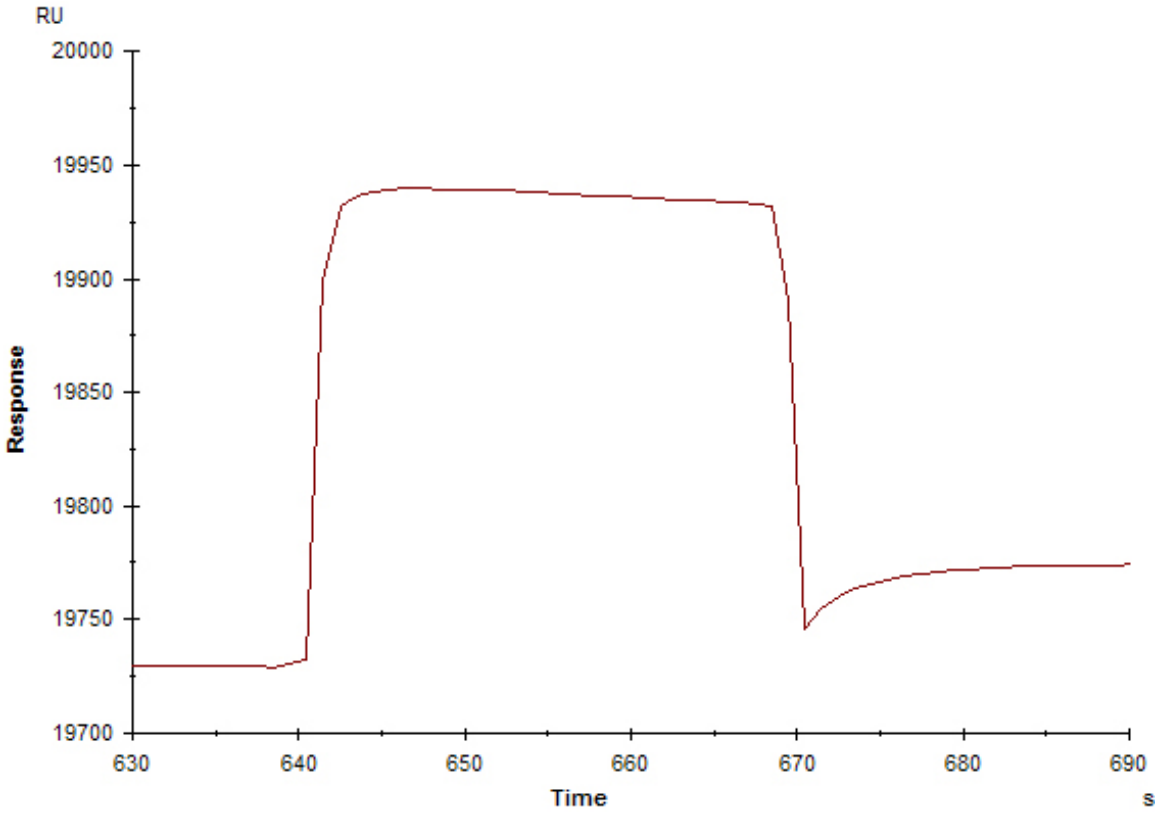

Figure 3-12 Binding of GS-2C4 to human plasma gelsolin coupled CM5 chip.

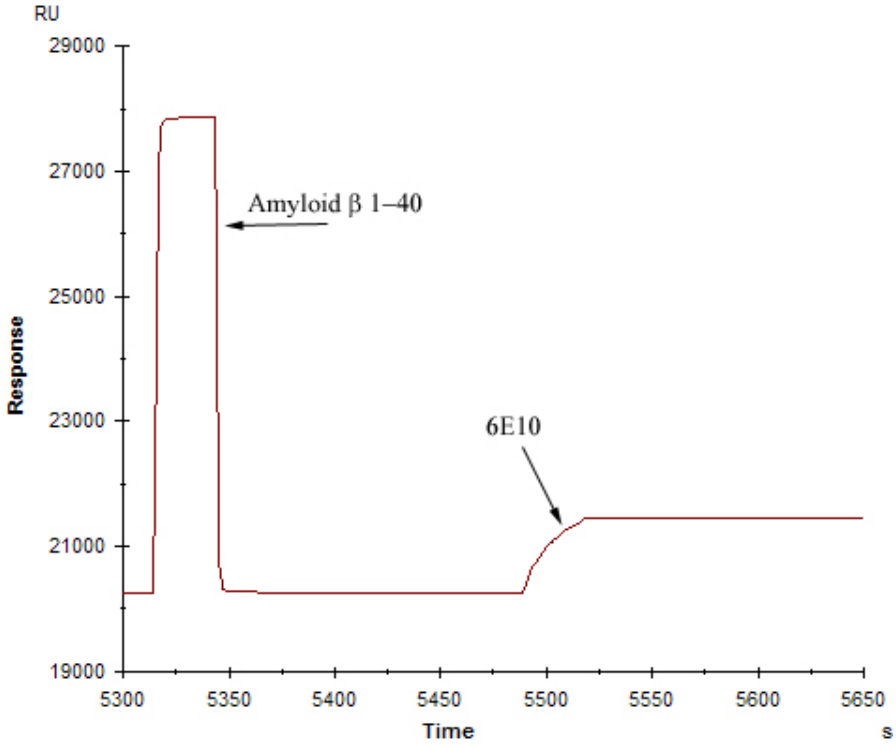

Figure 3-13 Binding of amyloid β 1-40 to human plasma gelsolin coupled CM5 chip.

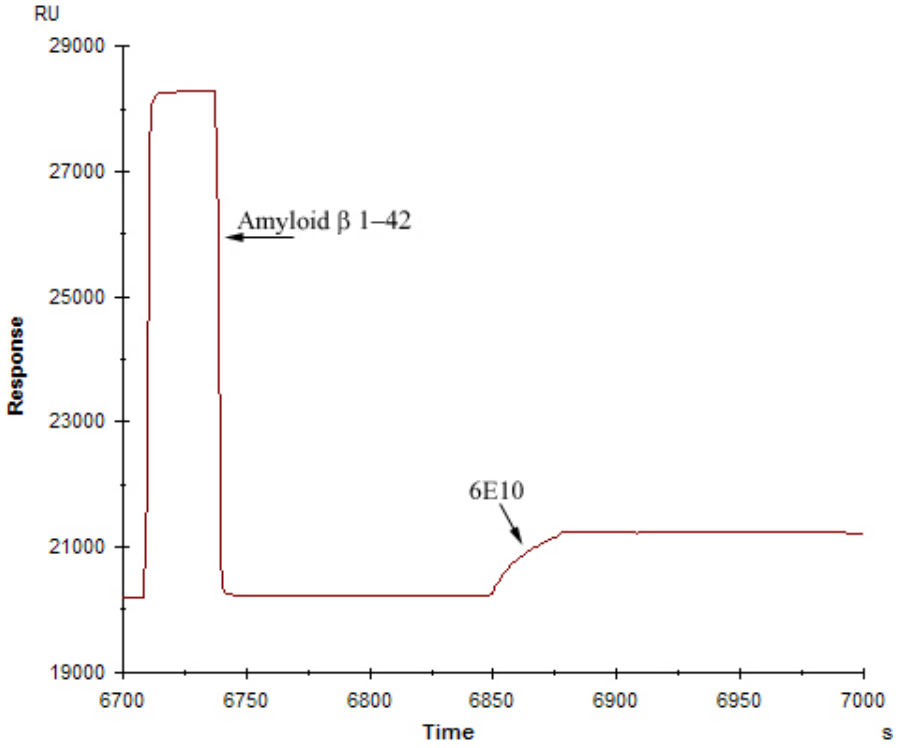

Figure 3-14 Binding of amyloid β 1-42 to human plasma gelsolin coupled CM5 chip.

CHAPTER 4
EXPRESSING PLASMA GELSOLIN AND EFFECTS IN TRANSGENIC MICE

Introduction

Gene therapy is a novel approach, which utilizes specific sequences of DNA to treat, cure, or ultimately prevent disease. There are major hurdles to overcome for it to be effective; the delivery of such large molecules to the target tissue offers a challenge because of vulnerability of degradation, due to endogenous nucleases. Another challenge is having the cells at the target tissue internalize the DNA and transport it into the nucleus. Finally, having the DNA transcribed and translated to produce a therapeutic protein that is transported to the proper site of action offers another hurdle to overcome.

Our target is the amyloid β that accumulates as senile plaques in the brains of those suffering from Alzheimer's disease. In the previous chapter we have demonstrated that human plasma gelsolin holds promise as an agent that can disassemble preformed amyloid fibrils. Because plasma gelsolin contains an amino-terminal 23 amino acid signal peptide which signals the cell producing it to secrete it towards the bloodstream, the site of action for our target can be in the bloodstream rather than the brain, simplifying delivery. Therefore expressing plasma gelsolin in any peripheral tissue should be enough to increase plasma gelsolin in the bloodstream.

The hydrodynamic gene delivery method offers an efficient technique for testing if peripheral expression of plasma gelsolin can have an effect on amyloid distribution and clearance in transgenic mice. The hydrodynamic gene delivery method was first developed by Dr. Dexi Liu (1999). This method involves injecting a large volume of a

DNA solution in a short period of time, via the tail vein of a mouse, and results in a high level of transgene expression in the liver. The mechanism for how this works seems to be that the initial rapid increase in blood volume causes an increase in venous pressure, which forces an enlargement of the liver fenestrae, and causes the formation of transient pores on the membranes of hepatocytes allowing the plasmid DNA to enter the cells (Zhang et al., 2004).

There is typically a high level of transgene expression following hydrodynamic gene delivery, followed by a quick drop off to a lower stable level of expression (Liu et al., 1999). Alino, Crespo, and Dasi showed that when the full length hAAT promoter was used to drive expression, after hydrodynamic gene delivery a stable therapeutic level of human alpha-1-antitrypsin (hAAT) is detected in the blood for up to 120 days, (2003).

The majority of plasmids delivered during hydrodynamic gene delivery studies are driven by human cytomegalovirus immediate-early promoter (CMV). Song et al showed that the CMV-chicken beta actin hybrid promoter (CBA) had well over 100 times the activity in the mouse liver than the CMV promoter (2001). We chose to incorporate the CBA promoter in our expression plasmid (Figure 2-1). We also included the woodchuck hepatitis virus post-transcriptional regulatory element (WPRE) in our plasmid. The WPRE functions to stabilize mRNA having the effect of increasing the half-life for mRNA and ultimately increasing the amount of gene product produced. We have previously described that incorporating the WPRE into vectors increased green fluorescent protein (GFP) and nerve growth factor (NGF) expression by more than ten fold in rats (Klein et al., 2002).

Results and Discussion

Conformation of Vector Product and Activity

To test that the vector we constructed pUFGL (Figure 2-1C) does in fact produce plasma gelsolin, we transfected 293 cells using the $Ca_3(PO_4)_2$ precipitation method, collected and concentrated media, and then performed a western blot to confirm size and identity of plasma gelsolin secreted into the media (Figure 4-1). There was a protein that ran at ~ 91kD that was immunoreactive with the anti-human gelsolin antibody, GS-2C4 (Sigma, St. Louis, MO), which was absent in the samples that had been transfected with the control plasmid pGFP.

To confirm that our gene product retained its amyloid binding activity we spiked some of the unconcentrated media with Aβ (1-42). Performed an immunoprecipitation using the GS-2C4 anti-human gelsolin antibody and then ran a Western blot with the precipitates. We found that Aβ 1-42 coprecipitated (Figure 4-2) with gelsolin in the pUFGL transfected, Aβ 1-42-spiked media and not with the pGFP transfected. Aβ 1-42-spiked media. Amyloid β 1-42 was not found in the precipitates when the media was not spiked with Aβ 1-42.

Hydrodynamic Gene Delivery in Mice

To determine the distribution and level of gene expression we should expect from using the hydrodynamic gene delivery technique mice were injected either pGFP or GWIZ luciferase expression plasmid via the hydrodynamic technique.

One day following injections with the GWIZ vector the two animals injected were imaged by the University of Florida's biomedical engineering department (Figure 4-3). Enough visible light was produced by the gene product luciferase that the liver was fully

illuminated for at least 30 minutes after an intraperitoneal injection of luciferin (luciferase's natural substrate).

Two and a half weeks after injecting mice with pGFP plasmid the animals were sacrificed and their livers were excised. Sections of the liver were made, 30μm thick, and the distribution of fluorescence was examined by fluorescence microscopy (Figure 4-4). At the two and a half week post-injection timepoint GFP fluorescence distribution was detected widely throughout the liver.

Transgenic mice expressing mutant presenilin-1M146L (mutant PS-1)(Duff et al., 1996) were injected via the hydrodynamic gene delivery method either pUFGL or pGFP. Plasma samples were taken at 24, 48 and 96 hours. These samples were used for a western blot (Figure 4-5). Plasma samples from pUFGL injected animals had clear bands corresponding to human plasma gelsolin that were not present in the pGFP injected animal.

Hematoxylin and Eosin Staining in Mice after Hydrodynamic Gene Transfer

Hematoxylin and eosin (H & E) staining is a routine stain that takes advantage of two separate dyes. Hematoxylin stains nuclear material a purplish color, while eosin stains membranes and connective tissue an orange-pinkish color. While unable to identify specific chemical markers for inflammation, H & E staining is useful at identifying, abnormal growth, division in the nucleus, or cellular death in tissues that may be related to disease or injury.

To determine if damage or inflammation affected the liver tissue 18 days after gene delivery via the hydrodynamic injections, livers were examined using H & E staining. Eighteen days after gene delivery of pGFP or pUFGL in double transgenic mice

expressing both human mutant APP695K670N,M671L (Tg2576)(Hsiao et al., 1996) and mutant presenilin-1M146L(Duff et al., 1996) ($_{hu}$APP/PS1$_{M146L}$ mice). H & E staining revealed no differences among livers from mice injected with pGFP, pUFGL or untreated mice (Figure 4-6).

Conclusions

In this chapter we demonstrate that our vector, pUFGL, does in fact produce human plasma gelsolin immunoreactivity, verified by western blot. We also show that our gene product maintains its Aβ binding activity verified by the co-immunoprecipitation of Aβ (1-42) with plasma gelsolin. We also show that by delivering vectors by the hydrodynamic technique we are able to obtain high levels of gene expression for at least two and a half weeks, and this expression does not result in damage or inflammation to the liver, detectable by H & E staining. Finally we are able to find detectable levels of human plasma gelsolin in the plasma of mice up to 96 hours after gene delivery by the hydrodynamic technique.

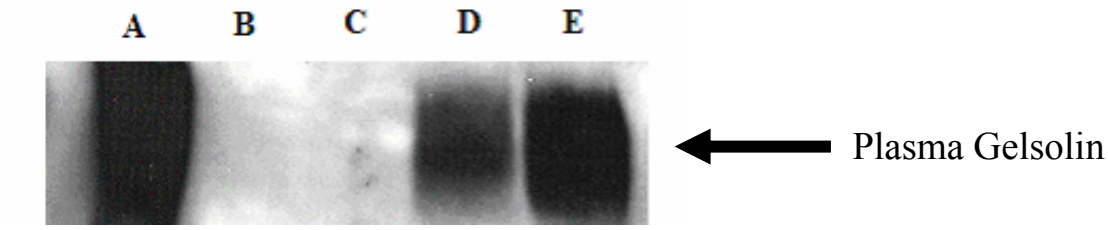

Figure 4-1 Immunoblot of transfected media. 293 cells at 50% confluency (lane B and D) or 80% confluency (lane C and lane E) were transfected using the $Ca_3(PO_4)_2$ precipitation method with either pGFP (lane B and lane C) or pUFGL (lane D and lane E). 48 hours after transfection, media was collected, concentrated, and then separated on a 7.5% PAGE and immunoblotted with a monoclonal anti-gelsolin antibody. Lane A contains 1 μg of human plasma gelsolin.

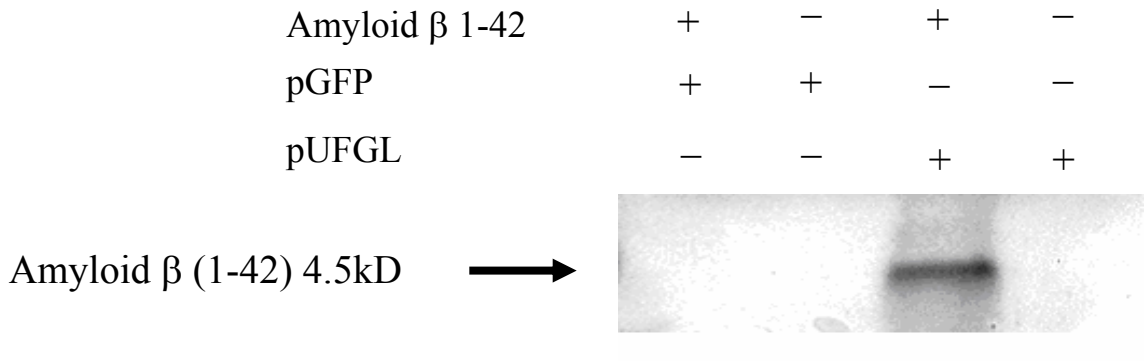

Figure 4-2 Immunoprecipitation**.** Amyloid β (1-42) co-immunoprecipitates with 293 expressed plasma gelsolin. The first lane contains immunoprecipitates from pGFP transfected media with Aβ 1-42. The second lane contains immunoprecipitates from pGFP transfected media with no Aβ. The third lane contains immunoprecipitates from pUFGL transfected media with Aβ 1-42. The fourth lane contains immunoprecipitates from pUFGL transfected media with no Aβ.

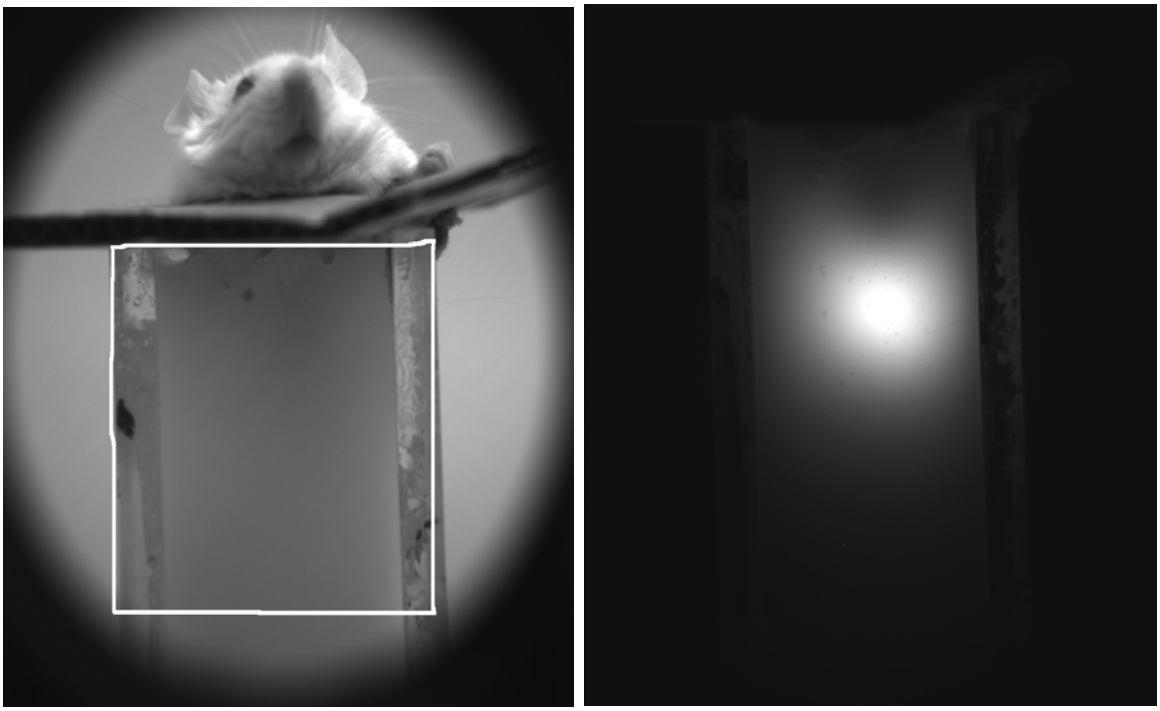

Figure 4-3 Bioluminescence resulting from hydrodynamic gene transfer. Imaging was done by the University of Florida's Department of Biomedical Engineering, as collaboration with fellow pharmaceutics graduate student Natalie Toussaint. The white rectangular shows the region imaged with a thermoelectrically cooled (-70°C), back illuminated CCD array (Roper Scientific Instrumentation, Trenton, NJ) coupled with an optical lens subsystem (Zoom 7000, Navitar, Rochester, NY).

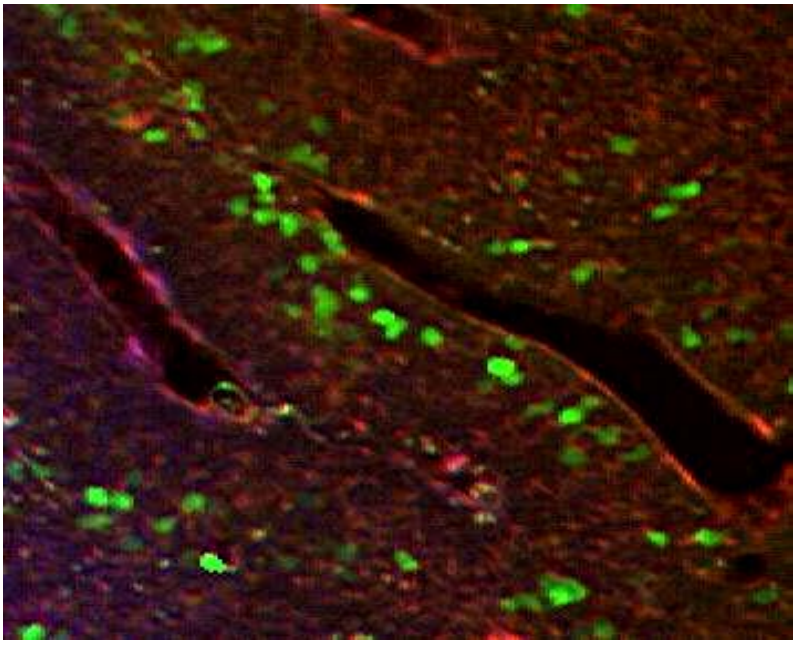

Figure 4-4 Green fluorescent protein. Expression observed in the liver of a mouse two and a half weeks after pGFP delivery via the hydrodynamic gene delivery technique. GFP expressing hepatocytes, green cells, are widely distributed throughout the liver. The red color resulted from background stained with Alexa Flour® 488 goat anti-mouse IgG (H+L). Dark empty spots are hepatic sinusoids.

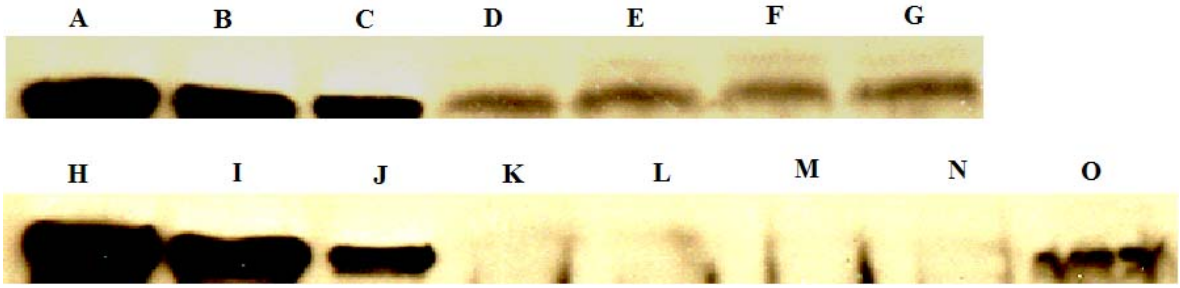

Figure 4-5 Western blot of plasma samples taken from PS-1 mice injected with pUFGL at 24 hours (Lanes D and E), 48 hours (Lane F), and 96 hours post injection (Lane G); or plasma taken from pGFP injected mice at 24 hours (Lane K), 48 hours (Lane L), and 96 hours post injection (Lane M). Lane N is plasma from a non injected mouse and Lane O is plasma from a non injected mouse spiked with 500ng of human plasma gelsolin. Lanes A and H contain 1500ng of human plasma gelsolin, Lanes B and I contain 1000ng of human plasma gelsolin, and Lanes C and J contain 500ng of human plasma gelsolin.

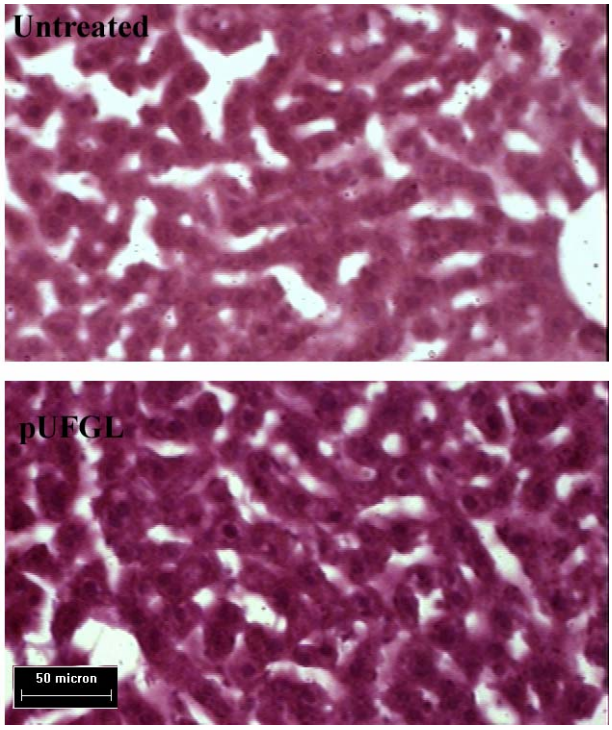

Figure 4-6 Hematoxylin and eosin staining of livers 18 days after hydrodynamic gene delivery. Upper image represents an untreated liver section, and lower image represents a pUFGL injected liver section. Scale bar represents 50 μm for both images.

CHAPTER 5
EFFECT OF GELSOLIN EXPRESSION ON AMYLOID DEPOSITION

Introduction

Since the discovery that senile deposits in Alzheimer's disease are composed mainly of the fibrillar amyloid β peptide (Glenner and Wong, 1984), researchers have discovered a number of mutations on either amyloid β's parent protein (APP), or proteins that process APP (PS1), that lead to inheritable forms of the disease. These discoveries have been quite useful in the development of transgenic mouse models of Alzheimer's disease pathology.

Achieving elevated levels of transgene expression was a critical step in the development of transgenic mice to model neurodegenerative diseases. It was recognized in the early 1990s that the gene encoding for mammalian prion protein (PrP) would make an effective expression package to produce foreign proteins in the central and peripheral nervous systems of mice (Hsiao et al., 1995; Scott et al., 1992; Telling et al., 1994). A 42 kb cosmid clone of the Syrian hamster PrP gene was made and it was noted that the entire open reading frame is contained in a single exon. (Basler et al., 1986). This exon can be excised and exchanged with the cDNA of a gene of interest, which can then be used for a pronuclear injection into mouse embryos to generate a transgenic line of mice expressing the protein of interest at high levels in the nervous system and heart of the mice (Borchelt et al., 1996).

In 1996, using this technique, Hsiao et al. developed a transgenic mouse model expressing the Swedish double mutant $APP_{K670N,M671L}$ (mutant APP, Tg2576) with a

C57/BI6 and SJL mouse background. These mice expressed the mutant APP about 5.5 times that of the endogenous murine APP. After 11 months of age amyloid plaque-like deposits are found throughout the cortex, hippocampus, presubiculum, subiculum, and the cerebellum (1996). These mice also demonstrated a deficit in memory-related behavior that correlated to the levels of insoluble amyloid β in the brain (Westerman et al., 2002).

Duff and coworkers developed mice that express a mutant form of presenilin-1_{M146L} (mutant PS-1). These mice had no detectable histopathology of Alzheimer's disease, however they did have elevated levels of amyloid β (1-42) (1996). When the mutant PS-1 mice are bred with the Tg2576 mice the resultant double transgenic progeny (APP/PS1) have an accelerated rate of amyloid β deposition, about 3-5 times that of the singly transgenic Tg2576, with a age of onset of between 3 and 6 months of age (Holcomb et al., 1998; Holcomb et al., 1999).

Using a similar strategy Borchelt et al. developed a transgenic model expressing a humanized version of murine APP695. This humanized gene was controlled by the mouse PrP promoter that drove expression of cDNA containing all murine sequence except for the amyloid β domain and the mutations (K595N, M596L) that are linked to the human Swedish form of familiar Alzheimer's disease. The level of transgene expression of these mice was about 2-3 times that over the endogenous APP expression in nontransgenic littermates (1996). These mice develop amyloid deposits around 18 months of age (1997).

Jankowsky and coworkers developed a line of mice that express the mouse human chimeric Swedish APP695 that Borchelt created along with a form of human presenilin-1

with exon nine deletion ($PS1_{\delta E9}$). They showed that these mice produce about 2.5 times the level of amyloid β (1-42) while amyloid β (1-40) levels remain constant (2004). The elevated levels of amyloid β (1-42) result in deposits occurring at a much accelerated rate as compared to the singly transgenic mice. These mice begin to develop deposits by the age of 6 months as compared to 18 months in the mice which don't co express $PS1_{\delta E9.}$

APP/PS1 mice have been useful as models to study treatments that target amyloid β. Morgan et al. successfully vaccinated APP/PS1 mice against Aβ, which had a dramatic effect on amyloid β deposition that protected against memory and learning deficits (2000). Deane et al. also saw dramatic effects on amyloid deposition by administering a soluble form of the receptor for advanced glyclation end products (RAGE)(2003). Matsuoka et al. treated young APP/PS1 mice with the amyloid binding agents GM1 and plasma gelsolin, and saw significant reductions in amyloid β levels in the brain (2003). This is why we believe APP/PS1 mice will make a good model to determine if peripheral expression of plasma gelsolin can effect amyloid β deposition.

Results

Mice Expressing Swedish Mutant Amyloid Precusor Protein (Mouse/Human Hybrid) and Exon 9 Deleted Mutant Presenilin-1

Message Detection

Nine month old double transgenic mice expressing both Swedish mutant mouse /human hybrid $APP695_{K594N,M595L}$ and mutant $presenilin\text{-}1_{\delta E9}$ ($_{mo/hu}APP$ /$PS1_{\delta E9}$) (Jankowsky et al., 2004) were injected with pUFGL, via the hydrodynamic gene delivery method. Two and one half weeks following injections the animals were sacrificed, along with three untreated littermates. RNA was purified from the liver and brain tissue, as described in the methods section. RT-PCR was performed using vector specific primers

designed to yield a 900 bp product from processed mRNA coded from pUFGL or an 1800bp fragment from unprocessed RNA or DNA.

All samples from animals that received an injection of pUFGL showed vector specific mRNA hybridization. In samples from animals that did not receive injections vector specific mRNA hybridization was not detected (Figure 5-1). All of the samples did show mRNA hybridization when reactions were run with primers specific for β-actin (data not shown) indicating that mRNA is present in all of the samples. Both samples from RNA purified from 293 cells transfected with pUFGL had positive bands. RNA samples purified from brain tissue did not show vector specific mRNA hybridization (data not shown) suggesting if there is vector gene expression in the brain it is below detectable quantities.

Total Brain Amyloid β (1-42) Concentrations

Enzyme linked immunosorbent assays (ELISA) were performed in order to measure the concentration of both soluble and insoluble fractions of amyloid β (1-42) in the hemi-brains from both pUFGL-injected and noninjected mice. All hemibrains were subjected to a guanidine extraction in order to obtain the total amount of Aβ contained within the brain tissue (Johnson-Wood et al., 1997; Masliah et al., 2001). The samples were run in duplicate on two separate occasions for a total of four samples assayed per animal. Untreated controls had a mean ± SEM amyloid β (1-42) concentration of 2,306 ± 202.6 picomoles per gram of brain tissue and the injected animals had 1,174 ± 334.7 picomoles per gram of brain tissue. A one- tailed t-test was performed and showed that these groups differ significantly with a P value = 0.0222 (Figure 5-2).

Plasma Amyloid β Concentrations

Blood was collected via the retro-orbital sinus using heparinized capillary tubes just prior to sacrifice. Samples were immediately centrifuged, followed by plasma collection which was flash frozen in liquid nitrogen. Samples were then thawed at a later time point and analyzed in duplicate by ELISA to determine amyloid β 1-40 and 1-42 concentrations. Untreated mice had a mean ± SEM plasma Aβ40 concentration of 315 ± 116.3 fmol/mL, while pUFGL-injected mice had 200.3 ± 86.5 fmol/mL (Figure 5-3A). Untreated mice had a mean ± SEM plasma Aβ42 concentration of 95.6 ± 23.2 fmol/mL, while pUFGL-injected mice had 150.9 ± 53.97 fmol/mL (Figure 5-3B). Trends but not significant changes in either Aβ42 or Aβ40 concentrations were observed; however a significant decrease in the ratio of Aβ40/ Aβ42 was observed in the pUFGL-injected mice (Figure 5-3C). Untreated mice had a mean Aβ40/ Aβ42 ratio of 3.0 ± 0.65, while pUFGL-injected mice had a mean Aβ40/ Aβ42 ratio of 1.24 ± 0.49 ($P = 0.045$).

Dense Cored Amyloid Deposits

Thioflavin S staining was used to examine the extent of dense cored amyloid Deposit pathology in injected and untreated mice (Sun et al., 2002). 50μm thick coronal sections were made. Four sections 0.3 mm apart were stained with thioflavin S and digital micrographs were made of epifluorescence images (Figure 5-6). Images were analyzed in a blinded manner using NIH Image J software. The area of the hippocampus and cortex, total stained area, area of each individual stained deposit, and the number of stained deposits was determined by thresholding segmentation. The amyloid burden was

determined by dividing the total area stained by the total area of the hippocampus and cortex.

Untreated animals had mean amyloid burden of 1.03 ± 0.13%, while pUFGL-injected animals had a mean amyloid burden of 0.39 ± 0.09%. A one-tailed t-test showed that these groups differ significantly with a P value = 0.0085 (Figure 5-4A). Untreated mice had a mean total stained area of 82,660 ± 10,150 pixels^2, while the pUFGL-injected mice had a mean total stained area of 33,740 ± 8429 pixels^2. These measurements were also determined to be significantly different by an unpaired one tailed t-test, P value = 0.0103 (Figure 5-4B). The average deposit size for untreated mice was determined to be 42.2 ± 4.8 pixels^2, while the average size for pUFGL was 34.2 ± 1.2 pixels^2. These were not found to be statistically different (P value = 0.0905, by an unpaired one-tailed t-test) (Figure 5-4C). Untreated mice had an average of 503 ± 84 deposits per section while pUFGL-injected mice averaged 244 ± 51 deposits per section. These were found to differ statistically (P value = 0.029, unpaired one-tailed t-test) (Figure 5-4D).

Diffuse Amyloid Deposits

Diffuse amyloid deposits were visualized by immunohistochemistry using the antibody 6E10, which recognizes the first 17 amino acids of human amyloid β. 50μm thick coronal sections were made. Three sections 0.3 mm apart were stained. Ditgital micrographs were made using light microscopy (Figure 5-7). Stained sections were analyzed in a blinded manner using NIH Image J software. The area of the hippocampus and cortex, total stained area, area of each individual stained deposit, and the number of stained deposits was determined by thresholding segmentation. The amyloid burden was

determined by dividing the total area stained by the total area of the hippocampus and cortex.

Untreated animals had a mean amyloid burden of 1.48 ± 0.19%, while pUFGL-injected animals had a mean amyloid burden of 1.12 ± 0.05%. An unpaired one-tailed t-test showed that these groups were not statistically different, however a strong trend towards significance was present (P value = 0.074) (Figure 5-5A). Untreated mice had a mean total stained area of 67,700 ± 10,590 pixels^2, while the pUFGL-injected mice had a mean total stained area of 48,570 ± 2643 pixels^2. These measurements were also not significantly different by an unpaired one tailed t-test, but again there was a trend (P value = 0.078) (Figure 5-5B).

The average deposit size for untreated mice was determined to be 16.9 ± 2.0 pixels^2, while the average size for pUFGL was 16.2 ± 1.2 pixels^2. These were not found to be statistically different (P value = 0.387, by an unpaired one-tailed t-test) (Figure 5-5C). Untreated mice had an average of 1326 ± 53 deposits per section while pUFGL-injected mice averaged 997 ± 123 deposits per section. These were found to differ statistically (P value = 0.035, by an unpaired one-tailed t-test) (Figure 5-5D).

Soluble Amyloid Oligomers

The distribution and relative quantities of soluble amyloid oligomers were examined by immunostaining with the A11 antibody. The A11 antibody recognizes an epitope that is common to soluble amyloid oligomers, but is not found in amyloidogenic monomers or mature amyloid fibrils(Kayed et al., 2003). Three sections from each animal were stained, all sections were incubated for equal amounts of time during the labeling procedure, and DAB reactions were carried out on slides containing one section from each animal, in order to minimize differences in reaction times or reagents. Digital

micrographs were prepared of the whole slides under the same light source using an Olympus BH-2 light microscope equipped with a motorized stage and focus control system (Prior Scientific). Image Pro plus version 4.0 software was used for tiling images together using a 4× nosepiece objective, a 1.25× internal magnification changer, and a 2.5× camera tube objective. To determine staining intensity and the relative amount of antigen present grey values were measured from negative images of each section using NIH Image J software.

Soluble amyloid oligomers appear to be widely distributed among both the pUFGL-injected mice and the untreated mice. Untreated mice had significantly lower negative grey values (127.6 ± 4.6) compared to pUFGL-injected mice (142 ± 1.8, P = 0.0220), which may indicate an increase in the concentration of soluble amyloid oligomers in pUFGL-injected mice (Figure 5-9). However, variability in fixation and section can also result in holes in the section that may correspond to less staining of the section. At high magnification the distribution of amyloid oligomer staining in both untreated mice and pUFGL-injected mice is mainly confined to the neuronal soma, axons, and dendritic processes (Figure 5-10). However in pUFGL-injected animals a number of glia cells and cells associated with the vasculature show an apparent immunoreactivity to the A11 antibody also (Figure 5-11).

Microglia

Microglia are a population of dendritic cells in the brain, thought to be of the same origin as monocytes and macrophages. Microglia can reside in the brain in a number of different states. Resting microglia (ramified) have long finely branched processes extending from all directions from the perinuclear cytoplasm (Giulian and Baker, 1986). Resting microglia, in response to a number of different insults to the nervous system,

begin to proliferate while still in non-phagocytic state, and are referred to as activated microglia. Activated microglia are recognizable by retracted cellular processes and mild hypertrophy resulting in a stout configuration. Further transformed microglia, with their processes even more retracted, are known as reactive or phagocytic microglia and are considered to be like "brain macrophages"(Streit et al., 1988). Reactive microglia have a round shape and can appear ruffled, due to short cytoplasmic projections, and are capable of releasing growth factors, cytokines, and free radicals.

The state of microglia cells in $_{mo/hu}$APP/PS1$_{\delta E9}$ brain sections was examined by immunostaining using the OX42 antibody. OX42 recognizes complement receptor 3 (CR3) which is expressed by microglia during all stages. Three sections per animal were examined and all sections were incubated for equal amounts of time during the labeling procedure. DAB reactions were carried out on slides containing one section from each animal, in order to minimize differences in reaction times. Calibrated digital micrographs were prepared of the whole slides with a constant light source, and relative grey values were measured from negative images for each section using NIH Image J software, to determine staining intensity.

Untreated mice had significantly lower relative negative grey values (130.7 ± 10.3) compared to pUFGL-injected mice (163.1 ± 11.1, P = 0.0496), indicating higher concentration of CR3 receptor in the pUFGL-injected animals (Figure 5-12 & 5-13). At higher magnification it is qualitatively clear that the increase in staining intensity observed in pUFGL treated mice is due to an increase in the number of activated and reactive microglia, distinguished by their retracted processes and condensed cell bodies (Figure 5-14).

Astrocytes

Astrocytes are a type of glial cell recognizable by numerous arms which give them a star shaped appearance. They play a number of roles in the brain including structuring the brain, providing neurons with nutrients, contributing to the blood brain barrier, altering cerebral blood flow, clearing neurotransmitters and regulating ion concentrations in the extracellular space (Pellerin, 2005; Sofroniew, 2005; Volterra and Meldolesi, 2005). Astrocytes become activated in response to disease or injury. One of the pathological features in Alzheimer's disease is the presence of activated astrocytes in and around amyloid deposits (McGeer and McGeer, 2003).

Astrocytic activation was examined in $_{mo/hu}$APP/PS1$_{\delta E9}$ brain sections by immunostaining for glial fibrillary acidic protein (GFAP). Two 50mm thick sections per animal were analyzed for total percent stained area of the hippocampus and cortex using NIH Image J software. Untreated mice had a mean ± SEM GFAP positive percent area of 11.06 ± 1.59 %, while pUFGL-injected mice had a mean ± SEM GFAP positive percent area of 14.15 ± 2.42 % (Figure 5-15). These values do not differ significantly however upon examination at a high magnification GFAP positive astrocytes in pUFGL-injected mice appear to have thicker and more numerous processes around areas corresponding to Congo Red positive amyloid deposits (Figure 5-16).

Mice Expressing Swedish Mutant Amyloid Precursor Protein (Human) and M146L Mutant Presenilin-1

Message Detection

Eight-month old double transgenic mice expressing both Swedish mutant human APP695 ($_{hu}$APP $_{K670N,M671L}$, Tg2576) (Hsiao et al., 1996) and mutant presenilin-1 $_{M146L}$ (PS–1$_{M146L}$) (Duff et al., 1996) were injected via the hydrodynamic gene delivery method

either pUFGL (5) or pGFP (3). Two and one half weeks following injections animals were sacrificed along with age-matched untreated mice (7). RNA was purified from the liver and brain tissue, as described in the methods section. RT-PCR was performed with primers designed to yield a 900 bp product from processed mRNA coded from our vector pUFGL. All samples from animals that received an injection of pUFGL had positive bands. Samples from animals that did not receive injections or received injections of pGFP did not have bands (Figure 5-16**,** not a complete data set, a representative gel). All samples did produce bands when reactions were run with primers for β-actin (data not shown) indicating that mRNA is present in the all of the samples. Sample from RNA purified from 293 cells transfected pUFGL had a positive band. None of samples purified from brain tissue had positive bands (data not shown) suggesting there is no vector gene expression in the brain.

Amyloid β (1-42) Quantification by ELISA

ELISA was used to quantify the concentration of guanidine extractable amyloid β (1–42) in brain homogenates of the $_{hu}$APP/PS1$_{M146L}$ mice. The resultant mean Aβ42 concentrations were 9179 ± 916 picomoles per gram of brain tissue for the untreated group, 10,928 ± 731 picomoles per gram of brain tissue for the pGFP-injected group, and 6740 ± 998 picomoles per gram of brain tissue for the pUFGL group. A one-way ANOVA showed that these means do not differ significantly, P = 0.069 (Figure 5-18A), however a trend toward significance was present.

In order to account for inter-litter variability, amyloid β 1–42 concentrations from pGFP and pUFGL-injected mice were divided by the amyloid β 1–42 concentrations obtained from their respective untreated littermates. These values were reported as the

fraction of amyloid β 1–42 of untreated littermates. The pGFP group had a mean fraction of 1.00 ± 0.06, while the pUFGL has a mean fraction of 0.797 ± 0.05. A unpaired one tailed t-test showed that these groups differ significantly with a P value = 0.022 (Figure 5-18B).

Plasma Amyloid β Concentrations

Blood was collected either via the retro-orbital sinus using heparinized capillary tubes or by intra cardiac puncture with an EDTA treated syringe just prior to sacrifice. Samples were immediately centrifuged; plasma collected and flash frozen in liquid nitrogen. Samples were then thawed and analyzed by ELISA in duplicate to determine amyloid β 1-40 and 1-42 concentrations. Untreated mice had a mean ± SEM plasma Aβ40 concentration of 1039 ± 244.6 fmol/mL, pGFP-injected mice had 971.7 ± 209 fmol/mL, and pUFGL-injected mice had 930 ± 252 fmol/mL (Figure 5-19A). Untreated mice had a mean ± SEM plasma Aβ42 concentration of 484.9 ± 143 fmol/mL, pGFP-injected mice had 453.5 ± 45.7 fmol/mL, and pUFGL-injected mice had 467 ± 43.3 fmol/mL (Figure 5-19B). There were no significant changes in either Aβ42 or Aβ40 concentration. There were also no significant changes measured in the Aβ40/ Aβ42 ratio; untreated mice had a mean concentration of 2.29 ± 0.22, pGFP-injected mice had a mean ratio of 2.1 ± 0.26, and pUFGL-injected mice had a mean ratio of 1.9 ± 0.46 (Figure 5-19C).

In light of the observation that amyloid β binds to heparins (Brunden et al., 1993; Leveugle et al., 1994), it is possible that the recovery of amyloid β may not have been the same between the two methods used for sample collection,. The data were examined in terms of collection method and differences were observed. Plasma collected retro-

orbitally had a mean amyloid β 1–40 concentration of 560.3 ± 164 fmol/mL and a mean amyloid β 1–42 concentration of 344.8 ± 59.1 fmol/mL; when collected via intra-cardiac puncture the mean amyloid β 1–40 concentration was 1185 ± 128 and a mean amyloid β 1–42 concentration of 531 ± 53.0 fmol/mL (P = 0.016 and 0.057 respectively, by unpaired two tailed t-test, Figure 5-19D &E). We concluded concentrations obtained from plasma samples collected with heparinized tubes are probably not accurate and cation should be used when analyzing such data. When two different collection methods are used, the samples are definitely not comparable.

Dense Cored Amyloid Deposits

Thioflavin S staining was used to examine the extent of dense cored amyloid deposit pathology in injected (pGFP and pUFGL) and untreated mice (Sun et al., 2002). 50μm thick coronal sections were made. Four sections 0.3 mm apart were stained with thioflavin S and digital micrographs were made (Figure 5-20) as described previously. Images were analyzed in a blinded manner using NIH Image J software. The area of the hippocampus and cortex, total stained area, area of each individual stained deposit, and the number of stained deposits was determined by thresholding segmentation. The amyloid burden was determined by dividing the total area stained by the total area of the hippocampus and cortex.

Untreated animals had a mean amyloid burden of 1.48 ± 0.16%, pGFP-injected animals had a mean amyloid burden of 1.59 ± 0.10%, pUFGL-injected animals had a mean amyloid burden of 1.09 ± 0.14%. A one-way ANOVA was performed, and the medians did not differ significantly with a P-value = 0.069 (Figure 5-21A).

Untreated mice had a mean total stained area of 115,329 ± 18,081 pixels^2, pGFP-injected mice had a mean total stained area of 140,952 ± 14,898 pixels^2, while the pUFGL-injected mice had a mean total stained area of 87,503 ± 14,622 pixels^2. These measurements were also found not to differ statistically (Figure 5-21B, P-value = 0.127, by one-way ANOVA).

There was also no difference observed in deposit size among the groups. Untreated mice had a mean deposit size of 75.62 ± 15.4 pixels^2, pGFP-injected mice had a mean Deposit size of 56.03 ± 5.6 pixels^2, and pUFGL-injected mice had a mean deposit size of 44.78 ± 6.3 pixels^2 (Figure 5-21C, P-value = 0.247, by one-way ANOVA).

Deposit numbers per section did not change between the treatment groups either. Untreated mice had an average of 458 ± 107 deposits per section; pGFP-injected mice had an average of 632 ± 53 deposits per section, and pUFGL-injected mice had an average of 513 ± 32 deposits per section.

Again to account for inter-litter variability, dense-cored amyloid burdens, average deposit sizes, and average number of deposits per section from pGFP and pUFGL-injected mice were divided by the values obtained from their respective untreated littermates. No differences were detected in dense-cored amyloid burden fractions or dense-cored deposit size fractions; pGFP-injected mice had a mean dense-cored amyloid burden fraction of 0.88 ± 0.05 and a mean dense-cored deposit size fraction of 1.06 ± 0.11, pUFGL-injected mice had a mean dense- cored amyloid burden fraction of 0.89 ± 0.16 and a mean dense-cored deposit size fraction of 0.86 ± 0.28 (Figure 5-22A &B).

An increase in the average number of deposits per section fraction was detected in pUFGL-injected mice; pGFP-injected mice had a mean average dense-cored deposit number per section fraction of 1.06 ± 0.11, pUFGL-injected mice had an average dense-cored deposit number per section fraction of 1.38 ± 0.13; P = 0.048 by unpaired two-tailed t-test (Figure 5-22C).

Diffuse Amyloid Deposits

Diffuse amyloid deposits were visualized by immunohistochemistry using the antibody 6E10, which recognizes the first 17 amino acids of human amyloid β. 50μm thick coronal sections were made. Three sections 0.3 mm apart were stained. Digital micrographs were made (Figure 5-23). Stained sections were analyzed in a blinded manner using NIH Image J software. The area of the hippocampus and cortex, total stained area, area of each individual stained deposit, and the number of stained deposits was determined. The amyloid burden was determined by dividing the total area stained by the total area of the hippocampus and cortex.

Untreated animals had mean amyloid burden of 4.25 ± 0.46%, pGFP-injected mice had a mean diffuse amyloid burden of 4.04 ± 0.46%, and pUFGL-injected animals had a mean amyloid burden of 2.83 ± 0.05%. A one-way ANOVA showed that these groups were not statistically different, (P value = 0.099) (Figure 5-24A).

The average diffuse deposit size for untreated mice was determined to be 20.3 ± 1.5 $pixels^2$, the average size for pGFP-injected mice was 26.3 ± 2.3 $pixels^2$, and the average size for pUFGL-injected mice was 20.9 ± 3.2 $pixels^2$. These were not found to be statistically different (P value = 0.271, by one-way ANOVA) (Figure 5-24B).

The average number of diffuse deposits per section for untreated mice was determined to be 3990 ± 481 deposits/section, 3437 ± 513 deposits/section for pGFP-injected mice, and 3623 ± 729 deposits/section for pUFGL-injected mice. These were not found to be statistically different (P value = 0.812, by one-way ANOVA) (Figure 5-23C).

Again to account for inter-litter variability, diffuse amyloid burdens, average diffuse deposit sizes, and average number of diffuse deposits per section from pGFP and pUFGL-injected mice were divided by the values obtained from their respective untreated littermates (Figure 5-25). No differences were detected; however a trend toward a reduction in diffuse amyloid burden fractions was seen, pGFP-injected mice had a mean diffuse amyloid burden fraction of 1.00 ± 0.13, and pUFGL-injected mice had a mean diffuse amyloid burden fraction of 0.72 ± 0.10 (P = 0.071, by unpaired one-tailed t-test). No trends were detected in diffuse deposit size fraction (pGFP-injected mice had a mean diffuse deposit size fraction of 1.06 ± 0.06, pUFGL-injected mice had a mean diffuse deposit size fraction of 1.06 ± 0.16) and average number of diffuse deposits per section fraction (pGFP-injected mice had an average number of diffuse deposits per section fraction of 1.13 ± 0.18, pUFGL-injected mice had had an average number of diffuse deposits per section fraction of 0.86 ± 0.11).

Microglia, Soluble Oligomers, and Astrocytes

The state of microglia and the degree of soluble amyloid oligomers in $_{hu}$APP/PS1$_{M146L}$ brain sections were examined by immunohistochemistry (Figure 5-26). Three sections per animal were examined and all sections were incubated for equal amounts of time during the labeling procedure. DAB reactions were carried out on slides containing one section from each animal, in order to minimize differences in reaction

times. Digital micrographs were prepared of the whole slides with a constant light source, and relative grey values were measured from negative images for each section using NIH Image J software, to determine staining intensity. Astrocytic activation was examined in $_{hu}$APP/PS1$_{M146L}$ brain sections by immunostaining for glial fibrillary acidic protein (GFAP). Two 50mm thick sections per animal were analyzed for total percent stained area of the hippocampus and cortex using NIH Image J software.

For microglia, untreated mice had a mean ± SEM relative negative grey value of 27.5 ± 4.8, pGFP-injected mice had 29.2 ± 3.3, and pUFGL-injected mice had 46.53 ± 16.0. These values did not differ significantly (Figure 5-27A). When examined in terms of fractions of their untreated littermates, pGFP-injected mice had a mean microglia stain fraction of 1.32 ± 0.05 and pUFGL-injected mice had a mean microglia stain fraction of 1.84 ± 0.60. These values values were also found not to be different statistically (Figure 5-27B)

When soluble amyloid oligomers were examined, untreated mice had a mean ± SEM relative negative grey value of 85.8 ± 4.7, pGFP-injected mice had 85.9 ± 1.3, and pUFGL-injected mice had 87.1 ± 8.5. These values did not differ significantly (Figure 5-27C). When examined in terms of fractions of their untreated littermates, pGFP-injected mice had a mean soluble amyloid oligomer stain fraction of 0.93 ± 0.01 and pUFGL-injected mice had a mean soluble amyloid oligomer stain fraction of 1.23 ± 0.18. These values were also found not to be different statistically although a trend was evident (Figure 5-27D).

Staining for astrocytes using GFAP revealed that untreated mice had 16.7 ± 1.4 % of their hippocampus and neocortex stained, pGFP-injected mice had 13.5 ± 0.89 %

stained, and pUFGL had 18.2 ± 2.8 % stained. These values did not differ statistically (Figure 27E). When examined in terms of fractions of their untreated littermates, pGFP-injected mice had a mean soluble amyloid oligomer stain fraction of 0.96 ± 0.04 and pUFGL-injected mice had a mean soluble amyloid oligomer stain fraction of 1.26 ± 0.16. These values were also found not to be different statistically although a trend was evident (Figure 5-27F).

Regression Analysis

Linear regression was employed to examine possible correlations in pUFGL-injected mice between the fractions of untreated littermate soluble amyloid oligomer staining, microglia staining, or % GFAP staining, and fraction of untreated littermate Aβ42 concentrations, diffuse or dense-core amyloid burdens. Slopes trended toward being significantly different from zero when soluble oligomers fractions (P = 0.079) and microglia fractions (P = 0.062) were compared with values for fractions of Aβ 42 concentrations (Figure 5-28A & B). Slopes also showed a strong trend toward being significantly different from zero when percent GFAP stain fractions were compared with dense-cored amyloid burden fractions (P = 0.084, Figure 28C).

When percent GFAP stain fractions were compared with fractions of diffuse amyloid burden, slope was significantly different than zero (P = 0.008, Figure 28D), indicating a strong correlation for an increase in the % area stained for GFAP compared to untreated littermates, with a decrease in diffuse amyloid burden compared to untreated littermates in pUFGL-injected mice.

Conclusion

In this study we examined the effects of peripheral plasma gelsolin expression on two different transgenic mouse models of Alzheimer's disease. Two different models were used due to a failure in our $_{hu}$APP/PS1$_{M146L}$ breeding colony. However, testing two separate models has advantages. Two separate models lets us examine gelsolin expression in animals that produce amyloid β at different rates ($_{hu}$APP/PS1$_{M146L}$, faster; $_{mo/hu}$APP/PS1$_{\delta E9}$, slower). They also allow us to test effects of gelsolin expression with mice of different genetic backgrounds. Studying the differences in response to gelsolin expression between the different models can allow us to make inferences on the efficiency and mechanisms of actions of plasma gelsolin expression may have.

These results demonstrate that both $_{mo/hu}$APP/PS1$_{\delta E9}$ mice and $_{hu}$APP/PS1$_{M146L}$ mice express pUFGL in the liver for at least two and a half weeks after gene delivery by hydrodynamic injection (Figures 5-1 & 5-16).

In $_{mo/hu}$APP/PS1$_{\delta E9}$ mice expression of pUFGL results in a significant decrease in the concentration of total brain amyloid β 1-42 (Figure 5-2). The decreased concentration of Aβ42 is accompanied with a significant decrease in the dense-cored amyloid deposit load when compared to untreated mice in $_{mo/hu}$APP/PS1$_{\delta E9}$ (Figure 5-4A). This reduction of dense-cored deposit load is accompanied with a significant decrease in number of both dense-cored and diffuse deposits observed per section of pUFGL-injected mice (Figure 5-4D & 5-5D). Surprisingly, the reduction in dense cored deposit load in $_{mo/hu}$APP/PS1$_{\delta E9}$ mice was not accompanied by significant reductions in diffuse deposit loads (Figure 5-5A). However, a strong trend toward significance was observed.

Our data indicates that the reduction of amyloid deposits may be associated with an increase in the apparent staining of soluble amyloid oligomers (Figure 5-9) and an increase in the apparent activation state of microglia in the brains of $_{mo/hu}$APP/PS1$_{\delta E9}$ mice injected with pUFGL (Figures 5-12 & 13). Although statistically significant, our results may just be an artifact due to variability of tissue treatment post-mortem. However an increase in oligomer staining could explain an increase in the activation state of microglia. It has been reported that soluble amyloid and not insoluble amyloid activates microglia (Floden and Combs, 2006; Lindberg et al., 2005). Activated microglia have been implicated of playing a role in antibody-mediated clearance of dense-cored amyloid deposits in transgenic mice (Wilcock et al., 2003). So it would not be surprising if microglia play a similar role in gelsolin mediated clearance of dense-cored deposits in our study also. This would be a significant observation because before clearance by peripheral amyloid binding agents was thought to be a result of mass action diffusion according to the peripheral sink hypothesis.

A decrease in total brain amyloid β 1-42 was also observed in $_{hu}$APP/PS1$_{M146L}$ mice when inter-litter variability is accounted for (Figure 5-18). In contrast to the $_{mo/hu}$APP/PS1$_{\delta E9}$ group, $_{hu}$APP/PS1$_{M146L}$ did not show a significant reduction in dense cored amyloid deposit load (Figure 5-21), nor was there a difference in diffuse amyloid deposit load (Figure 5-24). However both displayed a strong trend towards a reduction in amyloid load. No differences were evident among deposit size, but strangely when inter-litter variability was accounted for there was a significant increase in the dense-cored deposit number fraction (Figure 5-21).

There were also no differences observed in amyloid oligomers staining intensity, microglia staining intensity, or % GFAP stained. Only slight trends were seen when inter-litter variability were accounted for (Figure 5-26). The possibility of variability existing to the response of peripheral human plasma gene expression motivated us to examine if there were any correlations amyloid pathology and glial response. When correlations were examined (Figure 5-27) strong trends were evident indicating a possible correlation between decreasing total amyloid β 1–42 concentrations and increasing soluble oligomer or microglia staining intensity compared to untreated littermates.

A strong correlation was observed between decreases in diffuse amyloid deposits and increases in the % area stained for GFAP indicating astrocytes may be involved in the clearance of diffuse amyloid pathology. Evidence supporting this hypothesis has been observed in post-mortem studies of non-demented humans (Funato et al., 1998; Yamaguchi et al., 1998). Adult mouse astrocytes have also been observed to migrate toward and degrade immobilized amyloid β *in vitro* and *in situ* in transgenic mouse brain sections (Wyss-Coray et al., 2003).

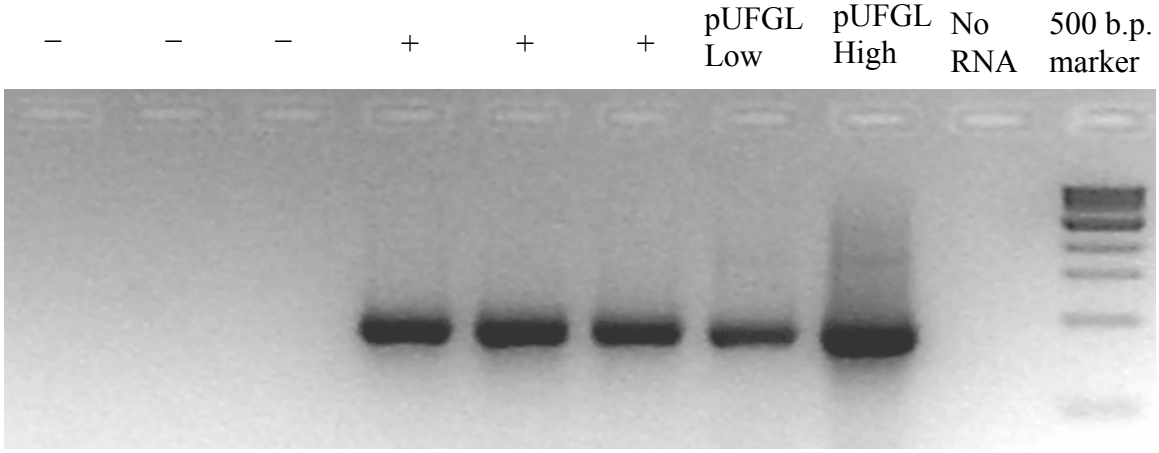

Figure 5-1 Detecting message in $_{mo/hu}$APP/PS1$_{\delta E9}$ mice. RT-PCR using primers specific for mRNA coded from pUFGL vector, using RNA purified from liver tissue from non-injected mice (– symbols), liver tissue from pUFGL-injected mice (+ symbols), and 293 cells transfected with pUFGL at a high or low confluency. No RNA refers to a product from a reaction mixture with no RNA. 500bp marker from Biorad was used.

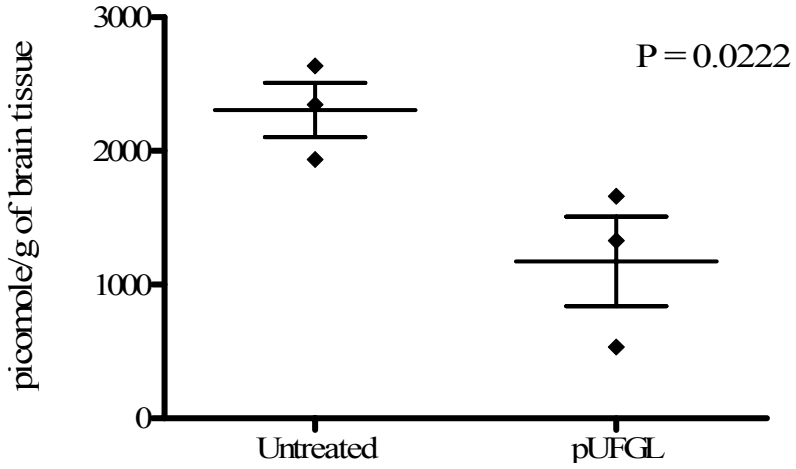

Figure 5-2 Amyloid β (1-42) concentrations in $_{mo/hu}$APP/PS1$_{\delta E9}$ brains. Diamonds represent individual animal means, bars represent means and standard error. Untreated mice had a mean ± SEM Aβ (1-42) concentration of 2,306 ± 202.6 pmoles/g of brain tissue, and the injected animals had 1,174 ± 334.7 pmoles/g of brain tissue. A one-tailed t-test was performed and showed that these groups differ significantly with a P value = 0.0222.

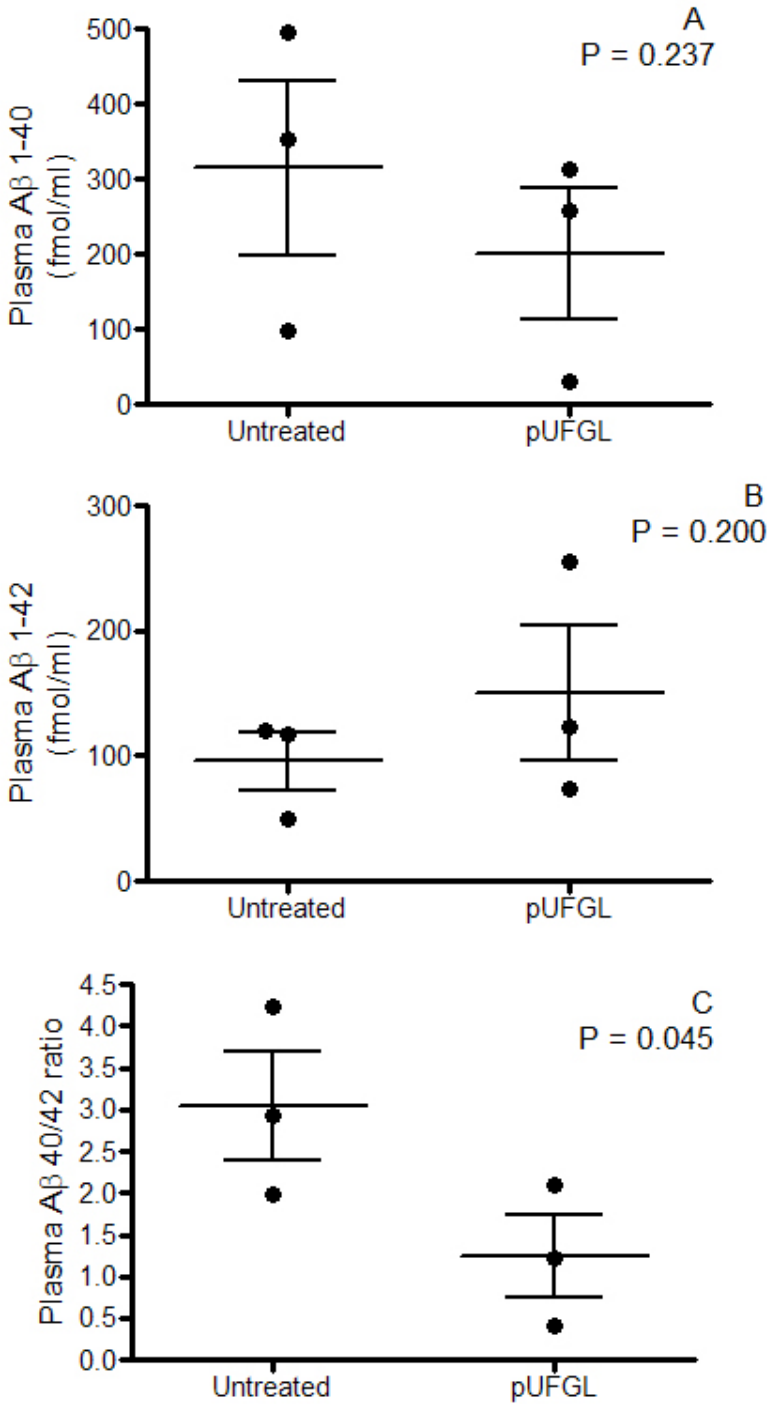

Figure 5-3 Plasma concentrations of amyloid in $_{mo/hu}$APP/PS1$_{\delta E9}$ mice. A) Amyloid β 1–40 Concentrations in fmol/mL. B) Amyloid β 1–42 Concentrations in fmol/mL. C) The Ratio of Amyloid β 1–40 to Amyloid β 1–42 Concentrations.

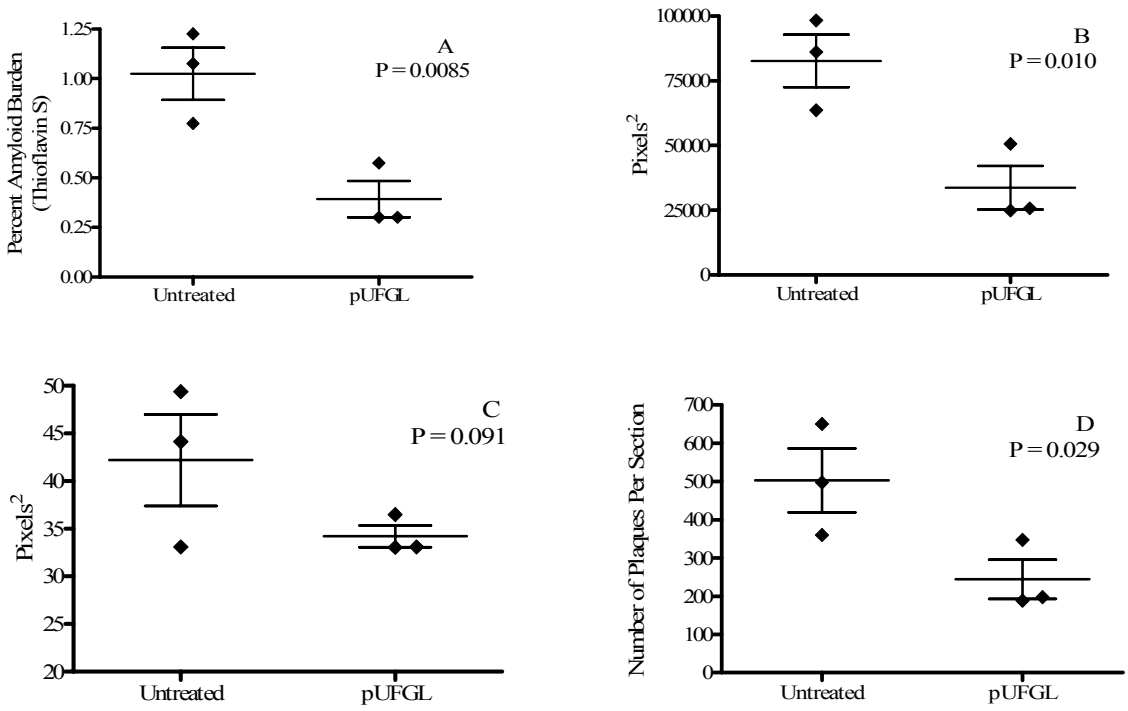

Figure 5-4 Analysis of dense-core amyloid deposits in $_{mo/hu}$APP/PS1$_{\delta E9}$ mice. Deposits visualized by thioflavin S staining of brain sections. A) Percent Amyloid Burden. B) Total Stained Area. C) Average Deposit Size. D) Average Number of Deposits per section. Diamonds represent individual animal means. Bars represent group means ± the standard error.

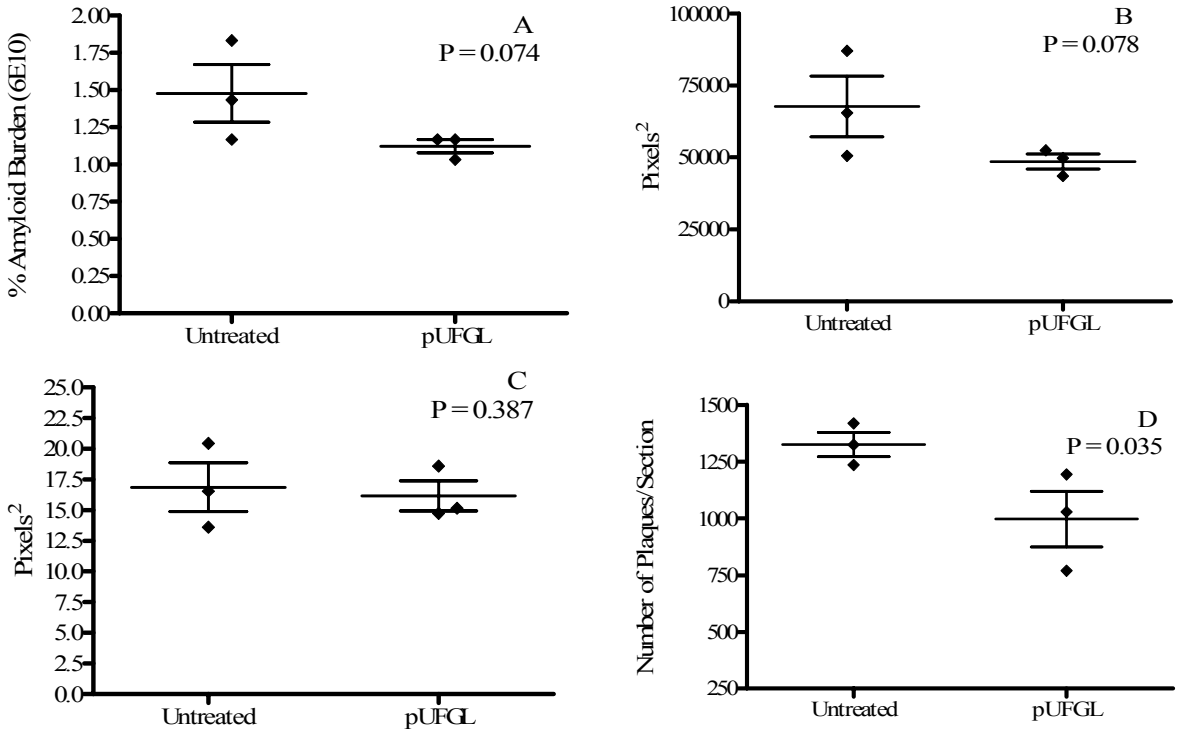

Figure 5-5 Analysis of diffuse amyloid deposits in $_{mo/hu}$APP/PS1$_{\delta E9}$ mice. Deposits visualized by immunostaining of brain sections. A) Percent Amyloid Burden. B) Total Stained Area. C) Average Deposit Size. D) Average Number of Deposits per section. Diamonds represent individual animal means. Bars represent group means ± the standard error.

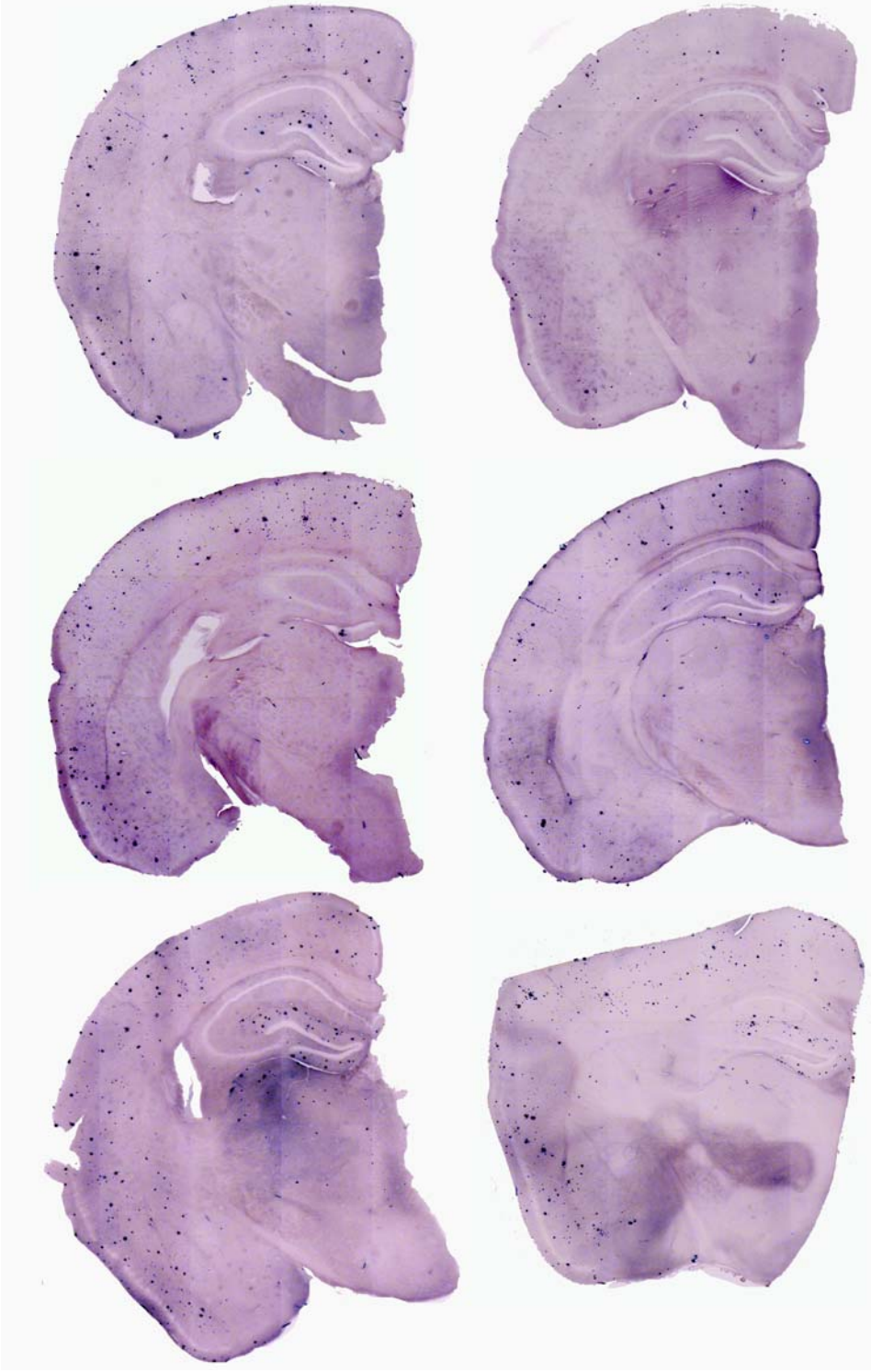

Figure 5-6 Dense-core amyloid deposits in $_{mo/hu}$APP/PS1$_{\delta E9}$ mice. Deposits visualized by thioflavin S Staining. Negative digital micrographs of untreated mice (left) and pUFGL-injected mice (right). One section is included from each animal.

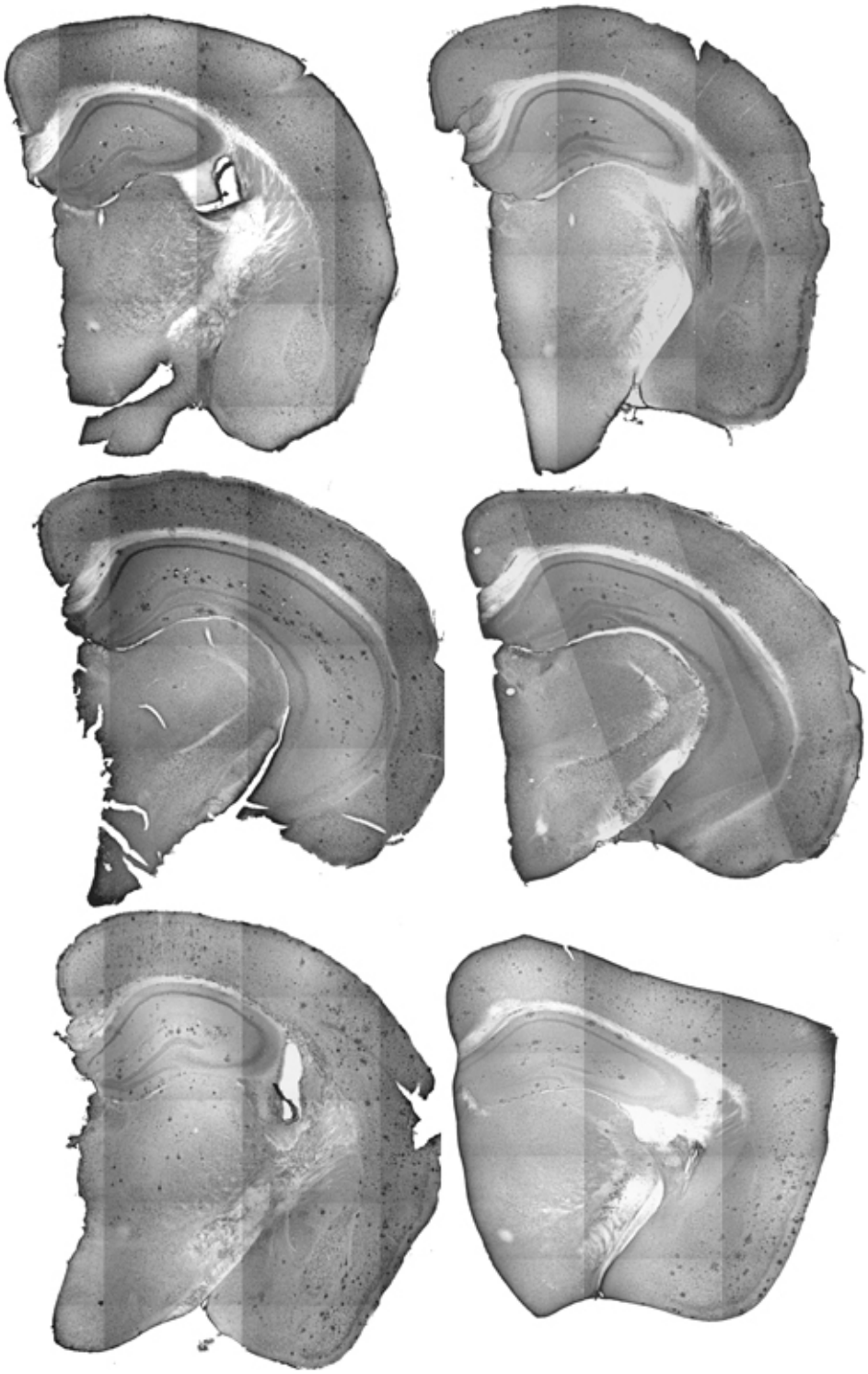

Figure 5-7 Diffuse amyloid deposits in $_{mo/hu}$APP/PS1$_{\delta E9}$ mice. Deposits visualized by immunostaining with 6E10, digital micrographs of untreated mice (left) and pUFGL-injected mice (right). One section is included from each animal.

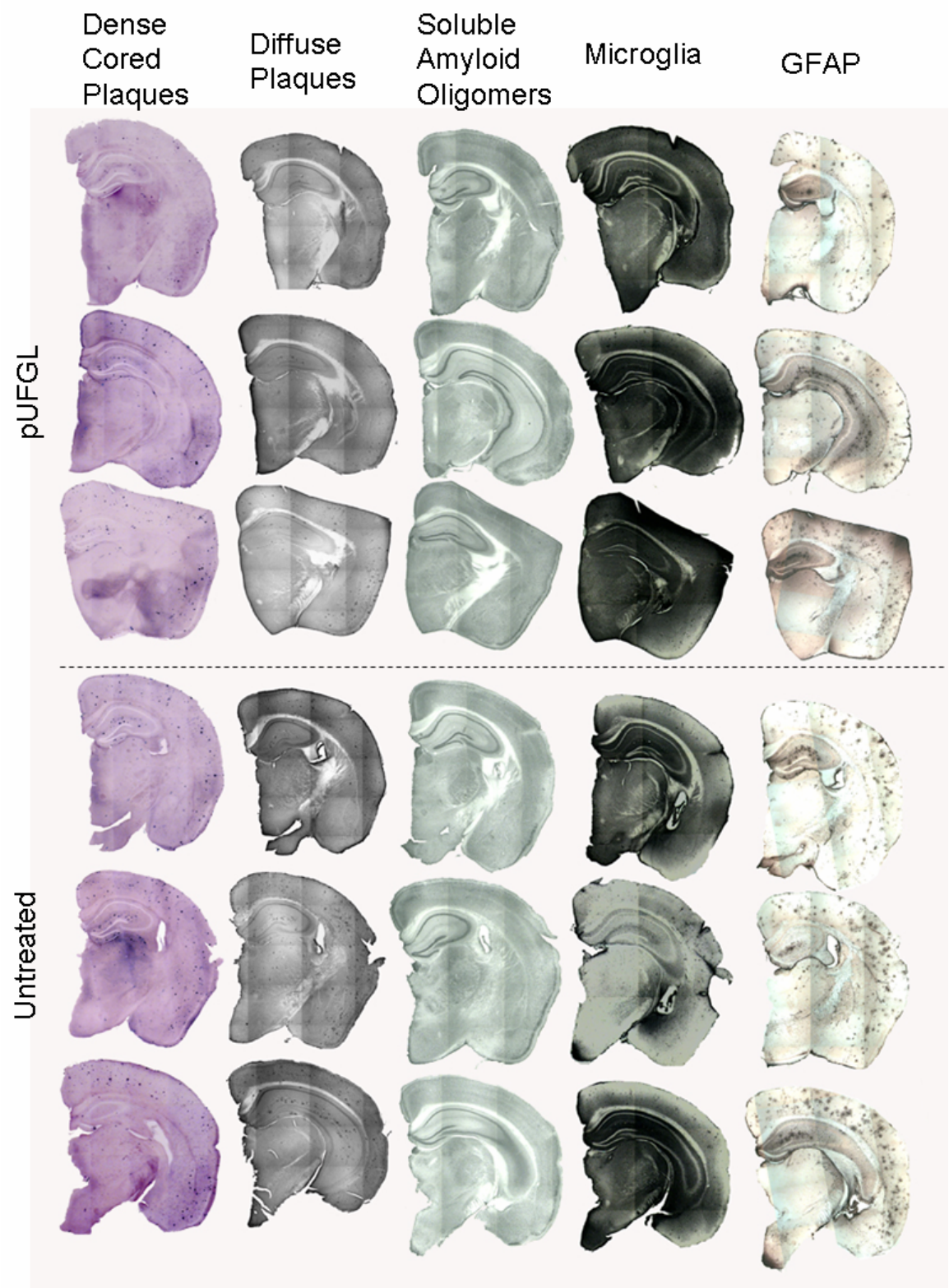

Figure 5-8 Side by side comparison of staining for dense cored amyloid deposits, diffuse amyloid deposits, soluble amyloid oligomers, microglia, and GFAP in $_{mo/hu}APP/PS1_{\delta E9}$ mice. Untreated are lower sections, pUFGL are upper.

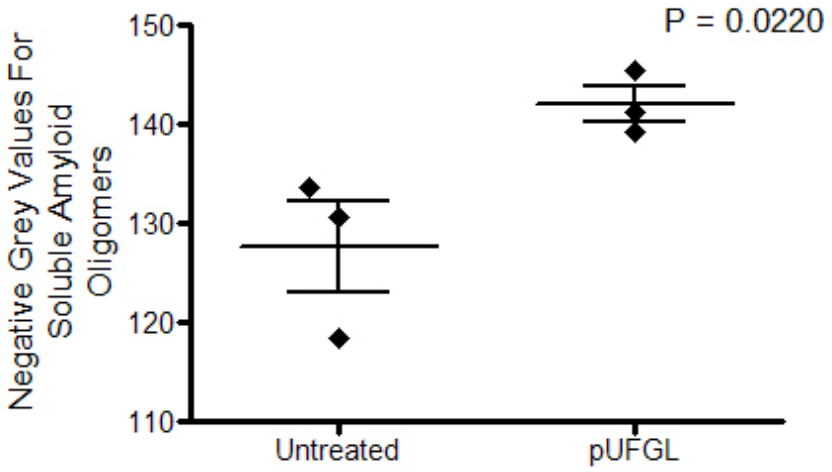

Figure 5-9 Staining intensity of soluble amyloid oligomers in $_{mo/hu}$APP/PS1$_{\delta E9}$ mice. Increasing negative grey values correspond to darker sections. Diamonds represent individual animal means determined from measurements from three sections, while bars represent group means ± SEM.

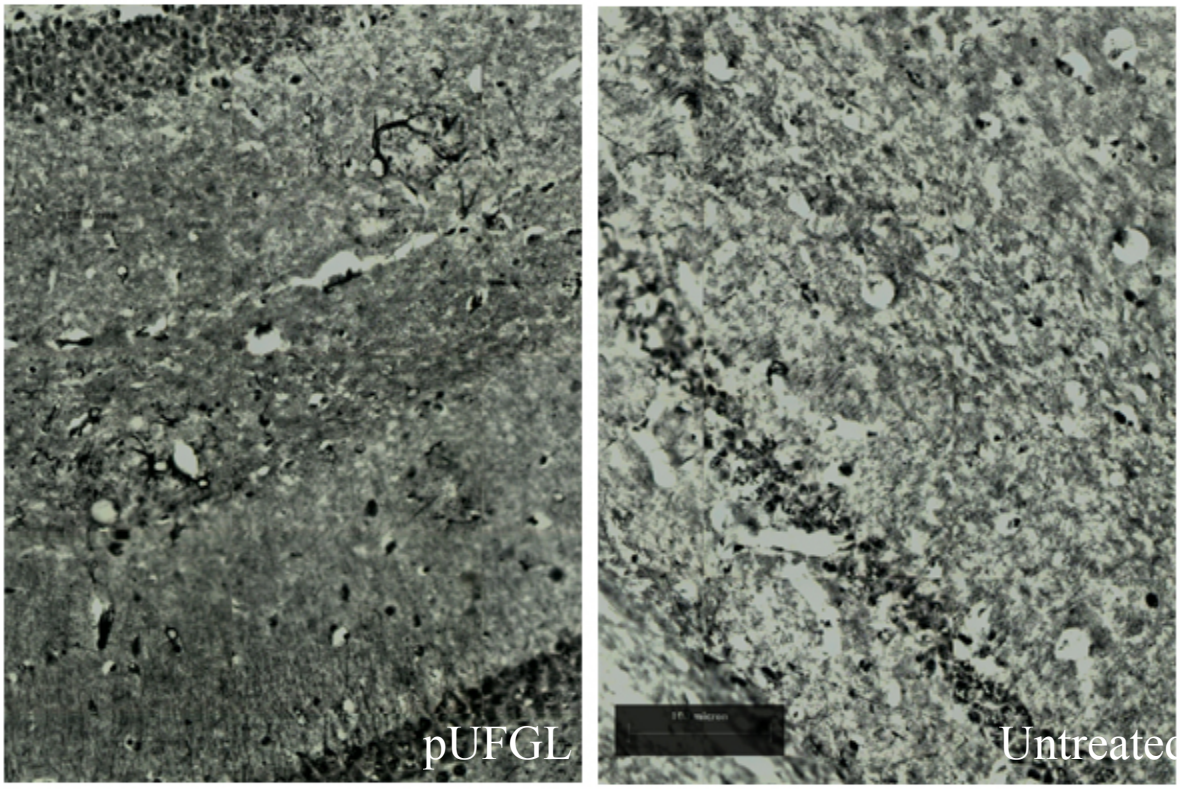

Figure 5-10 High magnification tiled images of amyloid oligomer staining. Untreated on the left, and pUFGL-injected on the right. Scale bar represents 100 μm for both images.

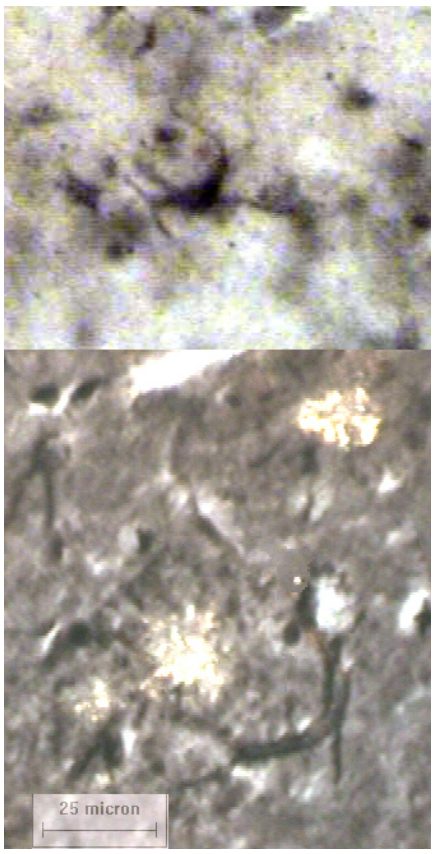

Figure 5-11 Cell types stained for soluble amyloid oligomers in pUFGL-injected mice. Upper photo displays an astrocyte containing soluble amyloid oligomers. Lower photo displays vasculature stained for soluble amyloid oligomers. Deposits in the lower photo were counterstained with congo red and visualized through a polarized light source. Scale bar represents 25μm for both images.

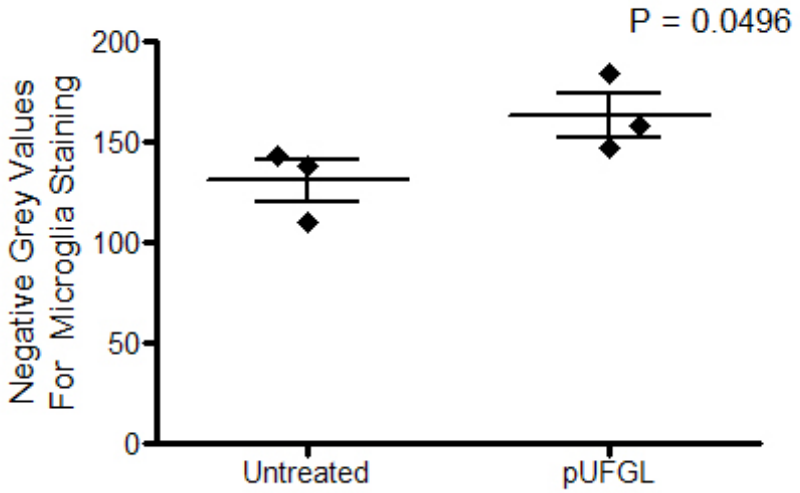

Figure 5-12 Staining intensity of microglia in $_{mo/hu}$APP/PS1$_{\delta E9}$ mice. P value calculated from an unpaired one-tailed t test.

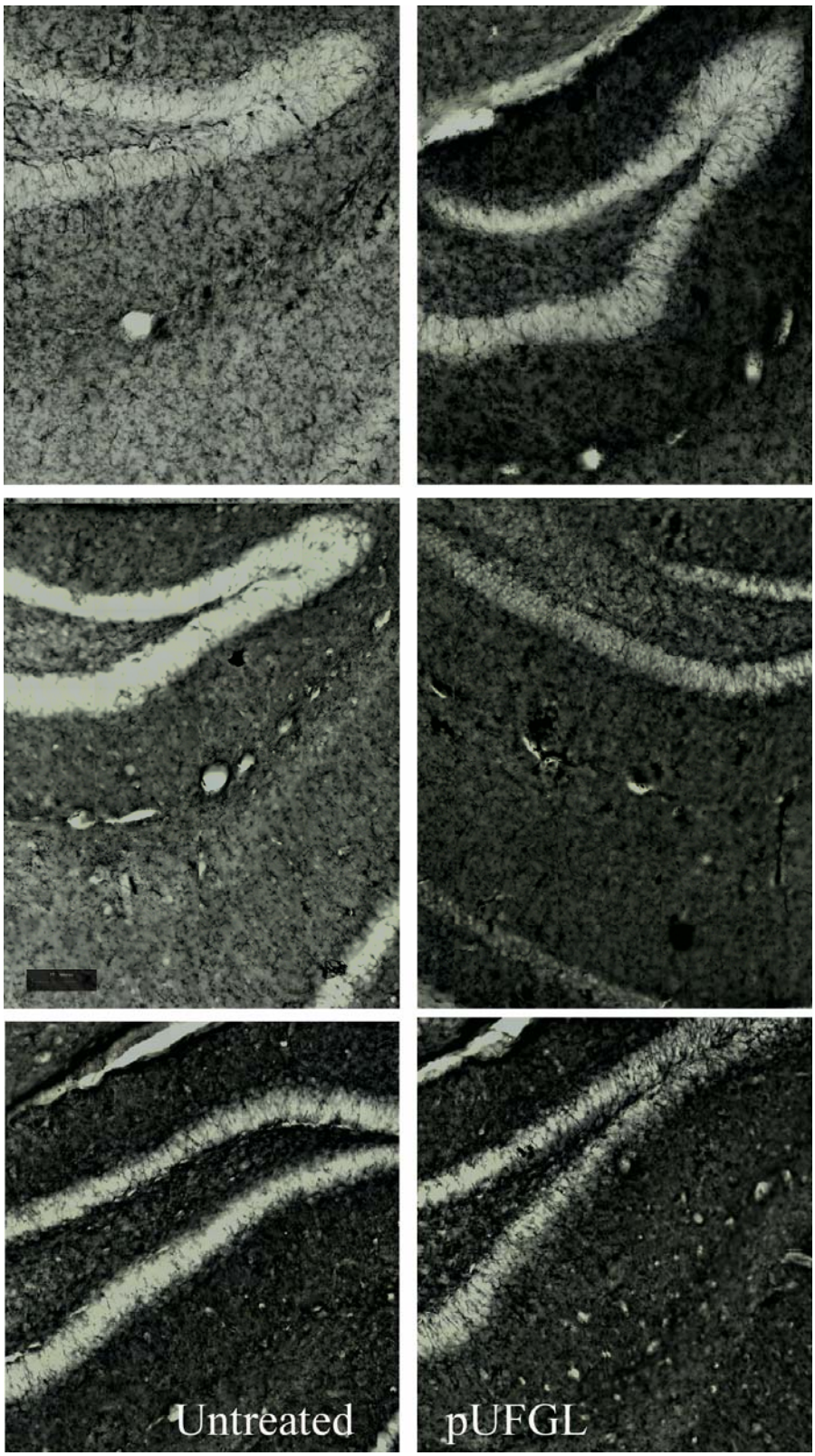

Figure 5-13 Low magnification images of microglia. Untreated (left), and pUFGL-injected (right) one image represented from each animal in the treatment groups (scale bar represents 100 μm).

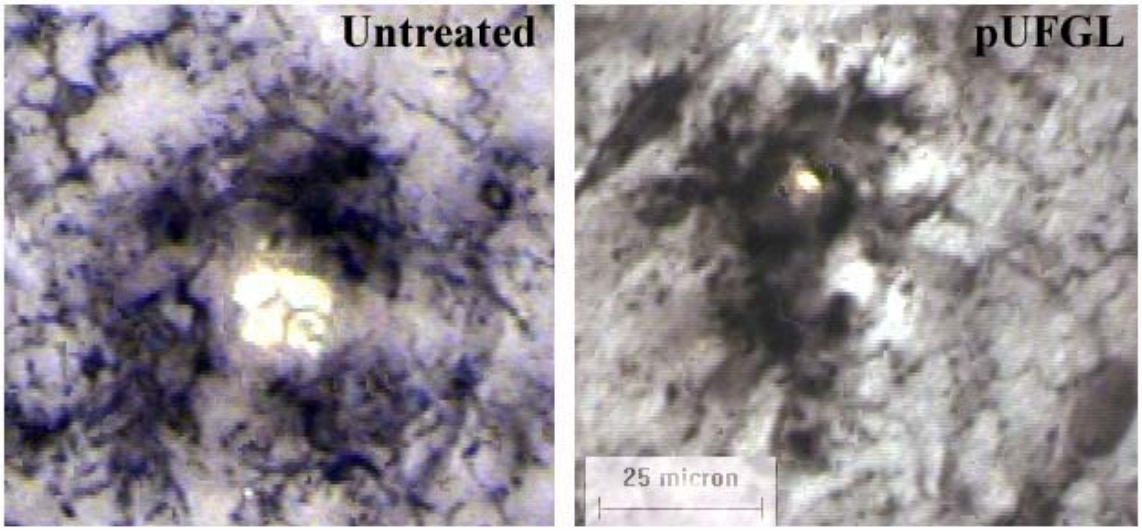

Figure 5-14 High magnification images of microglia staining. Untreated animal (right)and pUFGL-injected animal (left) are counterstained with Congo Red. (scale bar represents 25 μm).

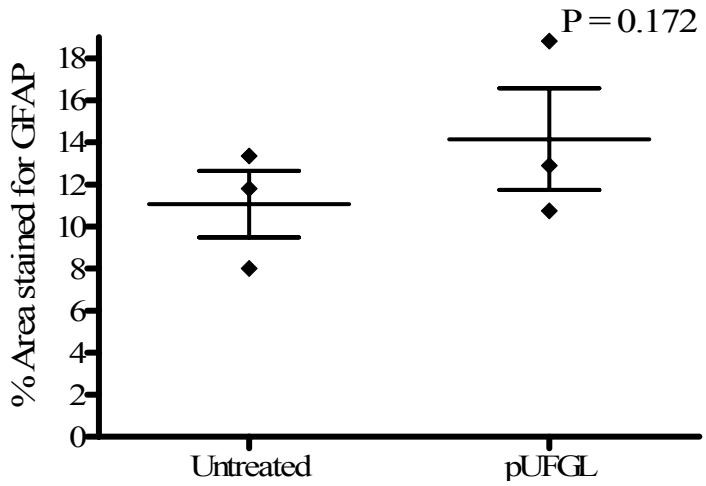

Figure 5-15 Average GFAP percent stained area in $_{mo/hu}$APP/PS1$_{\delta E9}$ cortex and hippocampus. P value calculated from an unpaired one-tailed t test.

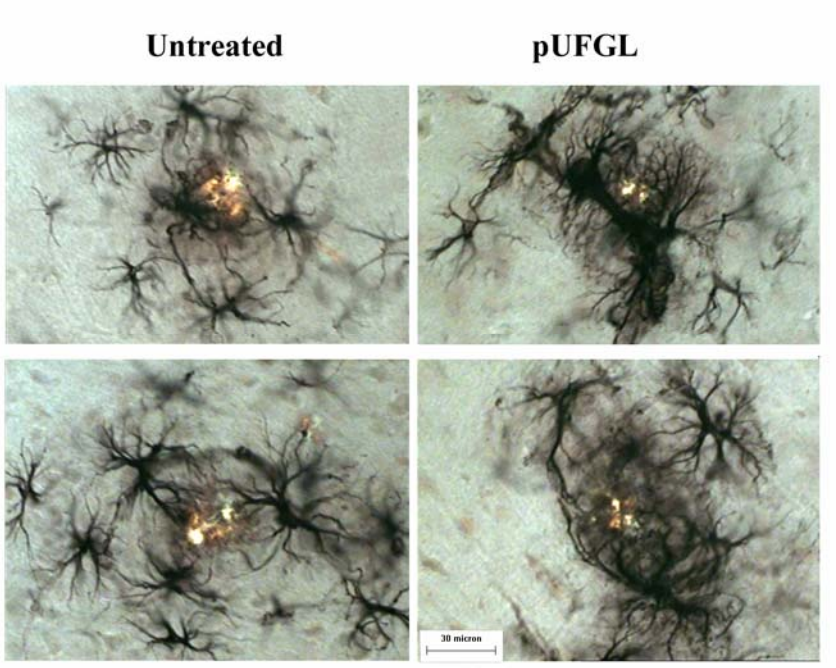

Figure 5-16 High magnification images of astrocytes surrounding congo red positive amyloid deposits. Untreated mice on the left and pUFGL-injected mice on the right. Scale bar represents 30 μm for all images.

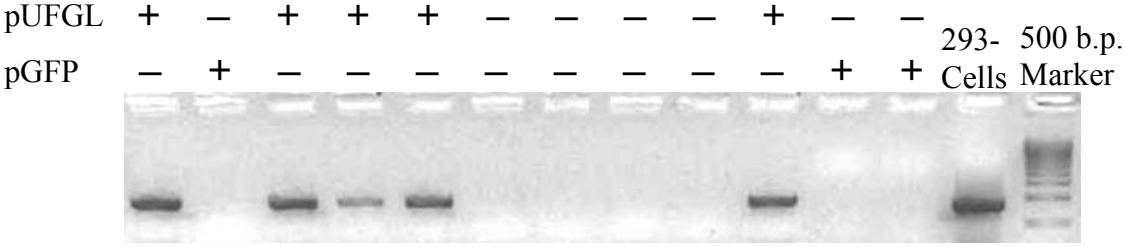

Figure 5-17 Message detection in $_{hu}$APP/PS1$_{M146L}$ mice. Specific for mRNA coded from pUFGL vector, using RNA purified from liver tissue from non-injected mice (– symbols), liver tissue from pGFP-injected mice (+ symbols), or liver tissue from pUFGL-injected mice (+ symbols), and 293 cells transfected with pUFGL 500 basepair marker from Biorad was used.

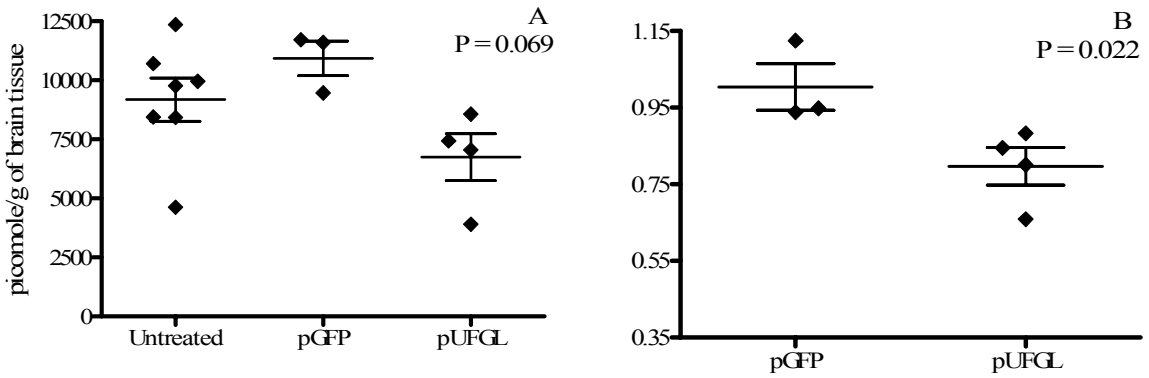

Figure 5-18 Amyloid β (1-42) cincentrations in $_{hu}$APP/PS1$_{M146L}$ brains. Amyloid β (1-42) concentrations (A). Fraction of Amyloid β (1-42) concentrations of untreated littermates (B). Diamonds represent individual animal means, bars represent means and standard error, P values calculated from one-way ANOVA (A) and an unpaired one tailed t-test (B).

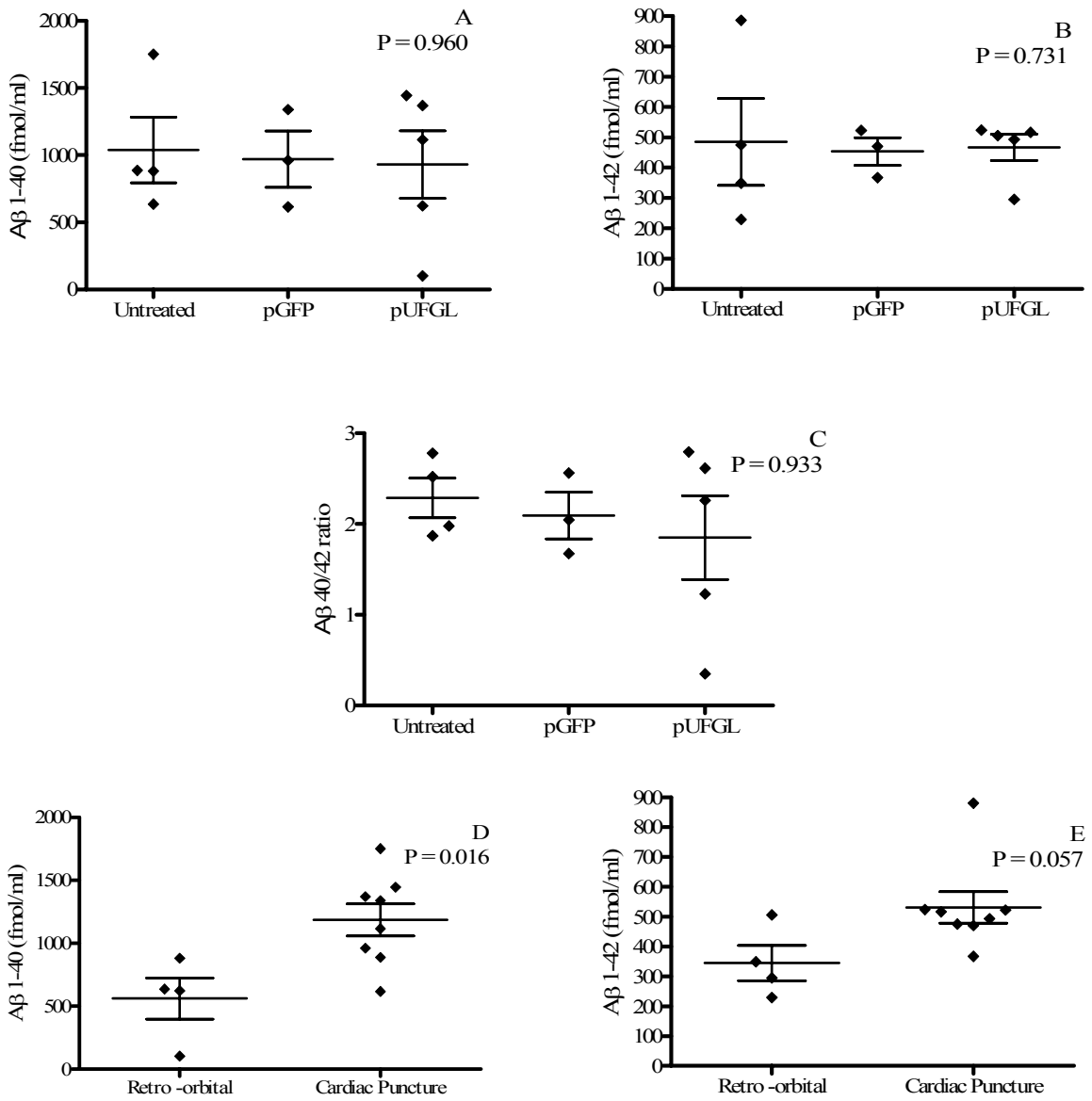

Figure 5-19 Plasma concentrations of amyloid in $_{hu}$APP/PS1$_{M146L}$ mice. A) Amyloid β 1–40 Concentrations in fmol/mL. B) Amyloid β 1–42 Concentrations in fmol/mL. C) The Ratio of Amyloid β 1–40 to Amyloid β 1–42 Concentrations. D) Amyloid β 1–40 and E) Amyloid β 1–42 Concentrations in fmol/mL in terms of sample collection method. P values determined one-way ANOVA or unpaired two-tailed t-test where appropriate.

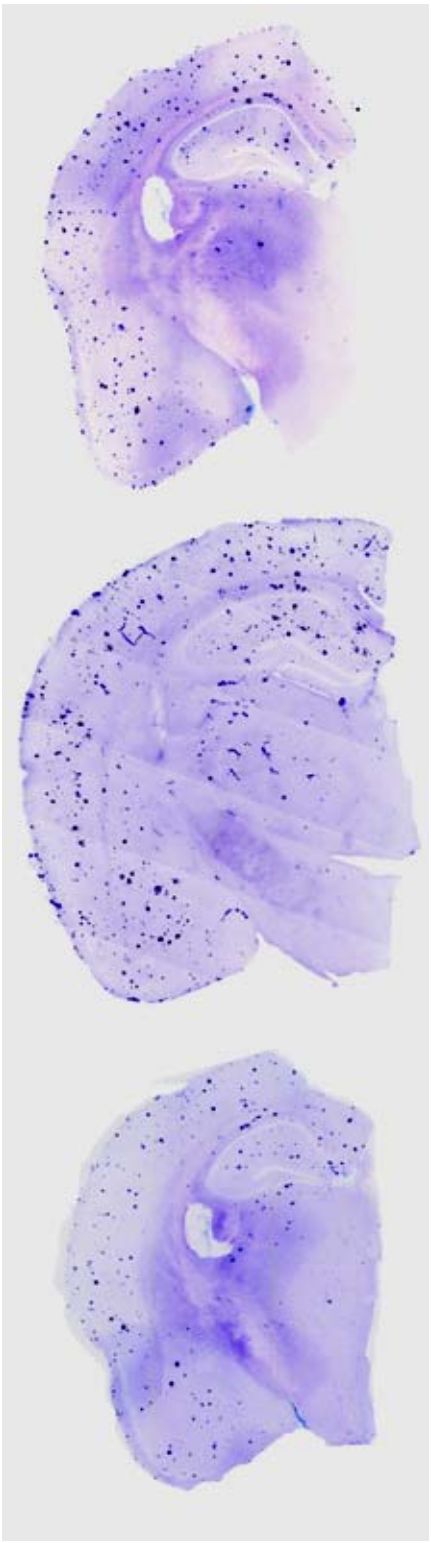

Figure 5-20 Dense-core amyloid deposits in $_{hu}$APP/PS1$_{M146L}$ mice. Deposits visualized by thioflavin S Staining. Negative digital micrographs of untreated mouse (top), pGFP-injected mouse (middle) and pUFGL-injected mouse (bottom).

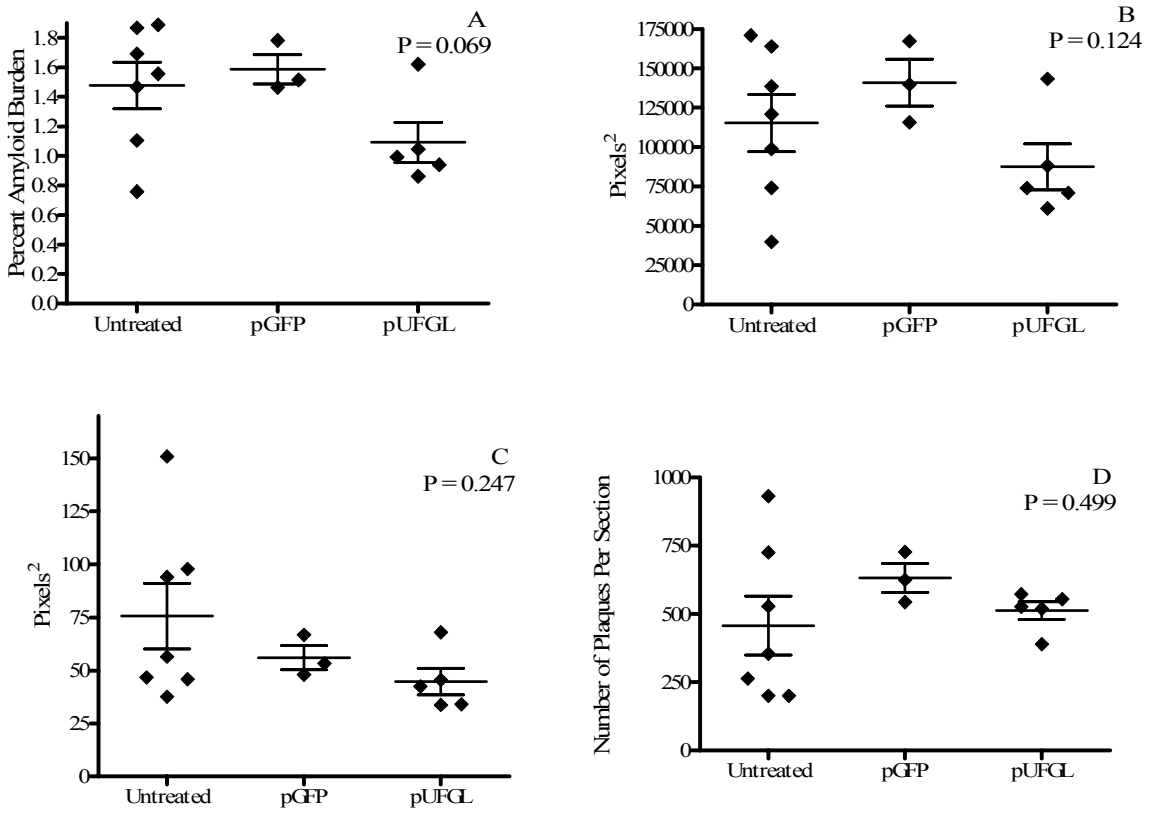

Figure 5-21 Analysis of dense-core amyloid deposits in $_{hu}$APP/PS1$_{M146L}$ mice. Deposits visualized by thioflavin S staining. A) Percent Amyloid Burden. B) Total Stained Area. C) Average Deposit Size. D) Average Number of Deposits per section. Diamonds represent individual animal means. Bars represent group means ± the standard error. P-values determined by ANOVA

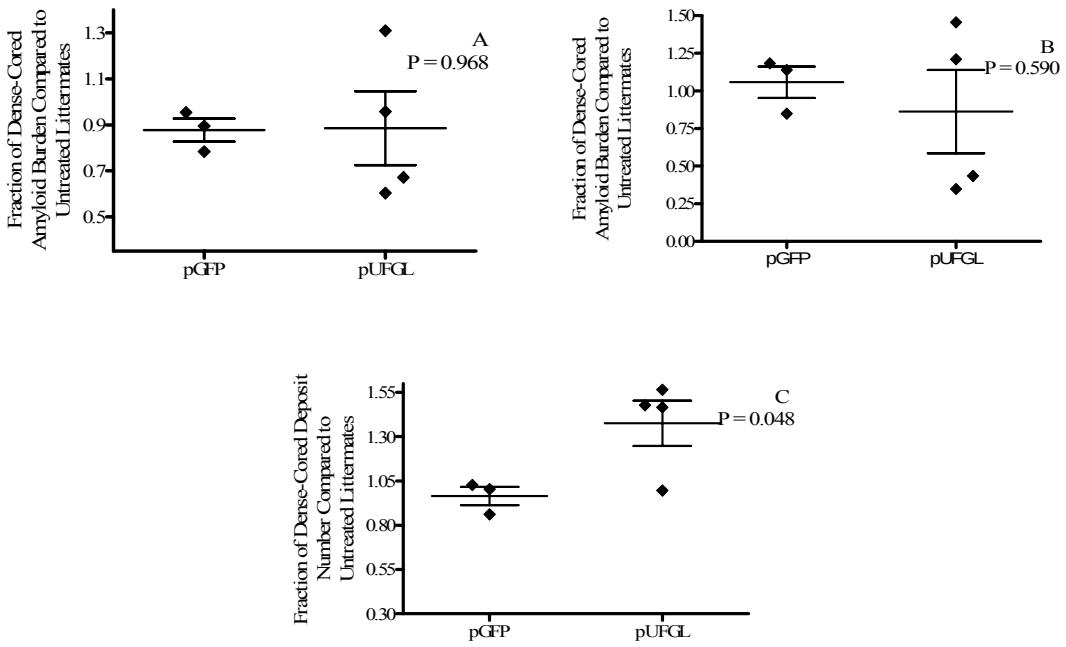

Figure 5-22 Analysis of dense-core amyloid deposits in terms of fractions compared to untreated littermates in $_{hu}APP/PS1_{M146L}$ mice. Deposits visualized by thioflavin S staining. A) Percent Amyloid Burden. B) Average Deposit Size. C) Average Number of Deposits per section. Diamonds represent individual animal means. Bars represent group means ± the standard error. P-value determined by two-tailed t-test.

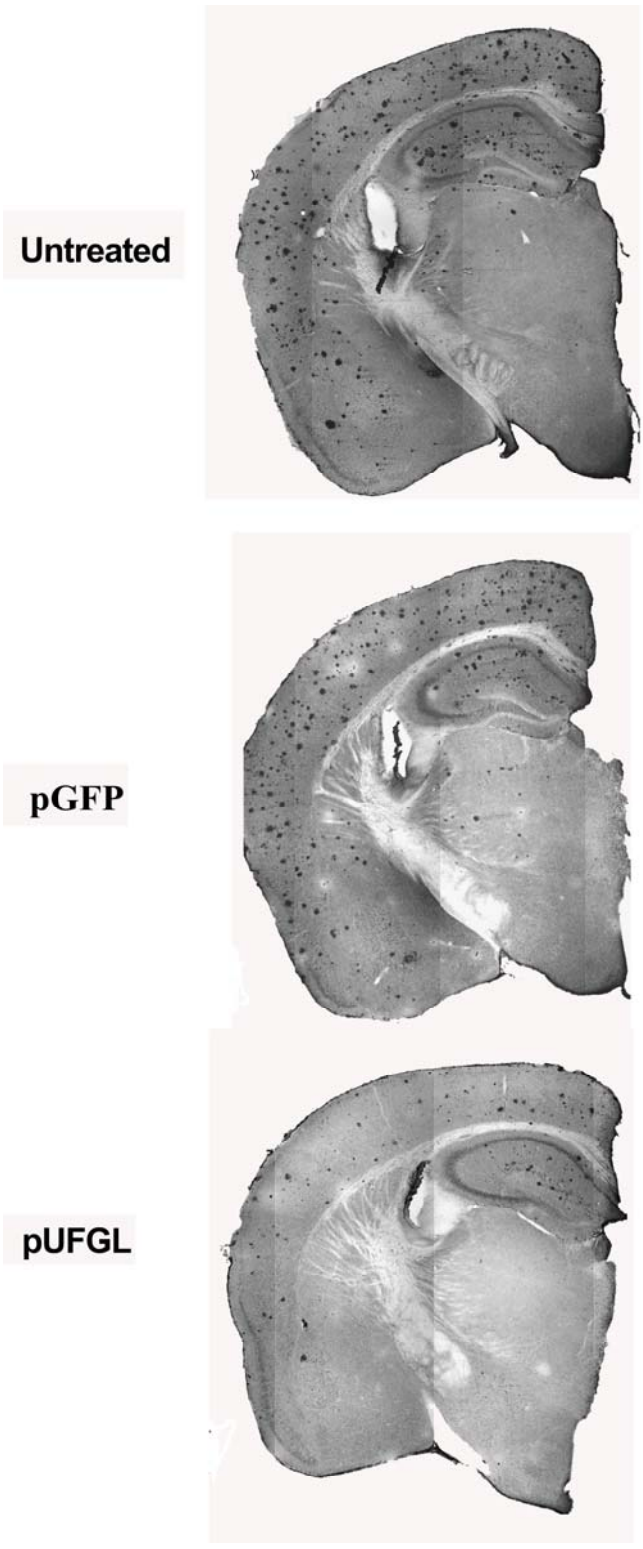

Figure 5-23 Diffuse amyloid deposits in $_{hu}$APP/PS1$_{M146L}$ mice. Deposits visualized by immunostaining with 6E10. Digital micrographs of untreated mouse (top), pGFP-injected mouse (middle) and pUFGL-injected mouse (bottom).

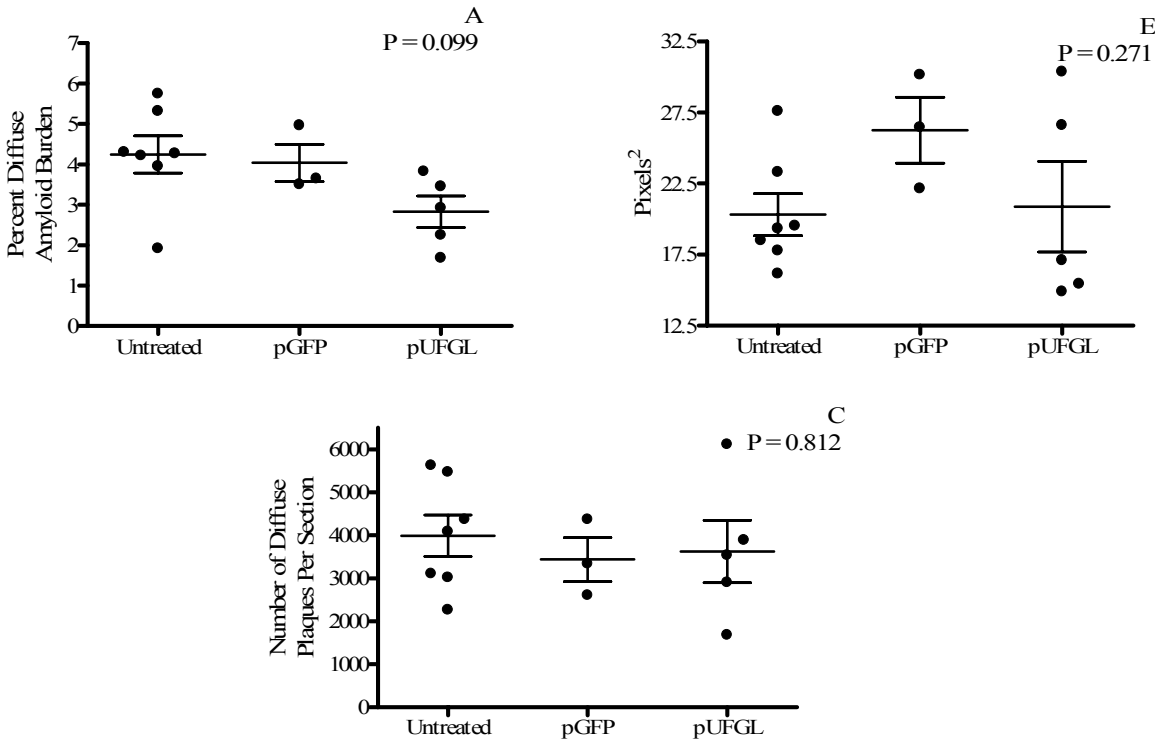

Figure 5-24 Analysis of diffuse amyloid deposits in $_{hu}$APP/PS1$_{M146L}$ mice. Deposits visualized by immunostaining. A) Percent Amyloid Burden. B) Average Deposit Size. C) Average Number of Deposits per section. Circles represent individual animal means. Bars represent group means ± the standard error. P-values determined by one-way ANOVA.

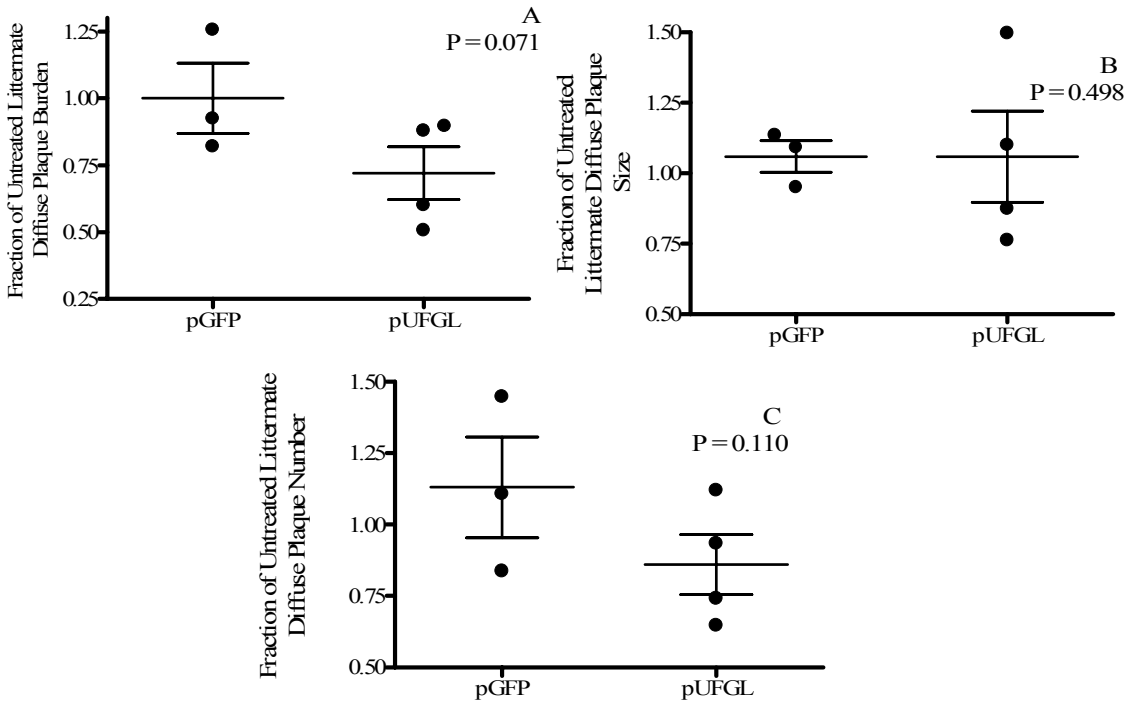

Figure 5-25 Analysis of diffuse amyloid deposits in terms of fractions compared to untreated littermates in $_{hu}$APP/PS1$_{M146L}$ mice. Deposits visualized by immunostaining. A) Percent Amyloid Burden. B) Average Deposit Size. C) Average Number of Deposits per section. Diamonds represent individual animal means. Bars represent group means ± the standard error. P-values determined by one-tailed t-test.

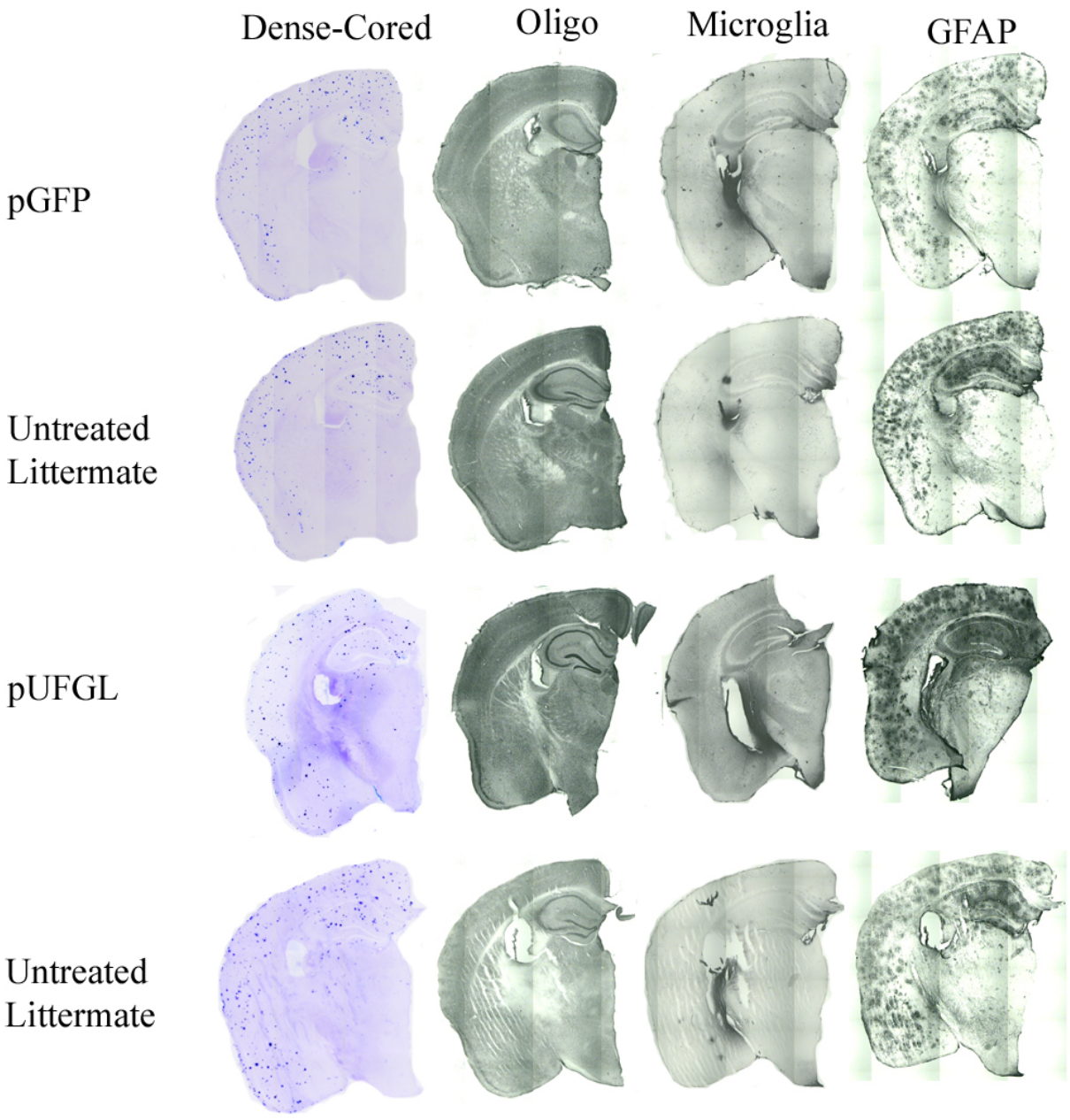

Figure 5-26 Side by side comparison of staining in $_{hu}$APP/PS1$_{M146L}$ mice for dense cored amyloid deposits, soluble amyloid oligomers, microglia, and GFAP positive cells in $_{hu}$APP/PS1$_{M146L}$ Mice. Untreateds represent littermates for both pGFP-injected animal (upper) and pUFGL-injected animal (lower).

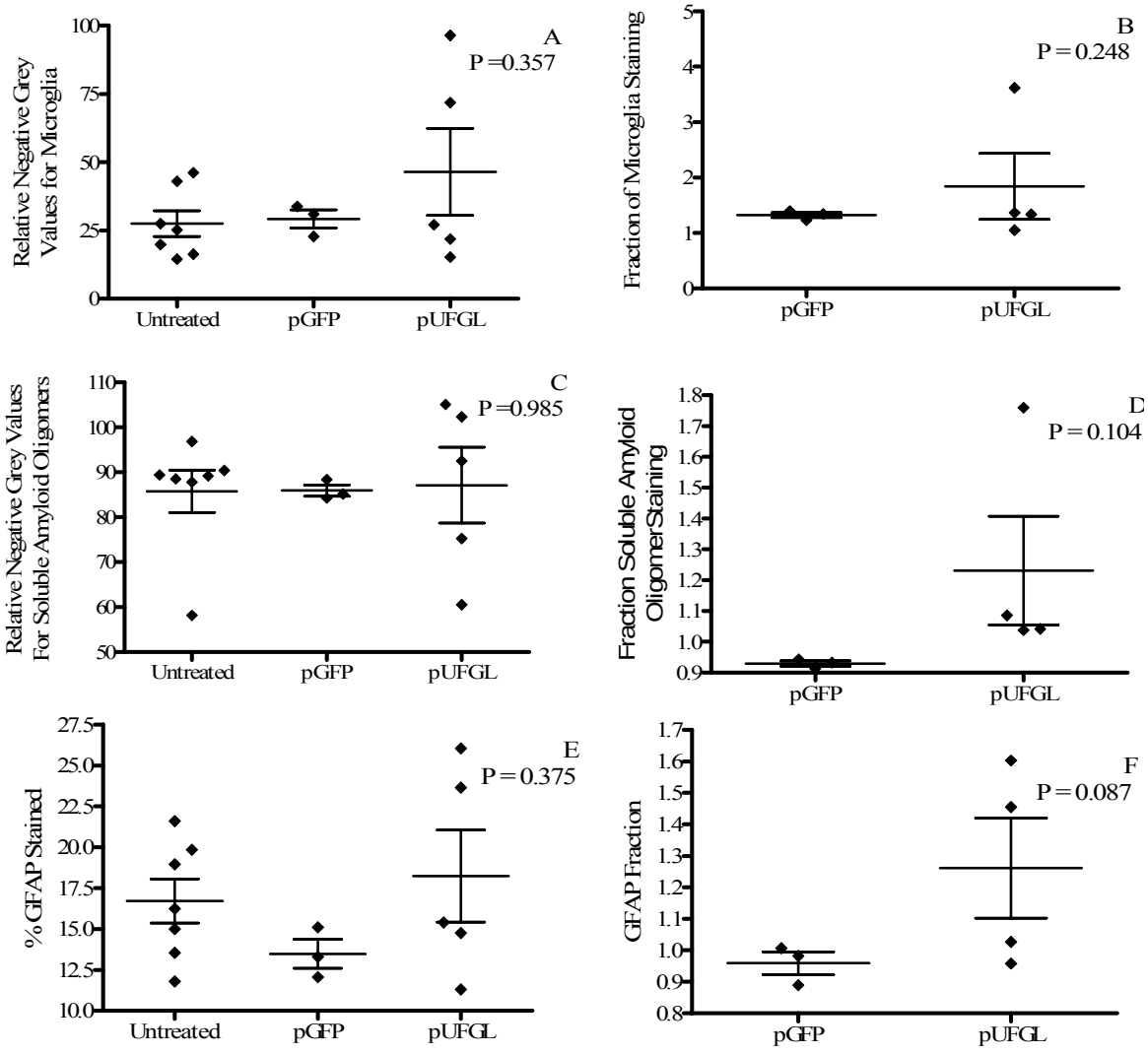

Figure 5-27 Analysis of microglia, soluble amyloid oligomers, and astrocytes in $_{hu}$APP/PS1$_{M146L}$ mice. A) Microglia. B) Microglia examined in terms of fractions of untreated littermates. C) Soluble amyloid oligomers. D) Soluble amyloid oligomers in terms of fractions of untreated littermates E) Astrocytes. F) Astrocytes in terms of fractions of untreated littermates. Diamonds represent individual animal means, and bars represent group means ± SEM. P-values determined one-way ANOVA or unpaired one-tailed t-test where appropriate.

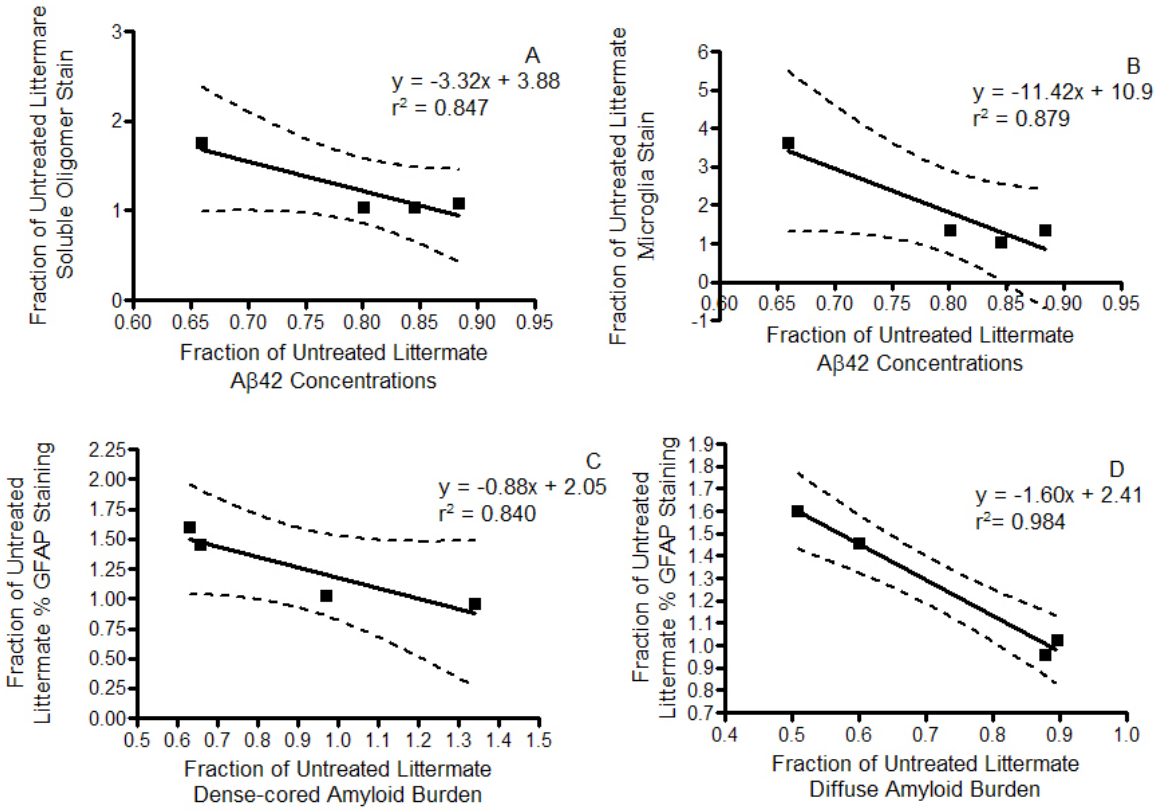

Figure 5-28 Linear regression analysis. Correlating soluble amyloid oligomer (A) and microglia stain fractions (B) to Aβ42 concentration fractions, and % GFAP stain fractions with dense-cored (C) and diffuse (D) amyloid burden fractions for pUFGL-injected $_{hu}$APP/PS1$_{M146L}$ mice. Dashed lines indicate a 95% confidence interval for the fitted lines.

CHAPTER 6
DISCUSSION AND FUTURE DIRECTIONS

Previous studies have demonstrated that human gelsolin purified from plasma has the ability bind to amyloid β (Chauhan et al., 1999). It has also been reported that human plasma gelsolin disassembles and prevents the assembly of amyloid fibrils (Ray et al., 2000). Matsouka et al. showed that administration of bovine plasma gelsolin reduces amyloid levels in $_{hu}$APP/PS1$_{M146L}$ mice (2003). We attempted to compare bovine and human plasma gelsolin's interaction with amyloid β due to these findings.

In our attempt to measure binding affinities for both the human and bovine forms of plasma gelsolin, by three separate experimental approaches, we discovered that in the presence of plasma gelsolin (both human and bovine) amyloid β is less 'sticky'. This is an important finding indicating that rather than gelsolin just having binding activity towards amyloid β, it appears to have enzymatic type activity, perhaps by maintaining amyloid β in a soluble α-helix state, rather than oligomerization prone β-sheet state. We compared the relative activity for both human and bovine plasma gelsolin to disassemble preformed amyloid fibrils, and our results confirm that both human and bovine plasma gelsolin have fibril disassembly activity, and that the human form is as efficient if not more so, as the bovine form.

We hypothesized that human plasma gelsolin would make an excellent candidate for a peripherally expressed gene therapy for AD based on several observations. Plasma gelsolin contains an internal signal peptide allowing for cellular export into the plasma

from peripheral expressing tissues. Plasma gelsolin has been shown to bind to and disassemble preformed Aβ fibers and prevent fibrillization of soluble amyloid β (Chauhan et al., 1999; Ray et al., 2000). Gelsolin concentrations appear to be reduced in the CSF of Alzheimer's patients (Chauhan, 2004). Administration of plasma gelsolin at a dose of 0.6 mg/kg every two days for three weeks significantly reduced the accumulation of deposits in young amyloid-depositing transgenic mice (Matsuoka et al., 2003).

To test this hypothesis we constructed a plasmid DNA mammalian expression vector, pUFGL. Our studies provide evidence that pUFGL does produce a human plasma gelsolin immunoreactive protein of the same molecular weight of plasma gelsolin when expressed by human embryonic kidney cells *in vitro*. We also demonstrate that the gene product recombinant human plasma gelsolin will bind to amyloid β 1-42. We are the first to demonstrate that recombinant plasma gelsolin maintains this activity.

We choose to use the hydrodynamic gene delivery technique to deliver our plasmid DNA. Our results confirm that delivering vectors by this method results in high levels of gene expression, which is widely distributed throughout the liver for at least two and a half weeks. Little if any damage or inflammation is observed as a result of the gene delivery and expression results in the liver.

We tested our vector in two separate mouse models of Alzheimer's disease, and saw significant reductions of amyloid β 1-42 concentrations in the brains of $_{mo/hu}$APP/PS1$_{\delta E9}$ mice, and a trend toward significant reductions in $_{hu}$APP/PS1$_{M146L}$ mice that was significant when inter-litter variability was accounted for. Only $_{mo/hu}$APP/PS1$_{\delta E9}$ mice had significant reductions in dense cored amyloid deposit load. However, $_{hu}$APP/PS1$_{M146L}$ mice did trend toward a decrease in dense cored amyloid deposit load; it

may be that a longer treatment regimen will result in a significant decrease in amyloid β 1-42 concentrations.

This difference between the two lines of transgenic mice may be accounted for by the fact that in $_{hu}$APP/PS1$_{M146L}$ mice there was only about a 20% reduction in amyloid β 1-42 concentration, while the $_{mo/hu}$APP/PS1$_{\delta E9}$ mice had nearly a 50% reduction. This difference in plasma gelsolin's apparent ability to clear amyloid from the brains of the two lines of mice may not be a function of gelsolin working better in one line rather than the other, but result from the fact that eight month old $_{hu}$APP/PS1$_{M146L}$ mice have an amyloid β 1-42 concentration that is nearly five times that of nine month old $_{mo/hu}$APP/PS1$_{\delta E9}$ mice, which is reflective of a much higher rate of amyloid β synthesis in $_{hu}$APP/PS1$_{M146L}$ mice as compared to $_{mo/hu}$APP/PS1$_{\delta E9}$ mice. Likewise the $_{hu}$APP/PS1$_{M146L}$ mice have a much higher dense cored amyloid deposit burden at the beginning of treatment, and our data is consistent with the commonly held belief that it should be harder to remove deposits that already exist, rather than prevent new deposits from forming (Levites et al., 2006).

The mechanism for this brain amyloid reduction is not clear. Peripheral sequestration is a possible explanation; however, increases in plasma Aβ often observed with immunization (DeMattos et al., 2001; DeMattos et al., 2002; Lemere et al., 2003) or other Aβ binding strategies (Deane et al., 2003; Matsuoka et al., 2005) are not detected in this study, agreeing with the previously reported study by Matsuoka and colleagues (Matsuoka et al., 2003). However, it is possible that there were increases in plasma Aβ at earlier time points that were not detected in this experiment.

Unlike Matsouka's study we did observe a decrease in the ratio of amyloid β 1-40/1-42. Normally amyloid depositing transgenic mice have much higher concentrations of amyloid β 1-40 than amyloid β 1-42 in the plasma (DeMattos et al., 2002; Lanz et al., 2005; Matsuoka et al., 2003). It has also been reported that in humans a decrease the ratio of plasma amyloid β 1-40/1-42 is assoiciated with an decreased risk for Alzheimer's disease (van Oijen et al., 2006). This observation may indicate that higher concentrations of amyloid β 1-42 in the plasma are a reflection of amyloid β 1-42's ability to be cleared from the CNS. Our observation that amyloid β 1-40/1-42 ratio is reduced in $_{mo/hu}$APP/PS1$_{\delta E9}$ mice may be associated with the activity described in this report of gelsolin's ability to solubilize amyloid β.

It is possible that plasma gelsolin enters the parenchyma across the blood brain barrier and directly solubilizes amyloid deposits. Transport mechanisms for gelsolin across the BBB are not known, though reports indicate that the BBB is compromised in mouse models of AD (Dickstein et al., 2006; Marco and Skaper, 2006). Gelsolin efficiently disassembles preformed amyloid fibrils (Ray et al., 2000), so this seems a feasible hypothesis. The possible increase of soluble amyloid oligomers observed in gelsolin expressing mice in this study supports this hypothesis. The increase in soluble amyloid could be an explanation for the increase in reactive and activated microglia observed in our study. It has been reported that soluble amyloid and not insoluble amyloid activates microglia (Floden and Combs, 2006; Lindberg et al., 2005).

An alternative to gelsolin entering the parenchyma and solubilizing amyloid is the activity we observed for gelsolin to shift the equilibrium of amyloid from forming fibrillar insoluble forms to monomeric or dimeric soluble forms of amyloid across a

membrane (Figure 3-6). Our data supports both the hypothesis of gelsolin entering the CNS and disassembling aggregates directly or the hypothesis gelsolin is not entering the CNS and just shifting the equilibrium of amyloid to a more soluble state.

A third possible explanation for our results is hypothesis that plasma gelsolin may have immunomodulatory functions based on its ability to bind a number of immunomodulatory chemicals (Bucki et al., 2005; Bucki et al., 2004; Chauhan et al., 1999; Lee et al., 2006; Lind and Janmey, 1984; Smith et al., 1987), since it has been shown to decrease the toxicity associated with inflammation after injury or trauma (Candiano et al., 2005; Christofidou-Solomidou et al., 2002a; Christofidou-Solomidou et al., 2002b; DiNubile et al., 2002; Mounzer et al., 1999). The roles of microglial and astrocytic activation during Alzheimer's are actively being studied. It has been proposed that in the presence of Aβ, glia become activated and secrete neurotoxic cytokines and chemicals (Dheen et al., 2005; Haas et al., 2002; von Bernhardi and Eugenin, 2004; Walker and Lue, 2005).

It has also been proposed that glia cells can serve neuroprotective roles. They have been shown to produce neurotrophins in response to injury or disease (Dougherty et al., 2000; Nakajima et al., 2001). Glia and immune cell production of brain derived neurotrophic factor (BDNF) has been shown to be important in hippocampal neurogenesis and spatial memory related behavior (Ziv et al., 2006). Astrocytes, microglia and macrophages have also been shown to internalize Aβ by phagocytosis; this function appears to be deficient in AD (Fiala et al., 2005) and amyloid depositing transgenic mice (Alarcon et al., 2005; Fiala et al., 2005; Rogers et al., 2002). Stimulating the immune system either by active or passive immunization against Aβ or

lipopolysaccharide administration restores phagocytosis of Aβ by microglia (Das et al., 2003; DiCarlo et al., 2001; Herber et al., 2004; Wilcock et al., 2003). If human gelsolin expression does affect amyloid by stimulating the immune system, it is most likely not the result of a global response to the expression of a foreign protein. If this were the case, GFP expression would cause similar effects and none are observed. Also, hematoxylin and eosin staining of liver sections reveals no differences between any of the treatment groups at the 18 day time point.

Gene therapy intends to treat, cure, or prevent diseases with the use of nucleic acid sequences. The vast majority of gene therapy approaches for AD involve delivery of vectors coding for either neurotrophic factors (nerve growth factor, NGF)(Bradbury, 2005; Klein et al., 2000; Wu et al., 2004), or amyloid degrading enzymes (neprilysin or insulin degrading enzyme) (Eckman and Eckman, 2005; Marr et al., 2003). The rationale behind delivering neurotrophic factors is to protect the neuronal populations that are lost due to AD pathology, and the rationale behind using amyloid degrading enzymes is to increase the clearance of amyloid. These approaches are promising; however both involve invasive surgery that requires an injection directly into the brain, which does not come without risks.

Treating AD through a peripherally administered gene therapy would be advantageous in this regard. NGF is also a secreted protein; however, peripheral expression is not a suitable treatment strategy due to significant side effects observed after systemic administration (Petty et al., 1994). In contrast because IDE activity is predominantly cytosolic (Affholter et al., 1990; Gao et al., 2004), and NEP is bound to the plasma membrane (Back and Gorenstein, 1990), these are not likely to be suitable

agents for peripheral therapy, however may prove to be effective if expressed locally in the brain (Eckman and Eckman, 2005; Leissring et al., 2003).

Future directions for this study will include determining if plasma gelsolin expressed in the brains has similar effects on amyloid and glia in the CNS of transgenic mice; also determine how much gelsolin can cross the blood brain barrier from the periphery. These studies will also examine behavior associated with memory and learning. Studies with multiple treatments at different time points will be important for learning how fast gelsolin works and for how long. *In vitro* studies will be carried out to determine if plasma gelsolin affects the ability of primary cultures of microglia and astrocytes to phagocytose amyloid β, and determine by what cellular mechanism gelsolin has this effect.

In conclusion our study demonstrates that a peripherally delivered and expressed gene therapeutic can affect amyloid dynamics in the central nervous system. Peripheral delivery offers significant advantages over the traditional gene therapeutic approaches for AD in that no invasive surgeries are required, thus reducing costs and complications. Plasma gelsolin is well suited as a peripherally expressed therapeutic in that it contains an internal signal peptide directing gelsolin to be secreted from the cells that make it at any peripheral location. Care should be taken using plasma gelsolin as a treatment strategy as we observed an increase in microglial activation and soluble oligomeric forms of Aβ, both of which are thought to be a possible source of neurotoxicity.

LIST OF REFERENCES

Affholter, J. A., Hsieh, C. L., Francke, U., and Roth, R. A. (1990). Insulin-degrading enzyme: stable expression of the human complementary DNA, characterization of its protein product, and chromosomal mapping of the human and mouse genes. *Mol Endocrinol* **4**, 1125-35.

Akama, K. T., Albanese, C., Pestell, R. G., and Van Eldik, L. J. (1998). Amyloid beta-peptide stimulates nitric oxide production in astrocytes through an NFkappaB-dependent mechanism. *Proc Natl Acad Sci U S A* **95**, 5795-800.

Alarcon, R., Fuenzalida, C., Santibanez, M., and von Bernhardi, R. (2005). Expression of scavenger receptors in glial cells. Comparing the adhesion of astrocytes and microglia from neonatal rats to surface-bound beta-amyloid. *J Biol Chem* **280**, 30406-15.

Alino, S. F., Crespo, A., and Dasi, F. (2003). Long-term therapeutic levels of human alpha-1 antitrypsin in plasma after hydrodynamic injection of nonviral DNA. *Gene Ther* **10**, 1672-9.

Allsop, D., Landon, M., and Kidd, M. (1983). The isolation and amino acid composition of senile plaque core protein. *Brain Res* **259**, 348-52.

Back, S. A., and Gorenstein, C. (1990). Localization of neutral endopeptidase-24.11 (enkephalinase) to N-methyl-D-aspartate sensitive cell populations in the rat forebrain. *Prog Clin Biol Res* **328**, 199-202.

Bacskai, B. J., Kajdasz, S. T., Christie, R. H., Carter, C., Games, D., Seubert, P., Schenk, D., and Hyman, B. T. (2001). Imaging of amyloid-beta deposits in brains of living mice permits direct observation of clearance of plaques with immunotherapy. *Nat Med* **7**, 369-72.

Bard, F., Cannon, C., Barbour, R., Burke, R. L., Games, D., Grajeda, H., Guido, T., Hu, K., Huang, J., Johnson-Wood, K., Khan, K., Kholodenko, D., Lee, M., Lieberburg, I., Motter, R., Nguyen, M., Soriano, F., Vasquez, N., Weiss, K., Welch, B., Seubert, P., Schenk, D., and Yednock, T. (2000). Peripherally administered antibodies against amyloid beta-peptide enter the central nervous system and reduce pathology in a mouse model of Alzheimer disease. *Nat Med* **6**, 916-9.

Basler, K., Oesch, B., Scott, M., Westaway, D., Walchli, M., Groth, D. F., McKinley, M. P., Prusiner, S. B., and Weissmann, C. (1986). Scrapie and cellular PrP isoforms are encoded by the same chromosomal gene. *Cell* **46**, 417-28.

Borchelt, D. R., Davis, J., Fischer, M., Lee, M. K., Slunt, H. H., Ratovitsky, T., Regard, J., Copeland, N. G., Jenkins, N. A., Sisodia, S. S., and Price, D. L. (1996). A vector for expressing foreign genes in the brains and hearts of transgenic mice. *Genet Anal* **13**, 159-63.

Borchelt, D. R., Ratovitski, T., van Lare, J., Lee, M. K., Gonzales, V., Jenkins, N. A., Copeland, N. G., Price, D. L., and Sisodia, S. S. (1997). Accelerated amyloid deposition in the brains of transgenic mice coexpressing mutant presenilin 1 and amyloid precursor proteins. *Neuron* **19**, 939-45.

Bradbury, J. (2005). Hope for AD with NGF gene-therapy trial. *Lancet Neurol* **4**, 335.

Brendza, R. P., Bales, K. R., Paul, S. M., and Holtzman, D. M. (2002). Role of apoE/Abeta interactions in Alzheimer's disease: insights from transgenic mouse models. *Mol Psychiatry* **7**, 132-5.

Brunden, K. R., Richter-Cook, N. J., Chaturvedi, N., and Frederickson, R. C. (1993). pH-dependent binding of synthetic beta-amyloid peptides to glycosaminoglycans. *J Neurochem* **61**, 2147-54.

Bucki, R., Georges, P. C., Espinassous, Q., Funaki, M., Pastore, J. J., Chaby, R., and Janmey, P. A. (2005). Inactivation of endotoxin by human plasma gelsolin. *Biochemistry* **44**, 9590-7.

Bucki, R., Pastore, J. J., Randhawa, P., Vegners, R., Weiner, D. J., and Janmey, P. A. (2004). Antibacterial activities of rhodamine B-conjugated gelsolin-derived peptides compared to those of the antimicrobial peptides cathelicidin LL37, magainin II, and melittin. *Antimicrob Agents Chemother* **48**, 1526-33.

Candiano, G., Bruschi, M., Pedemonte, N., Caci, E., Liberatori, S., Bini, L., Pellegrini, C., Vigano, M., O'Connor, B. J., Lee, T. H., Galietta, L. J., and Zegarra-Moran, O. (2005). Gelsolin secretion in interleukin-4-treated bronchial epithelia and in asthmatic airways. *Am J Respir Crit Care Med* **172**, 1090-6.

Chauhan, V. P. (2004). Anti-amyloidogenic Role of Gelsolin in Alzheimer's Disease. *In* " The 9th International Conference on Alzheimer's Disease and Related Disorders." (A. Chauhan, ed.).

Chauhan, V. P., Ray, I., Chauhan, A., and Wisniewski, H. M. (1999). Binding of gelsolin, a secretory protein, to amyloid beta-protein. *Biochem Biophys Res Commun* **258**, 241-6.

Chen, C. D., Huff, M. E., Matteson, J., Page, L., Phillips, R., Kelly, J. W., and Balch, W. E. (2001). Furin initiates gelsolin familial amyloidosis in the Golgi through a defect in Ca(2+) stabilization. *Embo J* **20**, 6277-87.

Chhabra, D., Nosworthy, N. J., and dos Remedios, C. G. (2005). The N-terminal fragment of gelsolin inhibits the interaction of DNase I with isolated actin, but not with the cofilin-actin complex. *Proteomics* **5**, 3131-6.

Christofidou-Solomidou, M., Scherpereel, A., Solomides, C. C., Christie, J. D., Stossel, T. P., Goelz, S., and DiNubile, M. J. (2002a). Recombinant plasma gelsolin diminishes the acute inflammatory response to hyperoxia in mice. *J Investig Med* **50**, 54-60.

Christofidou-Solomidou, M., Scherpereel, A., Solomides, C. C., Muzykantov, V. R., Machtay, M., Albelda, S. M., and DiNubile, M. J. (2002b). Changes in plasma gelsolin concentration during acute oxidant lung injury in mice. *Lung* **180**, 91-104.

Clark, R. F., and Goate, A. M. (1993). Molecular genetics of Alzheimer's disease. *Arch Neurol* **50**, 1164-72.

Cooper, J. A., Bryan, J., Schwab, B., 3rd, Frieden, C., Loftus, D. J., and Elson, E. L. (1987). Microinjection of gelsolin into living cells. *J Cell Biol* **104**, 491-501.

Corder, E. H., Saunders, A. M., Strittmatter, W. J., Schmechel, D. E., Gaskell, P. C., Small, G. W., Roses, A. D., Haines, J. L., and Pericak-Vance, M. A. (1993). Gene dose of apolipoprotein E type 4 allele and the risk of Alzheimer's disease in late onset families. *Science* **261**, 921-3.

Coyle, J. T., Price, D. L., and DeLong, M. R. (1983). Alzheimer's disease: a disorder of cortical cholinergic innervation. *Science* **219**, 1184-90.

Cruz, J. C., and Tsai, L. H. (2004). A Jekyll and Hyde kinase: roles for Cdk5 in brain development and disease. *Curr Opin Neurobiol* **14**, 390-4.

Curtain, C. C., Ali, F., Volitakis, I., Cherny, R. A., Norton, R. S., Beyreuther, K., Barrow, C. J., Masters, C. L., Bush, A. I., and Barnham, K. J. (2001). Alzheimer's disease amyloid-beta binds copper and zinc to generate an allosterically ordered membrane-penetrating structure containing superoxide dismutase-like subunits. *J Biol Chem* **276**, 20466-73.

Dahlgren, K. N., Manelli, A. M., Stine, W. B., Jr., Baker, L. K., Krafft, G. A., and LaDu, M. J. (2002). Oligomeric and fibrillar species of amyloid-beta peptides differentially affect neuronal viability. *J Biol Chem* **277**, 32046-53.

Das, P., Howard, V., Loosbrock, N., Dickson, D., Murphy, M. P., and Golde, T. E. (2003). Amyloid-beta immunization effectively reduces amyloid deposition in FcRgamma-/- knock-out mice. *J Neurosci* **23**, 8532-8.

Deane, R., Du Yan, S., Submamaryan, R. K., LaRue, B., Jovanovic, S., Hogg, E., Welch, D., Manness, L., Lin, C., Yu, J., Zhu, H., Ghiso, J., Frangione, B., Stern, A., Schmidt, A. M., Armstrong, D. L., Arnold, B., Liliensiek, B., Nawroth, P., Hofman, F., Kindy, M., Stern, D., and Zlokovic, B. (2003). RAGE mediates amyloid-beta peptide transport across the blood-brain barrier and accumulation in brain. *Nat Med* **9**, 907-13.

DeMattos, R. B., Bales, K. R., Cummins, D. J., Dodart, J. C., Paul, S. M., and Holtzman, D. M. (2001). Peripheral anti-A beta antibody alters CNS and plasma A beta clearance and decreases brain A beta burden in a mouse model of Alzheimer's disease. *Proc Natl Acad Sci U S A* **98**, 8850-5.

DeMattos, R. B., Bales, K. R., Cummins, D. J., Paul, S. M., and Holtzman, D. M. (2002). Brain to plasma amyloid-beta efflux: a measure of brain amyloid burden in a mouse model of Alzheimer's disease. *Science* **295**, 2264-7.

Dheen, S. T., Jun, Y., Yan, Z., Tay, S. S., and Ling, E. A. (2005). Retinoic acid inhibits expression of TNF-alpha and iNOS in activated rat microglia. *Glia* **50**, 21-31.

DiCarlo, G., Wilcock, D., Henderson, D., Gordon, M., and Morgan, D. (2001). Intrahippocampal LPS injections reduce Abeta load in APP+PS1 transgenic mice. *Neurobiol Aging* **22**, 1007-12.

Dickstein, D. L., Biron, K. E., Ujiie, M., Pfeifer, C. G., Jeffries, A. R., and Jefferies, W. A. (2006). Abeta peptide immunization restores blood-brain barrier integrity in Alzheimer disease. *Faseb J* **20**, 426-33.

DiNubile, M. J., Stossel, T. P., Ljunghusen, O. C., Ferrara, J. L., and Antin, J. H. (2002). Prognostic implications of declining plasma gelsolin levels after allogeneic stem cell transplantation. *Blood* **100**, 4367-71.

Dougherty, K. D., Dreyfus, C. F., and Black, I. B. (2000). Brain-derived neurotrophic factor in astrocytes, oligodendrocytes, and microglia/macrophages after spinal cord injury. *Neurobiol Dis* **7**, 574-85.

Duff, K., Eckman, C., Zehr, C., Yu, X., Prada, C. M., Perez-tur, J., Hutton, M., Buee, L., Harigaya, Y., Yager, D., Morgan, D., Gordon, M. N., Holcomb, L., Refolo, L., Zenk, B., Hardy, J., and Younkin, S. (1996). Increased amyloid-beta42(43) in brains of mice expressing mutant presenilin 1. *Nature* **383**, 710-3.

Eckman, E. A., and Eckman, C. B. (2005). Abeta-degrading enzymes: modulators of Alzheimer's disease pathogenesis and targets for therapeutic intervention. *Biochem Soc Trans* **33**, 1101-5.

Evans, D. A., Funkenstein, H. H., Albert, M. S., Scherr, P. A., Cook, N. R., Chown, M. J., Hebert, L. E., Hennekens, C. H., and Taylor, J. O. (1989). Prevalence of Alzheimer's disease in a community population of older persons. Higher than previously reported. *JAMA* **262**, 2551-6.

Fiala, M., Lin, J., Ringman, J., Kermani-Arab, V., Tsao, G., Patel, A., Lossinsky, A. S., Graves, M. C., Gustavson, A., Sayre, J., Sofroni, E., Suarez, T., Chiappelli, F., and Bernard, G. (2005). Ineffective phagocytosis of amyloid-beta by macrophages of Alzheimer's disease patients. *J Alzheimers Dis* **7**, 221-32; discussion 255-62.

Floden, A. M., and Combs, C. K. (2006). Beta-amyloid stimulates murine postnatal and adult microglia cultures in a unique manner. *J Neurosci* **26**, 4644-8.

Funato, H., Yoshimura, M., Yamazaki, T., Saido, T. C., Ito, Y., Yokofujita, J., Okeda, R., and Ihara, Y. (1998). Astrocytes containing amyloid beta-protein (Abeta)-positive granules are associated with Abeta40-positive diffuse plaques in the aged human brain. *Am J Pathol* **152**, 983-92.

Gao, W., Eisenhauer, P. B., Conn, K., Lynch, J. A., Wells, J. M., Ullman, M. D., McKee, A., Thatte, H. S., and Fine, R. E. (2004). Insulin degrading enzyme is expressed in the human cerebrovascular endothelium and in cultured human cerebrovascular endothelial cells. *Neurosci Lett* **371**, 6-11.

Giannakopoulos, P., Herrmann, F. R., Bussiere, T., Bouras, C., Kovari, E., Perl, D. P., Morrison, J. H., Gold, G., and Hof, P. R. (2003). Tangle and neuron numbers, but not amyloid load, predict cognitive status in Alzheimer's disease. *Neurology* **60**, 1495-500.

Gilman, S., Koller, M., Black, R. S., Jenkins, L., Griffith, S. G., Fox, N. C., Eisner, L., Kirby, L., Boada Rovira, M., Forette, F., and Orgogozo, J. M. (2005). Clinical effects of A{beta} immunization (AN1792) in patients with AD in an interrupted trial. *Neurology*.

Giulian, D., and Baker, T. J. (1986). Characterization of ameboid microglia isolated from developing mammalian brain. *J Neurosci* **6**, 2163-78.

Glenner, G. G., and Wong, C. W. (1984). Alzheimer's disease and Down's syndrome: sharing of a unique cerebrovascular amyloid fibril protein. *Biochem Biophys Res Commun* **122**, 1131-5.

Goate, A., Chartier-Harlin, M. C., Mullan, M., Brown, J., Crawford, F., Fidani, L., Giuffra, L., Haynes, A., Irving, N., James, L., and et al. (1991). Segregation of a missense mutation in the amyloid precursor protein gene with familial Alzheimer's disease. *Nature* **349**, 704-6.

Haas, J., Storch-Hagenlocher, B., Biessmann, A., and Wildemann, B. (2002). Inducible nitric oxide synthase and argininosuccinate synthetase: co-induction in brain tissue of patients with Alzheimer's dementia and following stimulation with beta-amyloid 1-42 in vitro. *Neurosci Lett* **322**, 121-5.

Hardy, J., and Allsop, D. (1991). Amyloid deposition as the central event in the aetiology of Alzheimer's disease. *Trends Pharmacol Sci* **12**, 383-8.

Harms, C., Bosel, J., Lautenschlager, M., Harms, U., Braun, J. S., Hortnagl, H., Dirnagl, U., Kwiatkowski, D. J., Fink, K., and Endres, M. (2004). Neuronal gelsolin prevents apoptosis by enhancing actin depolymerization. *Mol Cell Neurosci* **25**, 69-82.

Hasegawa, K., Yamaguchi, I., Omata, S., Gejyo, F., and Naiki, H. (1999). Interaction between A beta(1-42) and A beta(1-40) in Alzheimer's beta-amyloid fibril formation in vitro. *Biochemistry* **38**, 15514-21.

Herber, D. L., Roth, L. M., Wilson, D., Wilson, N., Mason, J. E., Morgan, D., and Gordon, M. N. (2004). Time-dependent reduction in Abeta levels after intracranial LPS administration in APP transgenic mice. *Exp Neurol* **190**, 245-53.

Holcomb, L., Gordon, M. N., McGowan, E., Yu, X., Benkovic, S., Jantzen, P., Wright, K., Saad, I., Mueller, R., Morgan, D., Sanders, S., Zehr, C., O'Campo, K., Hardy, J., Prada, C. M., Eckman, C., Younkin, S., Hsiao, K., and Duff, K. (1998). Accelerated Alzheimer-type phenotype in transgenic mice carrying both mutant amyloid precursor protein and presenilin 1 transgenes. *Nat Med* **4**, 97-100.

Holcomb, L. A., Gordon, M. N., Jantzen, P., Hsiao, K., Duff, K., and Morgan, D. (1999). Behavioral changes in transgenic mice expressing both amyloid precursor protein and presenilin-1 mutations: lack of association with amyloid deposits. *Behav Genet* **29**, 177-85.

Hoozemans, J. J., van Haastert, E. S., Veerhuis, R., Arendt, T., Scheper, W., Eikelenboom, P., and Rozemuller, A. J. (2005). Maximal COX-2 and ppRb expression in neurons occurs during early Braak stages prior to the maximal activation of astrocytes and microglia in Alzheimer's disease. *J Neuroinflammation* **2**, 27.

Hoshi, M., Sato, M., Matsumoto, S., Noguchi, A., Yasutake, K., Yoshida, N., and Sato, K. (2003). Spherical aggregates of beta-amyloid (amylospheroid) show high neurotoxicity and activate tau protein kinase I/glycogen synthase kinase-3beta. *Proc Natl Acad Sci U S A* **100**, 6370-5.

Hsiao, K., Chapman, P., Nilsen, S., Eckman, C., Harigaya, Y., Younkin, S., Yang, F., and Cole, G. (1996). Correlative memory deficits, Abeta elevation, and amyloid plaques in transgenic mice. *Science* **274**, 99-102.

Hsiao, K. K., Borchelt, D. R., Olson, K., Johannsdottir, R., Kitt, C., Yunis, W., Xu, S., Eckman, C., Younkin, S., Price, D., and et al. (1995). Age-related CNS disorder and early death in transgenic FVB/N mice overexpressing Alzheimer amyloid precursor proteins. *Neuron* **15**, 1203-18.

Jankowsky, J. L., Fadale, D. J., Anderson, J., Xu, G. M., Gonzales, V., Jenkins, N. A., Copeland, N. G., Lee, M. K., Younkin, L. H., Wagner, S. L., Younkin, S. G., and Borchelt, D. R. (2004). Mutant presenilins specifically elevate the levels of the 42 residue beta-amyloid peptide in vivo: evidence for augmentation of a 42-specific gamma secretase. *Hum Mol Genet* **13**, 159-70.

Janmey, P. A., Iida, K., Yin, H. L., and Stossel, T. P. (1987). Polyphosphoinositide micelles and polyphosphoinositide-containing vesicles dissociate endogenous gelsolin-actin complexes and promote actin assembly from the fast-growing end of actin filaments blocked by gelsolin. *J Biol Chem* **262**, 12228-36.

Janus, C., Pearson, J., McLaurin, J., Mathews, P. M., Jiang, Y., Schmidt, S. D., Chishti, M. A., Horne, P., Heslin, D., French, J., Mount, H. T., Nixon, R. A., Mercken, M., Bergeron, C., Fraser, P. E., St George-Hyslop, P., and Westaway, D. (2000). A beta peptide immunization reduces behavioural impairment and plaques in a model of Alzheimer's disease. *Nature* **408**, 979-82.

Johnson-Wood, K., Lee, M., Motter, R., Hu, K., Gordon, G., Barbour, R., Khan, K., Gordon, M., Tan, H., Games, D., Lieberburg, I., Schenk, D., Seubert, P., and McConlogue, L. (1997). Amyloid precursor protein processing and A beta42 deposition in a transgenic mouse model of Alzheimer disease. *Proc Natl Acad Sci U S A* **94**, 1550-5.

Johnstone, M., Gearing, A. J., and Miller, K. M. (1999). A central role for astrocytes in the inflammatory response to beta-amyloid; chemokines, cytokines and reactive oxygen species are produced. *J Neuroimmunol* **93**, 182-93.

Kang, J., Lemaire, H. G., Unterbeck, A., Salbaum, J. M., Masters, C. L., Grzeschik, K. H., Multhaup, G., Beyreuther, K., and Muller-Hill, B. (1987). The precursor of Alzheimer's disease amyloid A4 protein resembles a cell-surface receptor. *Nature* **325**, 733-6.

Kawas, C. H., and Brookmeyer, R. (2001). Aging and the public health effects of dementia. *N Engl J Med* **344**, 1160-1.

Kayed, R., Head, E., Thompson, J. L., McIntire, T. M., Milton, S. C., Cotman, C. W., and Glabe, C. G. (2003). Common structure of soluble amyloid oligomers implies common mechanism of pathogenesis. *Science* **300**, 486-9.

Kazmirski, S. L., Howard, M. J., Isaacson, R. L., and Fersht, A. R. (2000). Elucidating the mechanism of familial amyloidosis- Finnish type: NMR studies of human gelsolin domain 2. *Proc Natl Acad Sci U S A* **97**, 10706-11.

Klein, R. L., Hamby, M. E., Gong, Y., Hirko, A. C., Wang, S., Hughes, J. A., King, M. A., and Meyer, E. M. (2002). Dose and promoter effects of adeno-associated viral vector for green fluorescent protein expression in the rat brain. *Exp Neurol* **176**, 66-74.

Klein, R. L., Hirko, A. C., Meyers, C. A., Grimes, J. R., Muzyczka, N., and Meyer, E. M. (2000). NGF gene transfer to intrinsic basal forebrain neurons increases cholinergic cell size and protects from age-related, spatial memory deficits in middle-aged rats. *Brain Res* **875**, 144-51.

Koppel, R. (2002). Alzheimer's Disease: The Costs to U.S. Businesses in 2002. Alzheimer's Association, Washington, D.C.

Kothakota, S., Azuma, T., Reinhard, C., Klippel, A., Tang, J., Chu, K., McGarry, T. J., Kirschner, M. W., Koths, K., Kwiatkowski, D. J., and Williams, L. T. (1997). Caspase-3-generated fragment of gelsolin: effector of morphological change in apoptosis. *Science* **278**, 294-8.

Kraepelin, E. (1910). "Psychiatrie : ein Lehrbuch für Studierende und Ärzte," 8., vollst. umgearb. Aufl./Ed. Barth, Leipzig, Germany.

Kwiatkowski, D. J. (1999). Functions of gelsolin: motility, signaling, apoptosis, cancer. *Curr Opin Cell Biol* **11**, 103-8.

Kwiatkowski, D. J., Janmey, P. A., and Yin, H. L. (1989). Identification of critical functional and regulatory domains in gelsolin. *J Cell Biol* **108**, 1717-26.

Lakowicz, J. R. (2002). "Topics in fluorescence spectroscopy," Kluwer Academic, New York.

Lanz, T. A., Fici, G. J., and Merchant, K. M. (2005). Lack of specific amyloid-beta(1-42) suppression by nonsteroidal anti-inflammatory drugs in young, plaque-free Tg2576 mice and in guinea pig neuronal cultures. *J Pharmacol Exp Ther* **312**, 399-406.

Lashuel, H. A., Hartley, D., Petre, B. M., Walz, T., and Lansbury, P. T., Jr. (2002). Neurodegenerative disease: amyloid pores from pathogenic mutations. *Nature* **418**, 291.

Lee, P. S., Drager, L. R., Stossel, T. P., Moore, F. D., and Rogers, S. O. (2006). Relationship of plasma gelsolin levels to outcomes in critically ill surgical patients. *Ann Surg* **243**, 399-403.

Lee, W. M., and Galbraith, R. M. (1992). The extracellular actin-scavenger system and actin toxicity. *N Engl J Med* **326**, 1335-41.

Leissring, M. A., Farris, W., Chang, A. Y., Walsh, D. M., Wu, X., Sun, X., Frosch, M. P., and Selkoe, D. J. (2003). Enhanced proteolysis of beta-amyloid in APP transgenic mice prevents plaque formation, secondary pathology, and premature death. *Neuron* **40**, 1087-93.

Lemere, C. A., Spooner, E. T., LaFrancois, J., Malester, B., Mori, C., Leverone, J. F., Matsuoka, Y., Taylor, J. W., DeMattos, R. B., Holtzman, D. M., Clements, J. D., Selkoe, D. J., and Duff, K. E. (2003). Evidence for peripheral clearance of cerebral Abeta protein following chronic, active Abeta immunization in PSAPP mice. *Neurobiol Dis* **14**, 10-8.

Leveugle, B., Scanameo, A., Ding, W., and Fillit, H. (1994). Binding of heparan sulfate glycosaminoglycan to beta-amyloid peptide: inhibition by potentially therapeutic polysulfated compounds. *Neuroreport* **5**, 1389-92.

Levites, Y., Das, P., Price, R. W., Rochette, M. J., Kostura, L. A., McGowan, E. M., Murphy, M. P., and Golde, T. E. (2006). Anti-Abeta42- and anti-Abeta40-specific mAbs attenuate amyloid deposition in an Alzheimer disease mouse model. *J Clin Invest* **116**, 193-201.

Levy-Lahad, E., Wijsman, E. M., Nemens, E., Anderson, L., Goddard, K. A., Weber, J. L., Bird, T. D., and Schellenberg, G. D. (1995). A familial Alzheimer's disease locus on chromosome 1. *Science* **269**, 970-3.

Lind, S. E., and Janmey, P. A. (1984). Human plasma gelsolin binds to fibronectin. *J Biol Chem* **259**, 13262-6.

Lindberg, C., Selenica, M. L., Westlind-Danielsson, A., and Schultzberg, M. (2005). Beta-amyloid protein structure determines the nature of cytokine release from rat microglia. *J Mol Neurosci* **27**, 1-12.

Liu, F., Song, Y., and Liu, D. (1999). Hydrodynamics-based transfection in animals by systemic administration of plasmid DNA. *Gene Ther* **6**, 1258-66.

Liu, T., Perry, G., Chan, H. W., Verdile, G., Martins, R. N., Smith, M. A., and Atwood, C. S. (2004). Amyloid-beta-induced toxicity of primary neurons is dependent upon differentiation-associated increases in tau and cyclin-dependent kinase 5 expression. *J Neurochem* **88**, 554-63.

Lopez-Toledano, M. A., and Shelanski, M. L. (2004). Neurogenic effect of beta-amyloid peptide in the development of neural stem cells. *J Neurosci* **24**, 5439-44.

Lue, L. F., Kuo, Y. M., Roher, A. E., Brachova, L., Shen, Y., Sue, L., Beach, T., Kurth, J. H., Rydel, R. E., and Rogers, J. (1999). Soluble amyloid beta peptide concentration as a predictor of synaptic change in Alzheimer's disease. *Am J Pathol* **155**, 853-62.

Marco, S., and Skaper, S. D. (2006). Amyloid beta-peptide(1-42) alters tight junction protein distribution and expression in brain microvessel endothelial cells. *Neurosci Lett*.

Marr, R. A., Rockenstein, E., Mukherjee, A., Kindy, M. S., Hersh, L. B., Gage, F. H., Verma, I. M., and Masliah, E. (2003). Neprilysin gene transfer reduces human amyloid pathology in transgenic mice. *J Neurosci* **23**, 1992-6.

Masliah, E., Rockenstein, E., Veinbergs, I., Sagara, Y., Mallory, M., Hashimoto, M., and Mucke, L. (2001). beta-amyloid peptides enhance alpha-synuclein accumulation and neuronal deficits in a transgenic mouse model linking Alzheimer's disease and Parkinson's disease. *Proc Natl Acad Sci U S A* **98**, 12245-50.

Matsumoto, N., Kitayama, H., Kitada, M., Kimura, K., Noda, M., and Ide, C. (2003). Isolation of a set of genes expressed in the choroid plexus of the mouse using suppression subtractive hybridization. *Neuroscience* **117**, 405-15.

Matsuoka, Y., Saito, M., LaFrancois, J., Gaynor, K., Olm, V., Wang, L., Casey, E., Lu, Y., Shiratori, C., Lemere, C., and Duff, K. (2003). Novel therapeutic approach for the treatment of Alzheimer's disease by peripheral administration of agents with an affinity to beta-amyloid. *J Neurosci* **23**, 29-33.

Matsuoka, Y., Shao, L., Debnath, M., Lafrancois, J., Becker, A., Gray, A., Aisen, P., Mathis, C., Klunk, W., and Duff, K. (2005). An Abeta sequestration approach using non-antibody Abeta binding agents. *Curr Alzheimer Res* **2**, 265-8.

Mattson, M. P., Cheng, B., Davis, D., Bryant, K., Lieberburg, I., and Rydel, R. E. (1992). beta-Amyloid peptides destabilize calcium homeostasis and render human cortical neurons vulnerable to excitotoxicity. *J Neurosci* **12**, 376-89.

McGeer, E. G., and McGeer, P. L. (2003). Inflammatory processes in Alzheimer's disease. *Prog Neuropsychopharmacol Biol Psychiatry* **27**, 741-9.

McLaughlin, P. J., Gooch, J. T., Mannherz, H. G., and Weeds, A. G. (1993). Structure of gelsolin segment 1-actin complex and the mechanism of filament severing. *Nature* **364**, 685-92.

Moller, H. J., and Graeber, M. B. (1998). The case described by Alois Alzheimer in 1911. Historical and conceptual perspectives based on the clinical record and neurohistological sections. *Eur Arch Psychiatry Clin Neurosci* **248**, 111-22.

Morgan, D., Diamond, D. M., Gottschall, P. E., Ugen, K. E., Dickey, C., Hardy, J., Duff, K., Jantzen, P., DiCarlo, G., Wilcock, D., Connor, K., Hatcher, J., Hope, C., Gordon, M., and Arendash, G. W. (2000). A beta peptide vaccination prevents memory loss in an animal model of Alzheimer's disease. *Nature* **408**, 982-5.

Mounzer, K. C., Moncure, M., Smith, Y. R., and Dinubile, M. J. (1999). Relationship of admission plasma gelsolin levels to clinical outcomes in patients after major trauma. *Am J Respir Crit Care Med* **160**, 1673-81.

Nakajima, K., Honda, S., Tohyama, Y., Imai, Y., Kohsaka, S., and Kurihara, T. (2001). Neurotrophin secretion from cultured microglia. *J Neurosci Res* **65**, 322-31.

Naslund, J., Haroutunian, V., Mohs, R., Davis, K. L., Davies, P., Greengard, P., and Buxbaum, J. D. (2000). Correlation between elevated levels of amyloid beta-peptide in the brain and cognitive decline. *Jama* **283**, 1571-7.

Noble, W., Olm, V., Takata, K., Casey, E., Mary, O., Meyerson, J., Gaynor, K., LaFrancois, J., Wang, L., Kondo, T., Davies, P., Burns, M., Veeranna, Nixon, R., Dickson, D., Matsuoka, Y., Ahlijanian, M., Lau, L. F., and Duff, K. (2003). Cdk5 is a key factor in tau aggregation and tangle formation in vivo. *Neuron* **38**, 555-65.

Nodes, B. R., Shackelford, J. E., and Lebherz, H. G. (1987). Synthesis and secretion of serum gelsolin by smooth muscle tissue. *J Biol Chem* **262**, 5422-7.

Orgogozo, J. M., Gilman, S., Dartigues, J. F., Laurent, B., Puel, M., Kirby, L. C., Jouanny, P., Dubois, B., Eisner, L., Flitman, S., Michel, B. F., Boada, M., Frank, A., and Hock, C. (2003). Subacute meningoencephalitis in a subset of patients with AD after Abeta42 immunization. *Neurology* **61**, 46-54.

Pellerin, L. (2005). How astrocytes feed hungry neurons. *Mol Neurobiol* **32**, 59-72.

Petty, B. G., Cornblath, D. R., Adornato, B. T., Chaudhry, V., Flexner, C., Wachsman, M., Sinicropi, D., Burton, L. E., and Peroutka, S. J. (1994). The effect of systemically administered recombinant human nerve growth factor in healthy human subjects. *Ann Neurol* **36**, 244-6.

Pike, C. J., Walencewicz, A. J., Glabe, C. G., and Cotman, C. W. (1991). Aggregation-related toxicity of synthetic beta-amyloid protein in hippocampal cultures. *Eur J Pharmacol* **207**, 367-8.

Ray, I., Chauhan, A., Wegiel, J., and Chauhan, V. P. (2000). Gelsolin inhibits the fibrillization of amyloid beta-protein, and also defibrillizes its preformed fibrils. *Brain Res* **853**, 344-51.

Rogers, J., Strohmeyer, R., Kovelowski, C. J., and Li, R. (2002). Microglia and inflammatory mechanisms in the clearance of amyloid beta peptide. *Glia* **40**, 260-9.

Rothenbach, P. A., Dahl, B., Schwartz, J. J., O'Keefe, G. E., Yamamoto, M., Lee, W. M., Horton, J. W., Yin, H. L., and Turnage, R. H. (2004). Recombinant plasma gelsolin infusion attenuates burn-induced pulmonary microvascular dysfunction. *J Appl Physiol* **96**, 25-31.

Schenk, D., Barbour, R., Dunn, W., Gordon, G., Grajeda, H., Guido, T., Hu, K., Huang, J., Johnson-Wood, K., Khan, K., Kholodenko, D., Lee, M., Liao, Z., Lieberburg, I., Motter, R., Mutter, L., Soriano, F., Shopp, G., Vasquez, N., Vandevert, C., Walker, S., Wogulis, M., Yednock, T., Games, D., and Seubert, P. (1999). Immunization with amyloid-beta attenuates Alzheimer-disease-like pathology in the PDAPP mouse. *Nature* **400**, 173-7.

Scheuner, D., Eckman, C., Jensen, M., Song, X., Citron, M., Suzuki, N., Bird, T. D., Hardy, J., Hutton, M., Kukull, W., Larson, E., Levy-Lahad, E., Viitanen, M., Peskind, E., Poorkaj, P., Schellenberg, G., Tanzi, R., Wasco, W., Lannfelt, L., Selkoe, D., and Younkin, S. (1996). Secreted amyloid beta-protein similar to that in the senile plaques of Alzheimer's disease is increased in vivo by the presenilin 1 and 2 and APP mutations linked to familial Alzheimer's disease. *Nat Med* **2**, 864-70.

Scott, M. R., Kohler, R., Foster, D., and Prusiner, S. B. (1992). Chimeric prion protein expression in cultured cells and transgenic mice. *Protein Sci* **1**, 986-97.

Selkoe, D. J. (1989). The deposition of amyloid proteins in the aging mammalian brain: implications for Alzheimer's disease. *Ann Med* **21**, 73-6.

Selkoe, D. J. (1990). Deciphering Alzheimer's disease: the amyloid precursor protein yields new clues. *Science* **248**, 1058-60.

Sherrington, R., Froelich, S., Sorbi, S., Campion, D., Chi, H., Rogaeva, E. A., Levesque, G., Rogaev, E. I., Lin, C., Liang, Y., Ikeda, M., Mar, L., Brice, A., Agid, Y., Percy, M. E., Clerget-Darpoux, F., Piacentini, S., Marcon, G., Nacmias, B., Amaducci, L., Frebourg, T., Lannfelt, L., Rommens, J. M., and St George-Hyslop, P. H. (1996). Alzheimer's disease associated with mutations in presenilin 2 is rare and variably penetrant. *Hum Mol Genet* **5**, 985-8.

Shibata, M., Yamada, S., Kumar, S. R., Calero, M., Bading, J., Frangione, B., Holtzman, D. M., Miller, C. A., Strickland, D. K., Ghiso, J., and Zlokovic, B. V. (2000). Clearance of Alzheimer's amyloid-ss(1-40) peptide from brain by LDL receptor-related protein-1 at the blood-brain barrier. *J Clin Invest* **106**, 1489-99.

Sinha, S., and Lieberburg, I. (1999). Cellular mechanisms of beta-amyloid production and secretion. *Proc Natl Acad Sci U S A* **96**, 11049-53.

Sloane, P. D., Zimmerman, S., Suchindran, C., Reed, P., Wang, L., Boustani, M., and Sudha, S. (2002). The public health impact of Alzheimer's disease, 2000-2050: potential implication of treatment advances. *Annu Rev Public Health* **23**, 213-31.

Smith, D. B., Janmey, P. A., Herbert, T. J., and Lind, S. E. (1987). Quantitative measurement of plasma gelsolin and its incorporation into fibrin clots. *J Lab Clin Med* **110**, 189-95.

Sofroniew, M. V. (2005). Reactive astrocytes in neural repair and protection. *Neuroscientist* **11**, 400-7.

Song, S., Embury, J., Laipis, P. J., Berns, K. I., Crawford, J. M., and Flotte, T. R. (2001). Stable therapeutic serum levels of human alpha-1 antitrypsin (AAT) after portal vein injection of recombinant adeno-associated virus (rAAV) vectors. *Gene Ther* **8**, 1299-306.

Streit, W. J., Graeber, M. B., and Kreutzberg, G. W. (1988). Functional plasticity of microglia: a review. *Glia* **1**, 301-7.

Sun, A., Nguyen, X. V., and Bing, G. (2002). Comparative analysis of an improved thioflavin-s stain, Gallyas silver stain, and immunohistochemistry for neurofibrillary tangle demonstration on the same sections. *J Histochem Cytochem* **50**, 463-72.

Suzuki, N., Cheung, T. T., Cai, X. D., Odaka, A., Otvos, L., Jr., Eckman, C., Golde, T. E., and Younkin, S. G. (1994). An increased percentage of long amyloid beta protein secreted by familial amyloid beta protein precursor (beta APP717) mutants. *Science* **264**, 1336-40.

Tamaoka, A., Odaka, A., Ishibashi, Y., Usami, M., Sahara, N., Suzuki, N., Nukina, N., Mizusawa, H., Shoji, S., Kanazawa, I., and et al. (1994). APP717 missense mutation affects the ratio of amyloid beta protein species (A beta 1-42/43 and a beta 1-40) in familial Alzheimer's disease brain. *J Biol Chem* **269**, 32721-4.

Telling, G. C., Scott, M., Hsiao, K. K., Foster, D., Yang, S. L., Torchia, M., Sidle, K. C., Collinge, J., DeArmond, S. J., and Prusiner, S. B. (1994). Transmission of Creutzfeldt-Jakob disease from humans to transgenic mice expressing chimeric human-mouse prion protein. *Proc Natl Acad Sci U S A* **91**, 9936-40.

Terry, R. D., and Katzman, R. (1983). Senile dementia of the Alzheimer type. *Ann Neurol* **14**, 497-506.

Trinh, N. H., Hoblyn, J., Mohanty, S., and Yaffe, K. (2003). Efficacy of cholinesterase inhibitors in the treatment of neuropsychiatric symptoms and functional impairment in Alzheimer disease: a meta-analysis. *Jama* **289**, 210-6.

Turner, P. R., O'Connor, K., Tate, W. P., and Abraham, W. C. (2003). Roles of amyloid precursor protein and its fragments in regulating neural activity, plasticity and memory. *Prog Neurobiol* **70**, 1-32.

van Oijen, M., Hofman, A., Soares, H. D., Koudstaal, P. J., and Breteler, M. M. (2006). Plasma Abeta(1-40) and Abeta(1-42) and the risk of dementia: a prospective case-cohort study. *Lancet Neurol* **5**, 655-60.

Vasconcellos, C. A., Allen, P. G., Wohl, M. E., Drazen, J. M., Janmey, P. A., and Stossel, T. P. (1994). Reduction in viscosity of cystic fibrosis sputum in vitro by gelsolin. *Science* **263**, 969-71.

Volterra, A., and Meldolesi, J. (2005). Astrocytes, from brain glue to communication elements: the revolution continues. *Nat Rev Neurosci* **6**, 626-40.

von Bernhardi, R., and Eugenin, J. (2004). Microglial reactivity to beta-amyloid is modulated by astrocytes and proinflammatory factors. *Brain Res* **1025**, 186-93.

Vouyiouklis, D. A., and Brophy, P. J. (1997). A novel gelsolin isoform expressed by oligodendrocytes in the central nervous system. *J Neurochem* **69**, 995-1005.

Walker, D. G., and Lue, L. F. (2005). Investigations with cultured human microglia on pathogenic mechanisms of Alzheimer's disease and other neurodegenerative diseases. *J Neurosci Res* **81**, 412-25.

Weber, G. (1953). Rotational Brownian motion and polarization of the fluorescence of solutions. *Adv Protein Chem* **8**, 415-59.

Wegiel, J., Chauhan, A., Wisniewski, H. M., Nowakowski, J., Wang, K. C., and Le Vine, H., 3rd (1996). Promotion of synthetic amyloid beta-peptide fibrillization by cell culture media and cessation of fibrillization by serum. *Neurosci Lett* **211**, 151-4.

Weinstock, M. (1995). The pharmacotherapy of Alzheimer's disease based on the cholinergic hypothesis: an update. *Neurodegeneration* **4**, 349-56.

Westerman, M. A., Cooper-Blacketer, D., Mariash, A., Kotilinek, L., Kawarabayashi, T., Younkin, L. H., Carlson, G. A., Younkin, S. G., and Ashe, K. H. (2002). The relationship between Abeta and memory in the Tg2576 mouse model of Alzheimer's disease. *J Neurosci* **22**, 1858-67.

Wilcock, D. M., DiCarlo, G., Henderson, D., Jackson, J., Clarke, K., Ugen, K. E., Gordon, M. N., and Morgan, D. (2003). Intracranially administered anti-Abeta antibodies reduce beta-amyloid deposition by mechanisms both independent of and associated with microglial activation. *J Neurosci* **23**, 3745-51.

Wimo, A., Winblad, B., Stoffler, A., Wirth, Y., and Mobius, H. J. (2003). Resource utilisation and cost analysis of memantine in patients with moderate to severe Alzheimer's disease. *Pharmacoeconomics* **21**, 327-40.

Witke, W., Li, W., Kwiatkowski, D. J., and Southwick, F. S. (2001). Comparisons of CapG and gelsolin-null macrophages: demonstration of a unique role for CapG in receptor-mediated ruffling, phagocytosis, and vesicle rocketing. *J Cell Biol* **154**, 775-84.

Witke, W., Sharpe, A. H., Hartwig, J. H., Azuma, T., Stossel, T. P., and Kwiatkowski, D. J. (1995). Hemostatic, inflammatory, and fibroblast responses are blunted in mice lacking gelsolin. *Cell* **81**, 41-51.

Wu, K., Meyers, C. A., Guerra, N. K., King, M. A., and Meyer, E. M. (2004). The effects of rAAV2-mediated NGF gene delivery in adult and aged rats. *Mol Ther* **9**, 262-9.

Wyss-Coray, T., Loike, J. D., Brionne, T. C., Lu, E., Anankov, R., Yan, F., Silverstein, S. C., and Husemann, J. (2003). Adult mouse astrocytes degrade amyloid-beta in vitro and in situ. *Nat Med* **9**, 453-7.

Yamaguchi, H., Sugihara, S., Ogawa, A., Saido, T. C., and Ihara, Y. (1998). Diffuse plaques associated with astroglial amyloid beta protein, possibly showing a disappearing stage of senile plaques. *Acta Neuropathol (Berl)* **95**, 217-22.

Yankner, B. A., Duffy, L. K., and Kirschner, D. A. (1990). Neurotrophic and neurotoxic effects of amyloid beta protein: reversal by tachykinin neuropeptides. *Science* **250**, 279-82.

Yin, H. L., and Stossel, T. P. (1979). Control of cytoplasmic actin gel-sol transformation by gelsolin, a calcium-dependent regulatory protein. *Nature* **281**, 583-6.

Zhang, G., Gao, X., Song, Y. K., Vollmer, R., Stolz, D. B., Gasiorowski, J. Z., Dean, D. A., and Liu, D. (2004). Hydroporation as the mechanism of hydrodynamic delivery. *Gene Ther* **11**, 675-82.

Zheng, H., Jiang, M., Trumbauer, M. E., Hopkins, R., Sirinathsinghji, D. J., Stevens, K. A., Conner, M. W., Slunt, H. H., Sisodia, S. S., Chen, H. Y., and Van der Ploeg, L. H. (1996). Mice deficient for the amyloid precursor protein gene. *Ann N Y Acad Sci* **777**, 421-6.

Zheng, H., Jiang, M., Trumbauer, M. E., Sirinathsinghji, D. J., Hopkins, R., Smith, D. W., Heavens, R. P., Dawson, G. R., Boyce, S., Conner, M. W., Stevens, K. A., Slunt, H. H., Sisoda, S. S., Chen, H. Y., and Van der Ploeg, L. H. (1995). beta-Amyloid precursor protein-deficient mice show reactive gliosis and decreased locomotor activity. *Cell* **81**, 525-31.

Ziv, Y., Ron, N., Butovsky, O., Landa, G., Sudai, E., Greenberg, N., Cohen, H., Kipnis, J., and Schwartz, M. (2006). Immune cells contribute to the maintenance of neurogenesis and spatial learning abilities in adulthood. *Nat Neurosci* **9**, 268-75.

BIOGRAPHICAL SKETCH

The author was born in Pittsburgh, Pennsylvania, on May 9, 1972. In 1980, he moved to Gainesville, Florida, where he spent the remainder of his childhood. He graduated from Buchholz High School in 1990, and started studies at the University of Florida immediately afterward. After 2 years of studies at the University of Florida he left school and was trained as a commercial aircraft pilot. He returned to school in 1998, and obtained a part-time job in the laboratory of Dr. Edwin Meyer, where his interest in research first started. While working in Dr. Meyer's lab, he contributed to three articles published in scientific journals. Also while working there, he was introduced to and worked with Dr. Jeffrey Hughes, who later became his mentor. He graduated with honors with a bachelor's degree (food science and human nutrition) in 2000. In 2001 he matriculated as a graduate student under the tutelage of Dr. Jeffrey Hughes, in pursuit of a Ph.D. in the pharmaceutical sciences.